Anionentransport durch das Motorprotein Prestin

Von der Naturwissenschaftlichen Fakultät
der Gottfried Wilhelm Leibniz Universität Hannover
zur Erlangung des Grades
Doktor der Naturwissenschaften
Dr. rer. nat.
genehmigte Dissertation
von

Dipl.-Phys. Michael Schänzler

geboren am 03.03.1969 in Karlsruhe

2012

Referent: Prof. Dr. Christoph Fahlke
Korreferent: Prof. Dr. Anaclet Ngezahayo

Tag der Promotion: 22.08.2012

Zusammenfassung

Prestin ist das Motorprotein der äußeren Haarzellen. Es spielt eine zentrale Rolle im Hörprozess von Säugetieren. Die hohe Empfindlichkeit des Säugetierohres wird durch eine positive elektromechanische Rückkopplung innerhalb der Cochlea erreicht, indem die äußeren Haarzellen unter dem Einfluss von Schallwellen zu Längenänderungen im akustischen Frequenzbereich angeregt werden. Diese Längenänderungen finden aktiv mit Hilfe des Motorproteins Prestin statt, wobei Änderungen der Membranspannung unmittelbar in Konformationsänderungen des Proteins umgesetzt werden. Eine Eigenschaft die Elektromotilität genannt wird.

Das Prestin ist Mitglied einer größeren Familie von Anionentransportern, was für ein Motorprotein ungewöhnlich ist. Die Säugetierprestine nehmen innerhalb dieser, SLC26 genannten, Familie eine Sonderstellung ein. Nur sie zeigen die Eigenschaft der Elektromotilität. Während andere Proteine der SLC26-Familie eine Vielfalt von mono- und divalenten Ionen transportieren, ist bisher für die Säugetierprestine keine elektrogene Transportaktivität bekannt. Selbst Nicht-Säugetier-Prestine von *Danio rerio* und *Gallus gallus domesticus* sind ausgeprägte elektrogene Chlorid/Sulfat-Antiporter.

In der vorliegenden Arbeit konnte gezeigt werden, dass auch das Säugetierprestin von *Rattus norvegicus* zu einem elektrogenen Ionentransport in der Lage ist. Mit Hilfe von Patch-Clamp-Messungen sowie Fluoreszenzuntersuchungen konnte ein Transport des Thiocyanat-Anions nachgewiesen werden, indem der gemessene Strom mit dem Expressionsniveau des Prestins korreliert wurde. Es konnte gezeigt werden, dass der Transport stöchiometrisch nicht an den Kotransport anderer Ionen gekoppelt ist und nur geringe Auswirkungen auf die nichtlineare intrinsische Ladungsverschiebung des Prestins hat. Die Eigenschaften des Transportstroms deuten auf einen kanalartigen 'Slippage-Mode' hin. Der Strom konnte durch Salicylat, einen Inhibitor der Elektromotilität, nicht geblockt werden. Ein elektrophysiologischer Vergleich des Säugetierprestins mit dem Zebrafischprestin und einem Anionenkanal aus der SLC26-Familie (SLC26A7) zeigte, dass dieser Transportmodus bei Motorproteinen, Antiportern und Kanälen konserviert ist und keine spezifische Eigenschaft des Säugetierprestins darstellt.

Die Koexpression zweier Prestinmutanten mit unterschiedlichen nichtlinearen Ladungsverschiebungen in einer Zelle führte zu intermediären elektrischen Eigenschaften anstatt zu einer einfachen additiven Überlagerung, was darauf hinweist, dass ein funktionales Motorprotein aus zwei kooperierenden Untereinheiten aufgebaut ist.

Schlagworte: Motorprotein, Ionenkanal, Elektrophysiologie

Abstract

Prestin is the motor protein of outer hair cells. It has a crucial role in mammalian hearing. The extraordinary sensitivity of the mammalian ear is achieved by positive electromechanical feedback within the cochlea. Outer hair cells alter their length in response to sound-induced pertubations at acoustic rates. These length changes are driven by voltage-dependent conformational changes of the motor protein prestin which directly converts electrical energy into motion, a property called electromotility.

Prestin is a member of a family of anion transporters (SLC26). This is unusal for a motor protein. Mammalian prestin plays a special role among the SLC26. No other SLC26 protein has been shown to exhibit electromotility. While other SLC26 homologues were demonstrated to transport a wide variety of anions, no electrogenic transport activity has been assigned so far to mammalian prestin. Even non-mammalian prestin orthologs from *Danio rerio* and *Gallus gallus domesticus* are electrogenic chloride/sulfate exchangers.

In the present work we demonstrate the ability of a mammalian prestin from *Rattus norvegicus* to mediate electrogenic anion transport. Using patch-clamp recordings and fluorescence measurements, SCN^- transport was shown by correlating currents to expression levels of individual cells. SCN^- transport was not stoichiometrically coupled to other anions and caused only minor changes in non-linear charge movement. Transport activity was not abolished by salicylate, a known inhibitor of electromotility. SCN^--currents showed characteristics of a 'channel-like slippage mode'. An electrophysiological comparison of mammalian prestin with a non-mammalian prestin from *Danio rerio* and an SLC26 anion channel (SLC26A7) revealed that this transport mode is conserved in SLC26 proteins functioning as motor proteins, anion exchangers as well as anion channels and is not a unique property of mammalian prestin.

Co-expression of two mutant prestins with distinct voltage-dependent charge movements did not result in a mere superposition but showed intermediate electrical properties, indicating that two cooperating subunits are required to form a functional motor protein.

Keywords: Motor protein, Ion channel, Electrophysiology

Inhaltsverzeichnis

Abkürzungsverzeichnis

cDNA	Complementary DNA
CFTR	Cystic fibrosis transmembrane conductance regulator
DIC	Differentialinterferenzkontrast
EGTA	Ethylene glycol tetraacetic acid
FRET	Förster-Resonanzenergietransfer
HEK293T	Human embryonic kidney 293 cell
HEPES	Hydroxyethylpiperazin-Ethansulfonsäure
IHC	Inner hair cell
KCNQ4	Potassium voltage-gated channel, KQT-like subfamily, member 4
OHC	Outer hair cell
SCN	Thiocyanat
SD	Standard deviation
SEM	Standard error of the mean
SLC26	Solute carrier family 26
SLC26A5	Solute carrier family 26, member 5 (prestin)
SLC26A7	Solute carrier family 26, member 7
STAS	Sulphate Transporter and AntiSigma factor antagonist
SulP	Sulfat-Permease
TEA	Tetraethylammonium
TRP	Transient receptor potential channel
YFP	Yellow fluorescent protein

1 Einleitung

Der Gehörsinn von Säugetieren ist hoch entwickelt. Er kombiniert eine hohe Auflösung mit einem großen Dynamikumfang – gleichzeitig für die Amplitude des Schalldrucks und dessen Frequenz. Die absolute Lautstärkeempfindlichkeit ist so hoch, dass sie fast den Bereich thermischer Molekülbewegung erreicht [49][53]. Hinzu kommt bei vielen Arten eine ausgeprägte Fähigkeit zur räumlichen Lokalisierung von Schallquellen, die sich bei Fledermäusen und Walen bis hin zur Orientierung mittels Echoortung fortentwickelt hat.

Alle Wirbeltiere verfügen dagegen über ein morphologisch ähnliches Innenohr [37] und der grundsätzliche Mechanismus der Schallrezeption ist bei allen Wirbeltieren identisch. Die Umwandlung des mechanischen Reizes in elektrische Signale geschieht durch Mechanorezeptoren, die aufgrund ihrer charakteristischen Stereozilien Haarzellen genannt werden. Wird ein Haarbündel durch mechanische Störungen geschert, öffnen sich apikal Kationenkanäle, was zu einer Depolarisierung der Zelle führt. Die Depolarisation bewirkt im zweiten Schritt ein Freisetzen des afferenten Neurotransmitters und damit die Übertragung des Signals auf den Hörnerv. Durch mikromechanische oder elektrische Differenzierung können Haarzellen auf einzelne Frequenzbereiche abgestimmt werden, was zu einer frequenzselektiven Wahrnehmung führt [31].

Dieses Grundprinzip der Schallwahrnehmung ist evolutionär sehr alt und war vermutlich schon bei frühen Wirbeltieren vor 470 Mio. Jahren realisiert [21]. Man geht davon aus, dass die Hörorgane insgesamt homolog sind; sie haben einen gemeinsamen Vorfahren, eine vergleichbare Struktur und entwickeln sich aus dem gleichen genetischen Substrat. Bedeutsame evolutionäre Ereignisse, die später eintraten, waren [32]:

- die Entwicklung eines impedanzangepassten Mittelohres zur effektiven Schalleinleitung,
- die Verlängerung des *Ductus cochlearis*,
- die Differenzierung in zwei Arten von Haarzellen,
- das Aufrollen zur Hörschnecke verbunden mit einer weiteren Verlängerung der Cochlea,
- sowie die Entwicklung eines zweiten cochleären Verstärkers.

Wobei die letzten beiden Entwicklungsschritte im Wesentlichen nur bei Säugetieren stattgefunden haben. Seine außerordentliche Leistungsfähigkeit erreicht der zweite cochleäre Verstärker durch das unkonventionelle Motorprotein Prestin, das elektrische Energie unmittelbar in Konformationsänderungen umsetzen kann, ohne dabei selbst auf chemische Energiequellen zurückgreifen zu müssen [55].

1.1 Aktive mechanische Verstärkung im Innenohr

1.1.1 Haarzellen

Haarzellen oder auch Haarsinneszellen sind Epithelzellen, die aus einem in der Regel zylinderförmigen Zellkörper und dem namensgebenden Haarbündel bestehen. Das Haarbündel bildet die mechanosensitive Komponente und setzt sich wiederum zusammen aus einer Kinozilie und mehreren Stereovilli, oft insgesamt als Stereozilien bezeichnet. Das Kinozilium muss nicht immer vorkommen oder kann zurückgebildet sein, was beispielsweise bei adulten menschlichen Haarzellen der Fall ist und eine Rolle lediglich in der Entwicklung nahelegt [30].

Eine Haarzelle bildet etwa 20 – 300 Stereozilien, die in Reihen zunehmender Länge angeordnet sind. Die Stereozilien selbst bestehen aus parallelen Aktinfilamenten, die an der Basis verjüngt sind und nur dort ausgelenkt werden können. Untereinander sind die Aktinfilamente durch sogenannte Tip-Links gekoppelt, so dass eine Bewegung des Haarbündel stets als Ganzes erfolgt [30].

Die Tip-Links spielen eine entscheidende Rolle im Prozess der Schallwahrnehmung. Je nach Auslenkung des Haarbündels entsteht in den Tip-Links eine korrespondierende mechanische Spannung, die das Öffnen und Schließen von Ionenkanälen bewirkt. Der Kanal hat eine hohe Leitfähigkeit von mehr als 100 pS für K^+ und Ca^{2+} unter physiologischen Bedingungen. Man geht heute davon aus, dass es sich dabei um einen unspezifischen, mechanosensitiven Kationenkanal aus der TRP-Famile handelt [10]. Der Zustand der Ionenkanäle selbst wirkt zurück auf die Elastizität des Tip-Links [42], wobei das Öffnen von Kanälen seine Federkonstante verkleinert. Die Offenwahrscheinlichkeit des Kanals kann über das Binden von Ca^{2+} beeinflusst werden. Diese Modulation ist verantwortlich für den schnellen Adaptionsprozess von Haarzellen, der das Haarbündel am empfindlichsten Punkt seines Arbeitsbereiches hält [19]. Vermutet wird aber auch eine Rolle in der Frequenzabstimmung, da nicht nur die Offenwahrscheinlichkeit des Kanals beeinflusst werden kann, sondern auch dessen Leitfähigkeit. Die Frequenzselektivität von Haarzellen korreliert dabei mit der Einzelkanalamplitude des zugrundeliegenden Kanals [43].

Neben dieser schnellen elektrochemischen Anpassung exisitiert ein weiterer Adaptionsprozess im Bereich von zehntel Millisekunden, vermittelt durch einen ATP-abhängigen chemischen Motor, der den Aufhängepunkt des Tip-Links am Aktinfilament vertikal bewegt [22]. Als Motorprotein gilt Myosin-1C als wahrscheinlich. Der langsame Adaptionsprozess verschiebt die Auslenkungs-Antwort Kurve in Richtung des Stimulus. Indem das System auf eine fortgesetzte Auslenkung etwa durch eine Lage- oder Orientierungsänderung im Raum reagiert und den Arbeitspunkt verschiebt, bleibt es auch unter diesen neuen Bedingungen empfindlich für weitere Stimuli [30]. Beide Adaptionsprozesse sind aber nicht nur für die Einstellung des optimalen Arbeitspunktes von Bedeutung, sondern spielen eine zentrale Rolle im Verstärkungsprozess, indem sie dafür sorgen, dass unter bestimmten Bedingungen die Federkonstante der Tip-Links negativ werden kann [33]. Eine positive Federkonstante wirkt nach dem Hook'schen Gesetz einer Auslenkung entgegen und führt zu einer Beschleunigung in Richtung Ruhelage. Eine negative Steifigkeit verstärkt dagegen den Stimulus, was zu einer nichtlinearen Systemantwort führt. Das

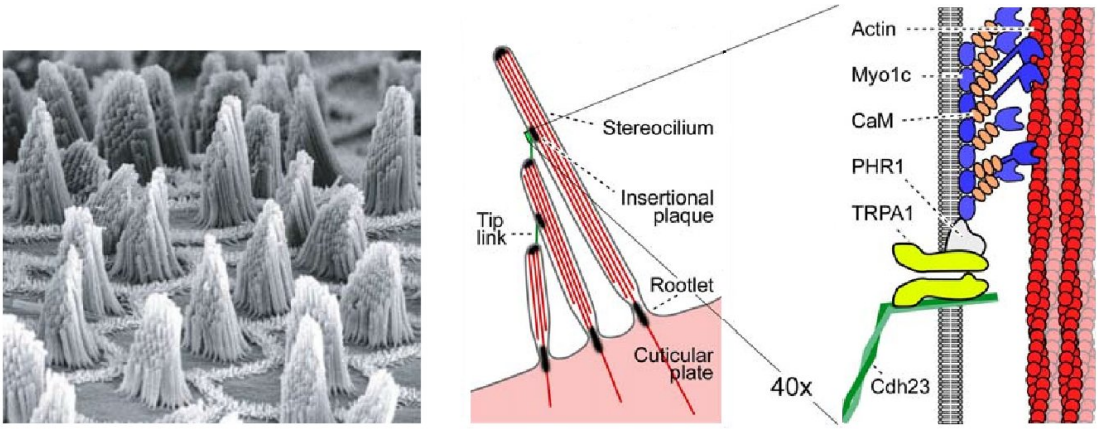

Abbildung 1.1: Links, rasterelektronenmikroskopische Aufnahme von Haarzellen und Stereozilien aus der Cochlea von *Gallus gallus*. Aufnahme aus Hudspeth 2008 [26]. Mitte und rechts, vergrößerte und schematisierte Darstellung des Aufbaus von Stereozilien und Tip-Links. Darstellung angepasst nach LeMasurier und Gillespie 2006 [30].

mechanische System eines kritischen Oszillators erklärt vier grundlegende Charakteristika des Innenohrs: aktive Verstärkung, Frequenzabstimmung, kompressive Nichtlinearität und spontane otoakustische Emissionen [26].

Ein kritischer Oszillator ist in der Lage, Energie in ein System einzuspeisen. Die durch aktive Verstärkung verrichtete Arbeit ist an Haarzellen von Fröschen direkt beobachtet worden. Für Reptilien, Vögel und Säugetiere existieren indirekte Nachweise etwa aus der Verletzung des Fluktuations-Dissipations-Theorems, was einen rein passiven Prozess ausschließt [26]. Als Folge der aktiven Verstärkung können Haarzellen elektrisch und mechanisch auf einzelne Frequenzbereiche abgestimmt werden. Damit kann eine deutlich höhere Frequenzselektivität erreicht werden als mit einem passiven harmonischen Oszillator, der in der Endolymphe zudem stark gedämpft ist.

Das Haarbündel besitzt die höchste Empfindlichkeit an seiner Eigenfrequenz. Je weiter die Anregung von dieser Frequenz entfernt liegt, umso stärker machen sich die passiven Eigenschaften des Bündels bemerkbar. Aktive und passive Eigenschaften skalieren unterschiedlich mit der Schallintensität, wobei die aktive Verstärkung langsamer mit der Intensität ansteigt als das für den passive Anteil der Fall ist. Bei hohen Schallintensitäten dominieren die passiven Eigenschaften, während umgekehrt bei geringen Intensitäten der aktive Prozess überwiegt. Die Frequenzselektivität ist demnach bei hohen Schallintensitäten am geringsten und wird mit abnehmender Schallintensität besser. Dieses Verhalten wird als kompressive Nichtlinearität bezeichnet [27].

Spontane Oszillationen des Haarbündels führen zur Emission reiner Töne aus dem Innenohr, otoakustische Emissionen genannt. Als Epiphänomen haben sie für den Hörprozess selbst keine Bedeutung.

1.1.2 Der zweite cochleäre Verstärker

Das archetypische Innenohr erster Landwirbeltiere war klein (~1 mm) und bestand wahrscheinlich aus nur wenigen hundert Haarzellen [31]. Erst durch die Ausbildung eines impedanzangepassten Mittelohres setzte eine Weiterentwicklung ein. Insbesondere konnten damit erstmals höhere Frequenzen verlustarm in das Innenohr eingekoppelt werden. Es entstand ein Selektionsdruck zur Leistungssteigerung des Innenohres. Der erste Schritt war dabei eine Verlängerung der Cochlea, um Platz für eine größere Anzahl Haarzellen zu schaffen [32]. Eine weitere Optimierung hin zu höheren Frequenzen, höherer Empfindlichkeit und besserer Frequenzauflösung war aber auf Ebene der einzelnen Haarzelle nur begrenzt möglich, etwa durch mikromechanische Differenzierung zusätzlich zur elektrophysiologischen Frequenzabstimmung.

Bei Säugetieren [8] und deutlich schwächer ausgeprägt bei Vögeln [25] bilden die makroskopischen Strukturen des Innenohres selbst ein schwingfähiges System. Die Antwort des Systems auf eine einfallende Schallwelle wird nicht mehr nur durch die einzelnen Haarzellen definiert, sondern zusätzlich durch die mechanischen Eigenschaften des Innenohres als Ganzes. Die weitere Beschreibung soll sich hier auf das Säugetierohr beschränken.

Einfallende Schallwellen werden vom Mittelohr auf die *Scala vestibuli* übertragen. Am hinteren Ende der Cochlea ist diese über das *Helicotrema* mit der darunter liegenden *Scala tympani* verbunden, deren Flüssigkeitssäule durch das bewegliche runde Fenster verschiebbar ist. Aufgrund der Inkompressibilität der Flüssigkeit bildet sich ein Volumenstrom mit entsprechendem Druckgefälle aus. Der Druckgradient zwischen *Scala vestibuli* und *Scala tympani* führt zu einer Auslenkung der mittig liegenden Basilarmembran innerhalb der *Scala media*. Druckunterschied und damit Kraft sind basal am größten. Diese Störung breitet sich als Wanderwelle längs der Basilarmembran aus. Eine einfallende longitudinale Schallwelle wird so in eine transversale Scherwelle umgewandelt [16] [44].

Das Schwingverhalten innerhalb der Cochlea wird nun wesentlich durch die elastischen Merkmale der Basilarmembran geprägt, wobei diese räumlich nicht konstant sind. So ändert sich längs der Basilarmembran sowohl die schwingfähige Masse als auch deren Elastizitätsmodul. Das hat zur Folge, dass die Resonanzbedingung für hohe Frequenzen am vorderen Ende und für tiefe Frequenzen am hinteren Ende der Cochlea erfüllt wird und eine räumliche Zerlegung nach Frequenzen stattfindet [7] [8] [44].

Die passiven Eigenschaften der Basilarmembran alleine genügen allerdings nicht, um die hohe Leistungsfähigkeit des Säugetierohres zu erreichen. Zudem können die experimentell gemessenen Werte für die Masseverteilung und die Steifigkeiten den großen hörbaren Frequenzbereich nicht ausreichend erklären [27] [39]. Ausgehend von dem vom Menschen hörbaren Frequenzumfang, der in etwa einem Faktor 1000 entspricht, wäre ein Quotient von Steifigkeit und Masse notwendig, der sich über sechs Größenordnungen erstrecken müsste, da die Resonanzfrequenz nur mit der Wurzel des Quotienten skaliert.

Schon früh wurde deshalb ein zusätzlicher aktiver Prozess postuliert [24]. Dieser konnte aber erst über dreißig Jahre später in Form der Elektromotilität der äußeren Haarzellen identifiziert werden [6]. Diese spezialisierten Haarzellen erfüllen keine Aufgabe der Signaltransduktion

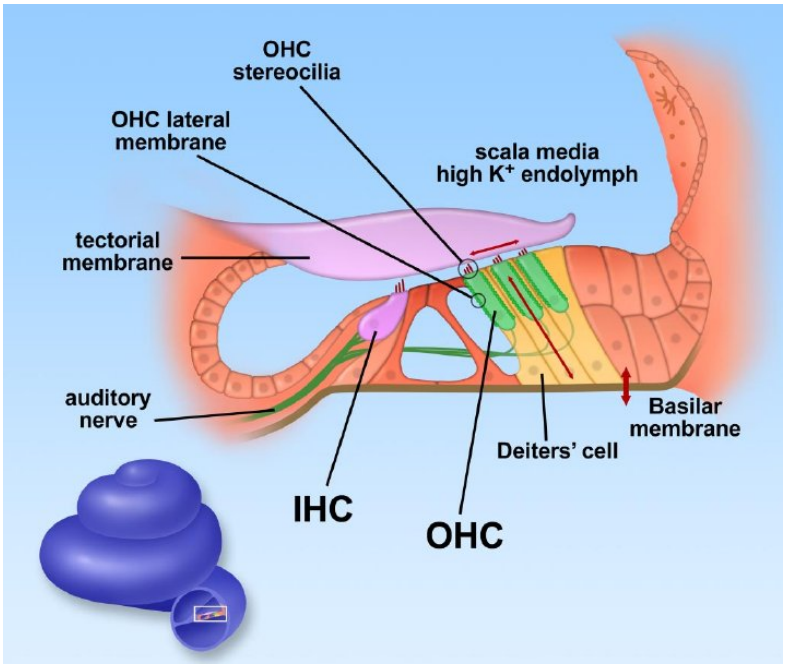

Abbildung 1.2: Querschnitt durch das Corti-Organ und dessen Lage innerhalb der Cochlea. Darstellung nach Ashmore 2008 [4]. OHC (äußere Haarzelle), IHC (innere Haarzelle).

mehr, sondern modulieren die mechanischen Eigenschaften der Basilarmembran, indem sie ihre Länge aktiv unter dem Einfluss der Wanderwelle ändern. Durch diese schallinduzierten Längenänderungen kann der Wanderwelle Energie zugeführt oder entzogen werden. Sie wirken also sowohl verstärkend als auch dämpfend. Das erhöht nicht nur insgesamt die Sensitivität, sondern führt zu schärfer ausgebildeten Maxima der Wanderwelle und verbessert so die Frequenzauflösung [27]. Die mathematische Beschreibung dieses Mechanismus ist Gegenstand aktueller Forschung und wird kontrovers diskutiert. Auch die Interaktion zwischen dem stereoziliären Verstärker einerseits und dem membranbasierten Verstärker andererseits ist noch weitgehend unklar [3].

Phänomenologisch sind die Eigenschaften der äußeren Haarzellen dagegen gut beschrieben. So verkürzt eine einzelne Zelle ihre Länge um bis zu 5% und erzeugt dabei Kräfte in der Größenordnung von 6 nN [28]. Ihre Länge ist spannungsabhängig und kann über das Zellmembranpotential gesteuert werden. Im Bereich hyperpolarisierter Membranpotentiale ist die Zelle elongiert, im depolarisierten Bereich dagegen verkürzt [6]. Physiologisch wird das Membranpotential über die intrazellulären Kaliumkonzentration reguliert. Kaliumeinstrom durch die Tip-Link-Kanäle depolarisiert und verkürzt die Zelle, was eine Ankopplung an des Schallfeld bewirkt. Kaliumausstrom über laterale KCNQ4-Kanäle repolarisiert und verlängert die Zelle [49]. Aufgrund der spannungsabhängigen Bewegung wurde der Begriff der Elektromotilität geprägt.

1.2 Das Motorprotein Prestin

Verursacht werden die Längenänderungen der äußeren Haarzellen durch Konformationsänderungen des Motorproteins Prestin, dass sich fundamental von den bekannteren Motorproteinen Myosin, Kinesin, Dynein unterscheidet. Während letztgenannte ATP-Hydrolyse als Energiequelle heranziehen, hängt der Zustand des Prestinmoleküls allein von der über der Zellmembran abfallenden elektrischen Potentialdifferenz ab. Es wandelt Spannungsdifferenzen in Kräfte um und bezieht seine Energie direkt aus dem elektrischen Feld [12][1].

Erst im Jahr 2000 gelang es Prestin zu klonieren. Unter der Annahme, dass das gesuchte Molekül in den äußeren, nicht aber in den nicht-motilen inneren Haarzellen vorkommt, konnten durch subtraktive Hybridisierung elf potentielle cDNA-Sequenzen isoliert werden. Anschließende Subklonierung und Expression in tsA201-Zellen ergab daraufhin eine Sequenz, mit der die Eigenschaften der äußeren Haarzellen in Kulturzellen reproduziert werden konnten, insbesondere konnten elektrisch induzierte Längenänderungen an den transfizierten Zellen nachgewiesen werden [55].

Prestin ist ein Membranprotein bestehend aus einer Sequenz von 744 Aminosäuren mit einem stark hydrophoben Kern von etwa 400 Aminosäuren [55]. Sowohl der relativ kurze N-Terminus als auch der ausgedehnte C-Terminus sind intrazellulär angelegt. Computerbasierte Verhersagen über die Zahl der Transmembrandomänen sind uneinheitlich und variieren zwischen 10 und 12. Aus diversen Experimenten gibt es Anhaltspunkte über die Lage einzelner Aminosäuren, sie ergeben aber noch kein vollständiges Bild der Transmembrantopologie [11]. Insgesamt favorisieren neuere Erkenntnisse das 12-Transmembrandomänen-Modell [14] [41] teilweise mit zwei Halbschleifen, die die Zellmembran nicht vollständig durchqueren [13].

Prestin wird in der basolateralen Membran von äußeren Haarzellen in hohen Konzentrationen akkumuliert. Die Verteilung ist ungleichmäßig und konzentriert sich auf cholesterinreiche Mikrodomänen [51]. Vermutet wird, dass es dort supramolekulare Motorkomplexe bildet [1], durch Oligomerisierung mit weiteren Prestinen und/oder durch geeignete Kopplung an andere Proteine oder Peptide [40]. Elektronenmikroskopische und rasterkraftmikroskopische Aufnahmen konnten einzelne 11 nm messende Partikel in der Membran von äußeren Haarzellen identifizieren [35].

Zur Quartärstruktur des Prestins selbst existieren widersprüchliche Angaben. Die Bildung von Homomultimeren ist unstrittig und wird durch biochemische Untersuchungen ebenso wie durch die Beobachtung von Förster-Resonanzenergietransfer (FRET) bestätigt [40]. Verkürzen der Aminosäurensequenz am N-Terminus um mehr als 20 Aminosäuren verhindert die Oligomerisierung und führt zum Funktionsverlust [40]. Über die Zahl der Untereinheiten herrscht dagegen keine Klarheit. Sie wird mit zwei [40] oder vier angegeben [54].

[1] Nach korrekter Terminologie wäre es damit kein Motor sondern ein piezoelektrischer Aktuator [4]. Es ist in der Literatur aber allgemein üblich, Prestin als Motorprotein zu bezeichnen.

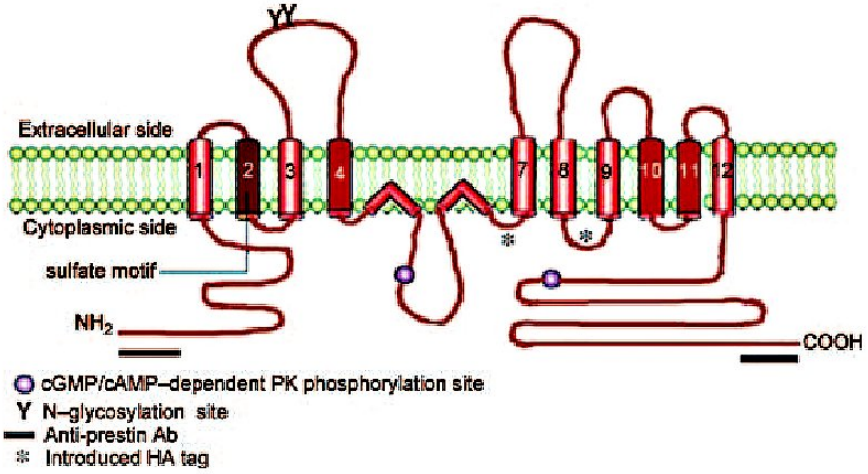

Abbildung 1.3: Vorgeschlagene Transmembrantopologie des Säugetierprestins. Darstellung aus Deák *et al.* 2005 [13].

1.2.1 Nichtlineare Kapazität

Neben der Fähigkeit zur Elektromotilität ist die nichtlineare Membrankapazität ein weiteres charakteristisches Merkmal von äußeren Haarzellen. Während der Versuchsdurchführung von elektrophysiologischen Patch-Clamp-Messungen wird die Membrankapazität der Zelle in der Regel elektronisch kompensiert. Für äußere Haarzellen gelingt dies nicht mehr vollständig über den gesamten Spannungsbereich. Trotz Kompensierung ergeben sich bei Spannungssprüngen deutliche kapazitive Ströme. Zurückgeführt werden sie auf Ladungsverschiebungen innerhalb der Zellmembran, die sich bei Spannungsänderungen als transiente Ströme zeigen [4].

Die mathematische Beschreibung geht hier fast immer von einem Zwei-Zustands-Systems aus, das heißt die Ladungen werden instantan zwischen zwei diskreten Zuständen verschoben. Die Besetzung der beiden Zustände ergibt sich dann aus der Boltzmannstatistik als Wahrscheinlichkeitsverteilung. Experimentell direkt zugänglich ist hier nicht die zahlenmäßige Besetzung der Zustände selbst sondern ihre Änderungsrate, die als spannungsabhängige Kapazität gemessen werden kann:

$$C(V) = \frac{\beta Q_{max} \, \mathrm{e}^{-\beta(V-V_{1/2})}}{\left(1+\mathrm{e}^{-\beta(V-V_{1/2})}\right)^2} + C_{lin} \tag{1.1}$$

mit

$$\beta = z\frac{e_0\delta}{k_B T} \tag{1.2}$$

Dabei ist Q_{max} die Ladungsmenge, die insgesamt bewegt werden kann, wenn alle aktiven Moleküle in den jeweils anderen Zustand übergehen. $V_{1/2}$ ist das Membranpotential, das zu einer

gleichmäßigen Verteilung der Moleküle auf die beiden Zustände führt und als unmittelbare Konsequenz, die Spannung bei der die Kapazität maximal ist; z beschreibt die Anzahl Elementarladungen e_0, die pro Molekül einen Bruchteil δ durch das Membrandielektrikum bewegt werden; k_B ist die Boltzmannkonstante und T die Temperatur in Kelvin [38]; C_{lin} ist die passive Membrankapazität und kann über begrenzte Spannungsbereiche mit ausreichender Genauigkeit als konstant angenommen werden [4] [18].

Die Spannung $V_{1/2}$ beträgt bei äußeren Haarzellen etwa -50 mV und liegt damit nahe am Ruhemembranpotential dieser Zellen. $V_{1/2}$ fixiert die Lage des Energieprofils des Zwei-Zustands-Systems relativ zur Membranspannung. Es ist daher nicht verwunderlich, dass $V_{1/2}$ durch eine Vielzahl innerer und äußerer Faktoren beeinflußt werden kann. Dazu zählen unter anderem die ionischen Bedingungen, die Temperatur, Membransteifigkeit und mechanische Spannung, Arzneimittel, der Phosphorylierungzustand des Prestins und schließlich Mutationen in dessen Aminosäurensequenz [4] [11] [47].

Der Steigungskoeffizient β ist deutlich weniger variabel und liegt bei etwa $0{,}03\,\mathrm{mV}^{-1}$. Er beinhaltet als Parameter die Ladungsmenge pro funktionaler Einheit und den Weg, den diese quer zur Membran verschoben wird. Genauer, welcher Bruchteil der über der Membran abfallenden Potentialdifferenz von der Ladung gesehen wird.

1.2.2 Nicht-Säugetier-Prestine

Von erheblichem wissenschaftlichem Interesse sind Prestin-Orthologe. Zum einen aus Sicht der phylogenetischen Entwicklung des Hörens, vor allem aber für das Verständnis der molekularen Grundlagen der Elektromotilität selbst. Hierfür sind die Prestine von Nicht-Säugetier-Spezies besonders geeignet, da sich ihre Eigenschaften deutlich vom Säugetierprestin unterscheiden. Gut untersucht sind sie von den beiden Modellorganismen Zebrafisch (*Danio rerio*) und Haushuhn (*Gallus gallus domesticus*). Beide sind elektrogene Chlorid/Sulfat-Antiporter mit 1:1 Austauschstöchiometrie [48], zeigen aber auch nichtlineare Kapazität; Elektromotilität konnte dagegen nicht nachgewiesen werden [52]. Verglichen mit dem Säugetierprestin ist die Kapazitäts-Spannungs-Kurve zu positiven Membranpotentialen hin verschoben und die Kinetik der Ladungsverschiebung auffallend langsamer [1]. Der Steigungsparameter β ist nur etwa ein drittel [52] bis halb so groß [1], was darauf hindeutet, dass die mit der Konformationsänderung verbundene Ladungsbewegung insgesamt geringer ausfällt.

1.2.3 Die SLC26-Transporterfamilie

Prestins Primärstruktur weist darauf hin, dass es zu einer Familie von Anionentransportern gehört. In dieser SLC26 (Solute Carrier 26) genannten Gruppe wird es als Mitglied A5 eingeordnet (SLC26A5). Die Aminosäurensequenz der SLC26-Familie ist gekennzeichnet durch ein Sulfat-Transportermotiv innerhalb des hydrophoben Kerns sowie der STAS-Domäne am C-Terminus. Die Familie umfasst bisher zehn Mitglieder bei Wirbeltieren, Homologe finden sich aber selbst bei weit entfernten Organismen wie Planzen, Hefen und Bakterien [4] auch wenn diese sich in

der Regel keinem einzelnen SLC26-Mitglied mehr zuordnen lassen. Die SLC26-Familie kann als Teil einer weit größeren Gruppe, der Sulfat-Permeasen (SulP) aufgefasst werden [36].

SLC26-Proteine transportieren eine ungewöhnliche Vielfalt an mono- und divalenten Anionen, SO_4^{2-}, Cl^-, I^-, HCO_3^-, OH^-, Formiat und Oxalat, oft in einem thermodynamisch gekoppelten Austausch. Die Austauschstöchiometrie kann innerhalb der Familie variieren [36]. Aber auch Ionenkanaleigenschaften sind für einzelne SLC26-Mitglieder wie SLC26A7 und SLC26A9 dokumentiert [15] [29]. Kürzlich (2011) gelang es Ohana *et al.* ungekoppelte NO_3^-- und SCN^--Transporte auch an SLC26A3 und SLC26A6 nachzuweisen.

Für das Motorprotein Prestin demonstrierten Bai *et al.* 2009 eine schwach ausgeprägte Aufnahme von radioaktivem Oxalat und Formiat in Zellen, die Säugetierprestin exprimieren [5]. Mit einer verbesserten Nachweismethode konnten Tan *et al.* später dagegen keinen signifikanten Unterschied zwischen prestin-exprimierenden Zellen und der Negativkontrolle feststellen [52].

Das Säugetierprestin ist damit das einzige SLC26-Protein, für das bisher ein Ionentransport noch nicht zweifelsfrei nachgewiesen werden konnte.

1.2.4 Mechanistische Modelle der Elektromotilität

Die Eigenschaft der Elektromotilität erfordert spannungsabhängige Konformationsänderungen von erheblichem Ausmaß. Die Zugehörigkeit des Prestins zur SLC26-Familie und die Antiporter-Eigenschaften der Nicht-Säugetier-Prestine legen die Vermutung nahe, dass diese sich evolutionär aus einem Transportzyklus entwickelt hat [48]. Ein wissenschaftlicher Konsens über die Ursache der Elektromotilität und der damit verbundenen nichtlinearen Membrankapazität besteht aber nicht. Verschiedene Modelle sind vorgeschlagen worden:

Unvollständiger Transportzyklus

Das älteste und zugleich einfachste Modell geht von einem unvollständigen Ionentransport aus [11]. Intrazelluläre Anionen wie Chlorid oder Bicarbonat binden dabei an einer vom Prestin gebildeten cytoplasmischen Pore und wandern unter dem Einfluss der Membranspannung durch diese Pore, wobei sie Konformationsänderungen des Proteins auslösen, die sich als spannungsabhängige Längenänderungen manifestieren. Das Modell führt ungezwungen auf ein Zwei-Zustands-System und erklärt das Fehlen eines offensichtlichen, intrinsischen Spannungssensors durch Anionen als externe Spannunsgsensoren. Damit war es in der Lage, die damalig bekannten Daten richtig zu erklären.

Es zeigte sich aber bald, dass dieses einfache Modell nicht konsistent mit neueren Beobachtungen war. Unter anderem kann der unvollständigen Transportprozess schlecht erklären, warum sich der Steigungsfaktor β nur geringfügig ändert, wenn das monovalente Cl^- durch das divalente SO_4^{2-} innerhalb des intrazellulären Mediums ersetzt wird. Nach Gleichung (1.2) ist β aber direkt proportional zur Valenz der verschobenen Ladung. Dieses Modell muss dafür annehmen, dass sich gleichzeitig der vom Spannungssensor zurückgelegte Weg δ verkürzt, was aus verschiedenen Gründen für wenig plausibel gehalten wird [45].

Allosterische Modulation

Um die Inkonsistenzen des einfachen Bildes eines unvollständigen Transporters zu beheben, wurde daraufhin das Modell der allosterischen Modulation entwickelt. Externe Anionen binden hier weiterhin an einer cytoplasmischen Bindungsstelle, werden aber nicht mehr selbst durch die Membran verschoben, sondern stoßen allosterisch eine Modifikation des Proteins an, die die Verschiebung einer intrinsischen Raumladung und damit eine Konformationsänderung auslöst [46]. So lassen sich einige experimentelle Beobachtungen deutlich besser erklären, wie zum Beispiel die geringe Variabilität des Steigungsfaktors β [38].

Anionen-Antiporter

Aufgrund theoretischer Überlegungen und Simulationen wurde von Muallem und Ashmore 2006 ein Modell basierend auf einem Chlorid/Sulfat-Austausch vorgeschlagen. Die Konformationsänderungen werden dabei einzelnen Übergängen des Zustandsdiagramms zugeschrieben. Attraktiv ist dieses Modell, da es gerade den für Nicht-Säugetier-Prestine gut dokumentierten Chlorid/Sulfat-Austausch heranzieht. Die Formulierung des Antiportermodells ist aber nicht auf Sulfat als solches festgelegt, sondern nimmt nur an, dass für jedes transportierte Chloridion zwei negative Elementarladungen in die Gegenrichtung bewegt werden. Die Formulierung ist in allgemeiner Form gültig für Austauschprozesse der Art Cl^-/A^{2-} oder $Cl^-/2A^-$ mit beliebigen Anionen A [38].

2 Ergebnisse

2.1 Publikationsliste

Diese Arbeit enthält folgende Originalpublikationen:

Conserved dimeric subunit stoichiometry of SLC26 multifunctional anion exchangers
Detro-Dassen S, Schänzler M, Lauks H, Martin I, zu Berstenhorst SM, Nothmann D, Torres-Salazar D, Hidalgo P, Schmalzing G, Fahlke C. *J Biol Chem.* 2008 Feb 15;283(7):4177–88.

Vom Verfasser wurde der elektrophysiologische Anteil bearbeitet. Gleichberechtigter Erstautor.

Anion transport by the cochlear motor protein prestin
Schänzler M, Fahlke C. *J Physiol.* 2012 Jan 15;590(Pt 2):259–72.

2.2 Unveröffentlichte Ergebnisse

SCN^--Ströme können durch Salicylat nicht unterdrückt werden

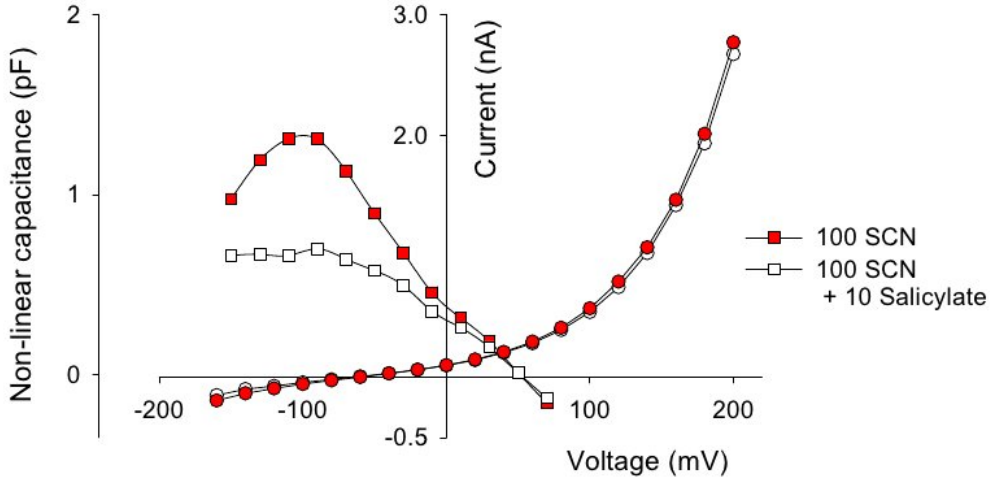

Abbildung 2.1: Repräsentative SCN^--Ströme (○) und nichtlineare Kapazitäten (□) einer HEK293T-Zelle, die transient SLC26A5(RAT)/Prestin exprimiert, vor und nach der Perfusion mit einer externen Lösung, die zusätzlich 10 mM Salicylat enthielt. Sonstige experimentelle Bedingungen wie beschrieben (Schänzler & Fahlke 2012).

Salicylat ist ein bekannter, reversibler Blocker der Elektromotilität äußerer Haarzellen. Die Überdosierung von Acetylsalicylsäure führt zu einer temporären Beeinträchtigung des Hörvermögens [50]. Elektrophysiologisch messbar ist die Hemmung der nichtlinearen Kapazität. Beim Zebrafischprestin reduziert es darüber hinaus den Chlorid/Sulfat-Transport konzentrationsabhängig um bis zu 95% [48].

Auch unter ionischen Bedingungen unter denen SCN^- einen großen Anteil der externen Lösung ausmacht, führt die Zugabe von Salicylat zu einer erheblichen Verringerung der nichtlinearen Kapazität. Der Kurvenverlauf weist keine wesentlichen Unterschiede zu Lösungen ohne SCN^- auf [14]. Es kann davon ausgegangen werden, dass Salicylat auch in Anwesenheit von SCN^- die Motoreigenschaften des Prestins hemmt. Demgegenüber hat die Zugabe von Salicylat praktisch keine Auswirkung auf den SCN^--Strom (Abb. 2.1). Er nimmt bei einer Membranspannung von 200 mV um nur $\Delta I = (60 \pm 59)$ pA ab (n=6).

3 Diskussion

Das Säugetierprestin nimmt innerhalb der SLC26-Familie eine Sonderstellung ein. So scheint es jegliche Transportaktivität verloren zu haben, selbst Nicht-Säugetier-Prestine sind ausgeprägte Chlorid/Sulfat-Antiporter. Dafür hat es die Fähigkeit zur Elektromotilität hinzugewonnen, die wiederum bei keinem anderen SLC26-Mitglied zu finden ist. Vergleichende Untersuchungen zwischen dem Säugetierprestin und anderen SLC26 mit Hilfe elektrophysiologischer Methoden werden dadurch erheblich erschwert.

Die Frage nach einer Transportaktivität stellt sich auch aus theoretischer Sicht. Bisher ist es nicht gelungen, ein mit wesentlichen experimentellen Beobachtungen konsistentes Modell von nichtlinearer Kapazität und Elektromotilität zu entwickeln. Alle vorgeschlagenen nichttransportierenden Modelle scheitern daran, die Abhängigkeit der verschiebbaren Ladungsmenge Q_{max} von der intrazellulären Chloridkonzentration zu erklären. Durch genügend stark hyperpolarisierte Membranspannungen oder umgekehrt durch ausreichend hohe Membranspannungen lassen sich nach diesen Modellen alle Prestinmoleküle in jeweils den elongierten oder verkürzten Zustand zwingen. Anders ausgedrückt, es lassen sich immer Spannungen finden, bei denen ein Zustand vollständig besetzt, der andere dagegen entleert ist. Solange die Anzahl der Chloridionen größer als die Zahl der Prestinmoleküle ist – was unter realistischen Bedingungen immer der Fall ist – wäre die maximal verschiebbare Ladungsmenge Q_{max} eine Konstante, entgegen der experimentell bestens bestätigten Abhängigkeit von der internen Chloridkonzentration [38] [46].

Das Antiportermodell von Muallem und Ashmore [38] ist zwar in der Lage alle wesentlichen experimentellen Befunde zumindest qualitativ richtig vorherzusagen, muss dafür aber einen elektrogenen Austauschprozess postulieren, für den es keinerlei experimentelle Bestätigung gibt. Ashmore äußerte die Vermutung, dass es gelingen könnte, die Ratenkonstanten des Antiportermodells zu optimieren und an die experimentellen Befunde anzupassen [4]. Die Chlorid/Sulfat-Leitfähigkeit müsste dafür sehr klein werden und wäre so vor dem Hintergrund endogener Ströme nicht detektierbar.

3.1 Elektrogener Transport

Die vorliegende Arbeit stützt das Antiportermodell durch den erstmaligen Nachweis eines elektrogenen Transportprozesses beim Säugetierprestin. Dieser konnte durch extrazelluläres Sulfat gehemmt werden (Abb. 4.13) und bietet damit einen Anhaltspunkt für eine externe Sulfat-Bindungstelle.

Ein Transportstrom war nur für das nicht-physiologische Thiocyanatanion SCN^- nachweisbar. Selbst für dieses waren die makroskopischen Leitfähigkeiten klein und es erforderte hohe Membranspannungen bis 200 mV, um Ströme deutlich oberhalb 1 nA zu erreichen. Mit hoher Sicherheit kann deshalb eine physiologische Rolle dieses konkreten Transports ausgeschlossen werden.

Trotz der insgesamt nur geringen Stromamplituden konnten die vom Prestin vermittelten Ströme sicher von endogenen Leitfähigkeiten unterschieden werden, indem der gemessene Strom mit dem Expressionsniveau korreliert wurde. Als Maß für die Expression wurden die nichtlineare Kapazität und die Zellfluoreszenz herangezogen. Die nichtlineare Kapazität ist besonders geeignet, da sie direkt proportional zu der Anzahl der funktionalen, in der Zellmembran eingebauten Prestine ist. Um potentielle Messartefakte durch die Überlagerung von hohen Stromamplituden und der nichtlinearen Kapazität zu vermeiden, wurden dieses Korrelationsverfahren nur für auswärtsgerichtete Ströme angewandt. Für einwärtsgerichtete Ströme wurde die Stärke der Zellfluoreszenz als Korrelationsgröße herangezogen.

In beiden Fällen gab es einen linearen Zusammenhang zwischen Expressionsniveau und Strom (Abb. 4.9, Abb. 4.12). Die Ergebnisse stellen zunächst lediglich eine Korrelation zwischen der Anzahl der Prestinmoleküle und dem SCN^--Strom her, begründen aber noch keine Ursache-Wirkungs-Beziehung. Allerdings konnte die Linearität über eine weiten Expressionsbereich nachgewiesen werden, ohne dass Anzeichen von Schwellwerten oder Sättigungen an den Enden des Messbereichs zu beobachten waren. Andere Erklärungsmuster, wie zum Beispiel eine durch das Prestin ausgelöste verstärkte Expression von endogenen Kanälen, würden kaum zu der beobachteten strengen Linearität führen. Es ist angebracht, den Strom auch ursächlich direkt dem Prestin zuzuschreiben.

Das SCN^--Anion ist eines der am schwächsten hydratisierten Ionen [34]. Möglicherweise ist das unphysiologische SCN^--Anion aufgrund der kaum vorhandenen Hydrationshülle eher in der Lage, die Selektivitätsfilter von Transportern oder Kanälen zu überwinden. Jedenfalls ist für viele Ionenkanäle eine hohe SCN^--Leitfähigkeit gut dokumentiert [17]. Stöchiometrisch streng gekoppelte Transporte werden oft entkoppelt [41] und in einen 'Channel-like slippage mode' geschaltet [2]. Auch in diesem Fall war der SCN^--Strom nicht thermodynamisch an einen etwaigen Chloridaustausch gebunden. Die gemessenen Umkehrpotentiale stimmen mit den berechneten Nernst-Potentialen des Thiocyanats überein (Abb. 4.13). Das SCN^--Anion nimmt demnach nicht die Rolle des Austauschpartners des Chlorids im Antiportermodell von Muallem und Ashmore ein.

Auch beim Zebrafischprestin kann ein Kotransport von SCN^- und Cl^- ausgeschlossen werden. Die Verschiebung des Umkehrpotential in Anwesenheit von Sulfat läßt darauf schließen, dass die Entkopplung des Transports unter diesen ionischen Bedingungen jedoch nicht vollständig erfolgt und ein Teil der Proteine weiterhin in einem Antiportermodus verbleibt (Abb. 4.13). Noch deutlicher wird es durch neuere Messungen belegt, die zeigen, dass der Chlorid/Sulfat-Austausch des Zebrafischprestins konzentrationsabhängig durch SCN^- und NO_3^- entkoppelt werden kann (Farshid Yazdan Shenas, persönliche Mitteilung).

Dieses Verhalten wird auch für das Säugetierprestin vorgeschlagen, mit dem Unterschied, dass die Entkopplung der nichtlinearen Ladungsverschiebung sehr viel schwächer ist, der SCN^--Strom also erheblich kleiner ausfällt. Die Spannungsabhängigkeit der nichtlinearen Kapazität wurde durch SCN^- nur unwesentlich geändert, insbesondere konnte keine Abnahme der verschobenen Ladungsmenge Q_{max} festgestellt werden (Tabelle 4.1). Angesichts des Verhaltens des Zebrafischprestins und bekannter Beobachtungen, dass gekoppelter und ungekoppelter Transport bei SLC26A3 und SLC26A6 durch die gleiche Pore erfolgt [41], erscheint die Annahme gerechtfertigt, dass auch SCN^--Strom und nichtlineare Ladungsverschiebung teilweise durch den gleichen Mechanismus vermittelt werden.

Eine Reihe von Beobachtungen sprechen dafür, dass der Thiocyanatstrom nicht auf Konformationsänderungen des transportierenden Proteins angewiesen ist, sondern über Diffusion durch eine Pore erfolgt: Bisher ist noch kein Uniporter-Transportmodus für ein SLC26-Protein beschrieben worden. Ein Uniport bedarf der elektroneutralen Reorientierung des unbeladenen Transporters. Dieser Schritt mit spannungsunabhängiger Ratenkonstante limitiert den maximal möglichen Strom. Für hohe Membranspannungen würde man einen Sättigungsverlauf der Strom-Spannungskennlinie erwarten. Dies konnte aber nicht beobachtet werden. Gerade beim Zebrafischprestin konnten sehr hohe Ströme gemessen werden (Abb. 4.11). Von diesem ist aber eine langsame Kinetik der nichtlineare Ladungsverschiebung dokumentiert [1].

Den wohl stärksten Hinweis liefern Perfusionsexperimente mit Salicylat. Salicylat blockiert sowohl die Konformationsänderungen des Säugetierprestins, als auch den Ionenaustausch des Zebrafischprestins. Ein Einfluss auf den ungekoppelten SCN^--Strom ließ sich aber nicht nachweisen (Abb. 2.1). Für das Zebrafischprestin ist es später gelungen, eine Mutante zu finden, deren Chlorid/Sulfat-Transport um etwa 70% reduziert war, bei gleichzeitig vom Wildtyp ununterscheidbarem SCN^--Strom (Farshid Yazdan Shenas, persönliche Mitteilung, Mutation G327C).

Die Beobachtungen zum elektrogenen SCN^--Transport sind konsistent mit einem möglichen Antiportermodell für das Säugetierprestin. Der die nichtlineare Kapazität generierende Austauschprozess des Chlorids und eines unbekannten Anions wird durch das Thiocyanat entkoppelt. Die Entkopplung ist ausreichend, um als Strom registriert zu werden, aber zu schwach, um die nichtlineare Ladungsverschiebung wesentlich zu beeinflussen. Der Transport des Thiocyanats erfolgt in einem kanalartigen 'Slippage Mode', wie er für den Anionen/Protonen-Austauscher ClC4 beschrieben wurde [2].

3.2 Kooperativität zwischen Untereinheiten

Die Spannungsabhängigkeit der nichtlinearen Kapazität kann durch Punktmutationen über weite Bereiche verschoben werden, besonders ausgeprägt durch die Mutationen D154N und D342Q [11]. Das Kapazitätsmaximum der Mutante D154N liegt bei -145 mV, während es für D342Q bei +15 mV liegt. Die Koexpression dieser zwei Prestinmutanten in einer Zelle führte nicht zu einer einfachen additiven Überlagerung, wie man es von unabhängigen Einzelmolekülen erwarten würde, sondern ergab intermediäre elektrische Eigenschaften. Die gemessene, spannungsabhän-

gige Kapazität zeigte ein einzelnes Maximum an einer Position mittig zwischen den Werten der jeweiligen Mutanten (Abb. 4.8). Erklärt werden kann dieses Verhalten mit dem Bilden von Heterodimeren, deren Merkmale gleichermaßen von beiden Proteinmutanten geprägt werden. Die nichtlineare Ladungsverschiebung ergibt sich dann als Summe von drei Komponenten, den zwei Homodimeren D154N-D154N, D342Q-D342Q und dem Heterodimer D154N-D342Q. Wobei die relative Aufteilung zwischen Homodimeren und Heterodimeren nach der Bernoulliverteilung erfolgt und damit die Bildung von Heterodimeren bevorzugt, was zu dem beobachteten nichtlinearen Kapazitätsverlauf mit nur einem Maximum führt (Abb. 4.8).

Dies schließt Monomere als funktionale Einheiten aus, im Einklang mit früheren Ergebnissen aus FRET-Messungen, dass die N-terminal vermittelte Verbindung zweier Untereinheiten Voraussetzung für nichtlineare Ladungsverschiebungen ist [40]. Eine eindeutige Aussage über den Oligomerisierungszustand des Prestins läßt sich allerdings nicht ableiten, da nicht zwangsläufig davon ausgegangen werden kann, dass die Untereinheiten aus lediglich einem Prestinmolekül bestehen. Die Beobachtung wäre auch verträglich mit einem Prestintetramer, aufgebaut aus zwei dimerisierten Motoreinheiten.

Unzweifelhaft muss dagegen eine Interaktion zwischen den Untereinheiten stattfinden. Zwei verschiedene Formen der Kooperativität sind denkbar. Beide Untereinheiten können Teile einer größeren Funktionseinheit darstellen und erst gemeinsam in der Lage sein, ihre Aufgabe wahrzunehmen. Oder jede Einheit bildet für sich einen funktionsfähigen Komplex, wird aber durch die Oligomerisierung allosterisch in ihrem Verhalten modifiziert. Für die Konformations- bzw. Längenänderungen eines Motorproteins können die Übergänge zwischen beiden Modellvorstellung fließend sein und ohne Detailkenntnisse über die Struktur und Arbeitsweise des molekularen Motors dürfte es schwer sein, sie zu unterscheiden.

Anders sieht es für den Ionentransport aus, hier besteht eine klare Abgrenzung zwischen zwei wohldefinierten Zuständen. Entweder wird von beiden Proteinen eine gemeinsame Pore geformt oder jedes Einzelmolekül bildet eine eigene Pore aus, deren Eigenschaften sich gegenseitig allosterisch beeinflussen. Im Rahmen dieser Arbeit konnte das nicht mehr untersucht werden. Möglicherweise bildet die G327C-Mutation des Zebrafischprestins einen Ansatzpunkt, um diese Frage zu klären.

3.3 Ausblick

Anhand einer ersten, allerdings nur grob aufgelösten, Kristallstrukturanalyse eines bakteriellen SLC26-Proteins vermuten Compton *et al.*, dass große Rotationsbewegungen der STAS-Domänen von SLC26-Dimeren den Transportvorgängen zugrundeliegen oder sie begleiten [9]. Durch Interaktion des 'Cystic Fibrosis Transmembrane Conductance Regulators' (CFTR) mit der STAS-Domäne kann das Verhalten von SLC26-Transportern reguliert werden [20].

Nach den Ergebnissen dieser Arbeit ist es äußerst unwahrscheinlich, dass der ungekoppelte Thiocyanatstrom ebenfalls solche Konformationsänderungen hervorruft. Vielmehr ist davon auszugehen, dass er kanalartig erfolgt und in Teilen unabhängig vom gekoppelten Transport und

der nichtlinearen Ladungsverschiebung abläuft. Vorstellbar ist, dass der Kanaltransport eine Fähigkeit des Einzelmoleküls an sich darstellt – jedes Molekül also eine Pore ausbildet – während der gekoppelte Transport den Zusammenschluss zu Dimeren voraussetzt und durch koordinierte Bewegungen der STAS-Domänen reguliert wird. Ohana *et al.* entwickelten computerbasiert eine räumliche Struktur von SLC26A6 in Anlehnung an ClC-ec1. Wie dieses wurde es als Dimer modelliert. Beide Untereinheiten besitzen jeweils eine Pore. Es gelang ihnen eine Aminosäure (E357) zu identifizieren, die Teil dieser Pore sein muss und maßgeblich das Verhalten des Transportprozesses beeinflusst [41].

Die Effekt des Salicylats könnte nun darin bestehen, spezifisch die Bewegung oder Funktion der STAS-Domäne zu unterbinden. Die ungekoppelte Diffusionen durch die beiden Poren wäre für Ionen, die energetisch dazu in der Lage sind, weiterhin möglich. Dass Salicylat die Bewegung des C-Terminus des Prestins stört, ist mit Hilfe von FRET-Messungen bestätigt [23]. Es konnte damit allerdings nicht zwischen Ursache und Wirkung unterschieden werden.

Die weitergehende Untersuchung der Kooperativität zwischen Untereinheiten bei gekoppeltem und ungekoppeltem Transport könnte so Informationen über die Struktur der SLC26-Proteine liefern. Ein Ansatzpunkt wäre die Koexpression von Wildtyp-Zebrafischprestin mit der Mutante G327C. Eine weitere Möglichkeit stellen am N-Terminus verkürzte Mutationen des Säugetierprestins dar, die zwar in die Zellmembran eingebaut werden, aber durch fehlende Dimerisierung keine nichtlineare Kapazität mehr aufweisen [40].

Auch unabhängig davon könnte sich der elektrogene SCN^--Strom des Säugetierprestins als nützliches Hilfsmittel zur weiteren Charakterisierung des Motorproteins Prestins herausstellen. Er ist experimentell leicht zugänglich und erweitert das Instrumentarium zur Untersuchung des Motorproteins Prestin um ein neues Messverfahren. Damit werden vergleichende elektrophysiologische Untersuchungen mit anderen SLC26 möglich. Nichtlineare Kapazität und SCN^--Strom können ohne größeren Aufwand gleichzeitig an einer Zelle gemessen werden.

Literaturverzeichnis

[1] JT Albert, H Winter, TJ Schaechinger, T Weber, X Wang, DZ He, O Hendrich, HS Geisler, U Zimmermann, K Oelmann, M Knipper, MC Göpfert and D. Oliver. "Voltage-sensitive prestin orthologue expressed in zebrafish hair cells". In: *J Physiol* **580** (2007), pp. 451–461.

[2] Alexi K. Alekov and Christoph Fahlke. "Channel-like slippage modes in the human anion/proton exchanger ClC-4". In: *J Gen Physiol* **133** (2009), pp. 485–496.

[3] J. Ashmore, P. Avan, W.E. Brownell, P Dallos, K. Dierkes, R. Fettiplace, K. Grosh, C.M. Hackney, A.J. Hudspeth, F. Jülicher, B. Lindner, P. Martin, J. Meaud, C. Petit, J.R. Santos Sacchi and B. Canlon. "The remarkable cochlear amplifier". In: *Hear Res* **266** (2010), pp. 1–17.

[4] Jonathan Ashmore. "Cochlear Outer Hair Cell Motility". In: *Physiol Rev* **88** (2008), pp. 173–210.

[5] JP Bai, A Surguchev, S Montoya, PS Aronson, J Santos-Sacchi and D Navaratnam. "Prestin's anion transport and voltage-sensing capabilities are independent". In: *Biophys J* **96** (2009), pp. 3179–3186.

[6] WE Brownell, CR Bader, D Bertrand and RY De. "Evoked mechanical responses of isolated cochlear outer hair cells". In: *Science* **227** (1985), pp. 194–196.

[7] G. Békésy. "Direct observation of the vibrations of the cochlear partition under a microscope". In: *Acta Otolaryngol* **42(3)** (1952), pp. 197–20.

[8] G. Békésy. "Zur Theorie des Hörens; die Schwingungsform der Basilarmembran." In: *Phys. Z.* **29** (1928), pp. 793–810.

[9] Emma L. R. Compton, Eleni Karinou, James H. Naismith, Frank Gabel and Arnaud Javelle. "Low Resolution Structure of a Bacterial SLC26 Transporter Reveals Dimeric Stoichiometry and Mobile Intracellular Domains". In: *J Biol Chem* **286** (2011), pp. 27058–27067.

[10] D.P. Corey. "New TRP channels in hearing and mechanosensation". In: *Neuron* **39** (2003), pp. 585–588.

[11] Oliver D, He DZ, Klöcker N, Ludwig J, Schulte U, Waldegger S, Ruppersberg JP, Dallos P and Fakler B. "Intracellular anions as the voltage sensor of prestin, the outer hair cell motor protein". In: *Science* **292** (2001), pp. 2340–2343.

[12] Peter Dallos, Jing Zheng and Mary Ann Cheatham. “Prestin and the cochlear amplifier”. In: *J Physiol* **576** (2006), pp. 37–42.

[13] Levente Deák, Jing Zheng, Alex Orem, Guo-Guang Du, Salvador Aguinaga, Keiji Matsuda and Peter Dallos. “Effects of cyclic nucleotides on the function of prestin”. In: *J Physiol* **563** (2005), pp. 483–496.

[14] S Detro-Dassen, M Schänzler, H Lauks, I Martin, SM zu Berstenhorst, Nothmann D, D Torres-Salazar, P Hidalgo, G Schmalzing and C Fahlke. “Conserved dimeric subunit stoichiometry of SLC26 multifunctional anion exchangers”. In: *J Biol Chem* **283** (2008), pp. 4177–4188.

[15] MR Dorwart, N Shcheynikov, Y Wang, S Stippec and S Muallem. “SLC26A9 is a Cl^- channel regulated by the WNK kinases”. In: *J Physiol* **584** (2007), pp. 333–345.

[16] T.A.J. Duke and F. Jülicher. *Critical oscillators as active elements in hearing*. Springer handbook of auditory research. Springer, 2008.

[17] C Fahlke, TH Rhodes, RR Desai and AL Jr George. “Pore stoichiometry of a voltage-gated chloride channel”. In: *Nature* **394** (1998), pp. 687–690.

[18] Brenda Farrell, Cythnia Do Shope and William E. Brownell. “Voltage-dependent capacitance of human embryonic kidney cells”. In: *Phys Rev E* **73** (2006).

[19] Robert Fettiplace. “Active hair bundle movements in auditory hair cells”. In: *J Physiol* **576** (2006), pp. 29–36.

[20] Peying Fong. “CFTR–SLC26 transporter interactions in epithelia”. In: *Biophys Rev* **4** (2012), pp. 1–10.

[21] Peter Forey and Philippe Janvier. “Agnathans and the origin of jawed vertebrates”. In: *Nature* **361** (1993), pp. 129–134.

[22] Peter G. Gillespie and David P. Corey. “Myosin and Adaptation by Hair Cells”. In: *Neuron* **19** (1997), pp. 955–958.

[23] KR Gleitsman, M Tateyama and Y Kubo. “Structural rearrangements of the motor protein prestin revealed by fluorescence resonance energy transfer”. In: *Am J Physiol Cell Physiol* **297** (2008), pp. C290–C298.

[24] T. Gold. “Hearing. II. The physical basis of the action of the cochlea”. In: *Proc R Soc Lond B Biol Sci* **135** (1948), pp. 492–498.

[25] AW Gummer, JW Smolders and R Klinke. “Basilar membrane motion in the pigeon measured with the Mössbauer technique”. In: *Hear Res* **29(1)** (1987), pp. 63–92.

[26] A. J. Hudspeth. “Making an Effort to Listen: Mechanical Amplification in the Ear”. In: *Neuron* **59** (2008), pp. 530–545.

[27] A. J. Hudspeth, Frank Jülicher and Pascal Martin. “A Critique of the Critical Cochlea: Hopf–a Bifurcation–Is Better Than None”. In: *J Neurophysiol* **104** (2010), pp. 1219–1229.

[28] K. H. Iwasa and M. Adachi. “Force generation in the outer hair cell of the cochlea”. In: *Biophys. J* **73** (1997), pp. 546–555.

[29] KH Kim, N Shcheynikov, Y Wang and S Muallem. “SLC26A7 is a Cl^- channel regulated by intracellular pH”. In: *J Biol Chem* **280** (2005), pp. 6463–6470.

[30] M LeMasurier and PG Gillespie. “Hair-Cell Mechanotransduction and Cochlear Amplification”. In: *Neuron* **48** (2005), pp. 403–415.

[31] G.A. Manley, A.N. Popper and R.R. Fay. *Evolution of the vertebrate auditory system*. Springer handbook of auditory research. Springer, 2004.

[32] Geoffrey A. Manley. “Cochlear mechanisms from a phylogenetic viewpoint”. In: *Proc. Natl. Acad. Sci. USA* **97**.22 (2000), pp. 11736–11743.

[33] P. Martin, A. D. Mehta and A. J. Hudspeth. “Negative hair-bundle stiffness betrays a mechanism for mechanical amplification by the hair cell”. In: *Proc. Natl. Acad. Sci. USA* **97(22)** (2000), pp. 12026–12031.

[34] P. E. Mason, G. W. Neilson, C. E. Dempsey, A. C. Barnes and J. M. Cruickshank. “The hydration structure of guanidinium and thiocyanate ions: Implications for protein stability in aqueous solution”. In: *Proc Natl Acad Sci USA* **100** (2003), pp. 4557–4561.

[35] K Mio, Y Kubo, T Ogura, T Yamamoto, F Arisaka and C Sato. “The motor protein prestin is a bullet-shaped molecule with inner cavities”. In: *J Biol Chem* **283(2)** (2008), pp. 1137–1145.

[36] DB Mount and MF Romero. “The SLC26 gene family of multifunctional anion exchangers”. In: *Pflugers Arch* **447(5)** (2004), pp. 710–721.

[37] Christopher D. Moyes and Patricia M. Schulte. *Tierphysiologie*. Pearson Studium, 2007.

[38] Daniella Muallem and Jonathan Ashmore. “An Anion Antiporter Model of Prestin, the Outer Hair Cell Motor Protein”. In: *Biophys J* **90** (2006), pp. 4035–4045.

[39] RC Naidu and DC Mountain. “Measurements of the stiffness map challenge a basic tenet of cochlear theories”. In: *Hear Res* **124(1-2)** (1998), pp. 124–131.

[40] D Navaratnam, JP Bai, H Samaranayake and J Santos-Sacchi. “N-terminal-mediated homomultimerization of prestin, the outer hair cell motor protein”. In: *Biophys J* **89(5)** (2005), pp. 3345–3352.

[41] E Ohana, N Shcheynikov, D Yang, I So and S Muallem. “Determinants of coupled transport and uncoupled current by the electrogenic SLC26 transporters”. In: *J Gen Physiol* **137(2)** (2011), pp. 239–251.

[42] A. J. Ricci, A. C. Crawford and R. Fettiplace. “Mechanisms of Active Hair Bundle Motion in Auditory Hair Cells”. In: *J Neurosci* **22** (2002), pp. 44–52.

[43] AJ Ricci, AC Crawford and R Fettiplace. “Tonotopic variation in the conductance of the hair cell mechanotransducer channel”. In: *Neuron* **40** (2003), pp. 983–990.

[44] Luis Robles and Mario A. Ruggero. “Mechanics of the Mammalian Cochlea”. In: *Physiol Rev* **81(3)** (2001), pp. 1305–1352.

[45] V Rybalchenko and J Santos-Sacchi. “Anion control of voltage sensing by the motor protein prestin in outer hair cells”. In: *Biophys J* **95(9)** (2008), pp. 4439–4447.

[46] V Rybalchenko and J Santos-Sacchi. “Cl- flux through a non-selective, stretch-sensitive conductance influences the outer hair cell motor of the guinea-pig”. In: *J. Physiol* **547** (2003), pp. 873–891.

[47] J. Santos-Sacchi and M. Wu. “Protein- and lipid-reactive agents alter outer hair cell lateral membrane motor charge movement”. In: *J Membr Biol* **200** (2004), pp. 83–92.

[48] TJ Schaechinger and D. Oliver. “Nonmammalian orthologs of prestin (SLC26A5) are electrogenic divalent/chloride anion exchangers”. In: *Proc Natl Acad Sci USA* **104(18)** (2007), pp. 7693–7698.

[49] R. Schmidt, F. Lang and G. Thews. *Physiologie des Menschen*. 30. Auflage. Heidelberg: Springer Medizin Verlag, 2007.

[50] WE Shehata, WE Brownell and R Dieler. “Effects of salicylate on shape, electromotility and membrane characteristics of isolated outer hair cells from guinea pig cochlea”. In: *Acta Otolaryngol* **111** (1991), pp. 707–718.

[51] AK Sturm, L Rajagopalan, D Yoo, WE Brownell and FA Pereira. “Functional expression and microdomain localization of prestin in cultured cells”. In: *Otolaryngol Head Neck Surg* **136(3)** (2007), pp. 434–439.

[52] Xiaodong Tan, Jason L. Pecka, Jie Tang, Oseremen E Okoruwa, Qian Zhang, Kirk W. Beisel and David Z. Z. He. “From Zebrafish to Mammal: Functional Evolution of Prestin, the Motor Protein of Cochlear Outer Hair Cells”. In: *J Neurophysiol* **105** (2011), pp. 36–44.

[53] Helmut Vogel. *Gerthsen Physik*. 19. Auflage. Berlin, Heidelberg: Springer Verlag, 1997.

[54] J Zheng, GG Du, CT Anderson, JP Keller, A Orem, P Dallos and M. Cheatham. “Analysis of the oligomeric structure of the motor protein prestin”. In: *J Biol Chem* **281(29)** (2006), pp. 19916–19924.

[55] Jing Zheng, Weixing Shen, David Z. Z. He, Laird D. Long Kevin B. Madison and Peter Dallos. “Prestin is the motor protein of cochlear outer hair cells”. In: *Nature* **405** (2000), pp. 149–155.

4 Publikationen

Conserved Dimeric Subunit Stoichiometry of SLC26 Multifunctional Anion Exchangers

Silvia Detro-Dassen[‡1], Michael Schänzler[§1], Heike Lauks[‡], Ina Martin[§], Sonja Meyer zu Berstenhorst[§], Doreen Nothmann[§], Delany Torres-Salazar[§], Patricia Hidalgo[§], Gunther Schmalzing[‡2,4], and Christoph Fahlke[§¶3,4]

From the [‡]Abteilung Molekulare Pharmakologie, Rheinisch-Westfalische Technische Hochschule Aachen University, Wendlingweg 2, Aachen 52074, the [¶]Institut für Neurophysiologie, Medizinische Hochschule Hannover, Carl-Neuberg-Strasse 1, Hannover 30625, and the [¶]Zentrum für Systemische Neurowissenschaften Hannover 30625, Hannover, Germany

[1]Both authors contributed equally to this work as first authors.

[2] To whom correspondence may be addressed. Tel.: 49-241-808-9130; Fax: 49-241-808-2433;
E-mail: gschmalzing@ukaachen.de.

[3] To whom correspondence may be addressed. Tel.: 49-511-532-2777; Fax: 49-511-532-2776;
E-mail: fahlke.christoph@mh-hannover.de.

[4] Both authors contributed equally to this work as senior authors.

The *SLC26* gene family encodes multifunctional transport proteins in numerous tissues and organs. Some paralogs function as anion exchangers, others as anion channels, and one, prestin (SLC26A5), represents a membrane-bound motor protein in outer hair cells of the inner ear. At present, little is known about the molecular basis of this functional diversity. We studied the subunit stoichiometry of one bacterial, one teleost, and two mammalian SLC26 isoforms expressed in *Xenopus laevis* oocytes or in mammalian cells using blue native PAGE and chemical cross-linking. All tested SLC26s are assembled as dimers composed of two identical subunits. Co-expression of two mutant prestins with distinct voltage-dependent capacitances results in motor proteins with novel electrical properties, indicating that the two subunits do not function independently. Our results indicate that an evolutionarily conserved dimeric quaternary structure represents the native and functional state of SLC26 transporters.

The abbreviations used are: SLC26, solute carrier 26; BN, blue native; EndoH, endoglycosidase H; HEK293, human embryonic kidney 293; NTA, nitrilotriacetic acid; PFO, perfluoro-octanoate; PNGase F, peptide:N-glycosidase F; YFP, yellow fluorescent protein; DTT, dithiothreitol; WT, wild type; zf, zebrafish; zfprestin, zebrafish prestin; rprestin, rat prestin; PASulP, bacterial isoform from *P. aeruginosa*; DIDS, 4,4'-diisothiocyanostilbene disulfonic acid; DMA, dimethyl adipimidate; GA, glutardialdehyde; GlyR: glycine receptor.

The solute carrier 26 (SLC26) gene family was defined ten years ago by expression cloning of a Na_2-independent SO_4^{2-} transporter from rat liver (1). Subsequently, many homologs were found in mammals, non-mammals, plants, fungi, and bacteria (2). The functional importance of this family is highlighted by several inherited human diseases caused by mutations in SLC26 genes (3, 4), such as diastrophic dysplasia (SLC26A2), congenital chloride diarrhea (SLC26A3), Pendred syndrome (a syndrome comprising sensorineural deafness and enlarged thyroid (SCL26A4)), and inner ear deafness (SLC26A5 or pres). The symptomatic variety of these diseases illustrates the diversity of cellular functions per- formed by this class of transport proteins.

Mammalian SLC26s are the members of this family that have been functionally studied the best. Most of them operate as anion exchangers, and distinct isoforms differ significantly in anion specificity. Some transport monovalent and divalent anions, whereas others transport only monovalent anions (1, 5–9). There are also family members that do not function as anion exchangers, most notably, SLC26A5 or prestin, the motor protein in the outer hair cells (10). Outer hair cells in the mammalian cochlea change length in response to acoustic signals, and this mechan- ical amplification enhances the hearing sensitivity by >40 db. The basis for these length changes are voltage-dependent conformational changes of prestin that are transformed into somatic length changes of outer hair cells (11). Moreover, recent work suggested that SLC26A7 and SLC26A9 are not anion carriers, but anion channels (12, 13).

The SLC26 family thus exhibits an amazing variety of functions, yet the molecular basis of this diversity is poorly understood. As a fundamental step to understand structure-function relationships, we decided to study the subunit stoichiometry of various SLC26 homologs from humans, rat, zebrafish, and Pseudomonas aeruginosa. We demonstrate that all tested isoforms exhibit a dimeric subunit stoichiometry.

Experimental Procedures

Expression of His- or YFP Fusion Proteins in *Xenopus* Oocytes or in Mammalian Cells pGEMHE-hSLC26A3-HisCT (poly-histidine tag at the carboxyl-terminal end) encoding the human SLC26A3 (GenBank accession number NM_000111) (14), pGEMHE-rprestin-His_{CT} encoding the rat prestin (GenBank accession number NM_030840), pGEMHE-zfprestin-His_{CT} encoding prestin from Danio rerio (zebrafish) (GenBankTM accession number BX571796) (15), and pGEMHE-His_{NT}-hClC-1 (polyhistidine tag at the amino-terminal end; GenBankTM accession number NM_000083) plasmids were generated by adding a cDNA fragment encoding six histidine residues carboxyl- or amino-terminal to the coding region by PCR and subcloning into pGEMHE vector (16). A construct encoding a rat prestin concatamer was generated by covalently linking two prestin copies in a single open reading frame by a cDNA sequence containing four repeats of the tripeptide AGS (17). PASulP (GenBank accession number NP_250338) was identified by searches for rat prestin homologues using BLAST searches at the National Center for Biotechnology Information (NCBI). It was amplified by PCR from genomic P. aeruginosa

DNA and subcloned into pGEMHE using BamHI and HindIII restriction sites. Transcription of cRNAs and handling of oocytes was performed as described (18).

To create YFP fusion proteins, the YFP cDNA was excised from pEYFP-N1/pECFP-N1 (Clontech) and inserted into pcDNA3.1 (Invitrogen) connected to the coding sequences of rat and zebrafish prestin and human SLC26A3 by short linker sequences in a single open reading frame. SLC26 proteins were expressed in tsA201 cells as described (19). For some experiments, stable inducible cell lines, generated by selecting Flp-In T-REx cells (Invitrogen) transfected with pcDNA5/FRT/TO-YFP-rprestin, were used after 24 h incubation with 1 µg/ml tetracycline. Point mutations were introduced using the QuikChange^{TM} method. All constructs were verified by restriction analysis and DNA sequencing. Supplemental Fig. S1 gives an alignment of the SLC26 isoforms characterized in this study.

Functional Characterization of SLC26A3 and Prestin Radioactive chloride uptake into oocytes was studied 4–5 days after cRNA injection. Oocytes were preincubated for 10 min in chloride-free medium (98 mM potassium gluconate, 1.8 mM calcium gluconate, 5 mM HEPES-Tris, pH 7.5) and then transferred to the uptake solution (100 mM potassium gluconate, 5 mM HEPES-Tris, 3 mM ^{36}Cl, pH 7.5) above 300 µl of mineral oil. After various time periods, ^{36}Cl uptake was terminated by centrifuging the oocytes into the mineral oil layer. Scintillation counting was performed after lysis of the oocytes in scintillation counting tubes containing 100 µl of 0.5% SDS. For each incubation period, uptake was also determined for at least two uninjected oocytes. These control values were averaged and subtracted from radioactive uptake levels measured on injected oocytes. Additional control experiments were performed with oocytes expressing SLC26A3 transporters incubated in the uptake solution supplemented by 100 µM DIDS. DIDS was dissolved in Me_2SO at a concentration of 10 mM and diluted into the uptake solution.

Transfected HEK293 or tsA201 cells were studied through whole cell patch clamping using an Axopatch 200B amplifier. In experiments measuring voltage-dependent capacitances, the external solution contained (in mM): 140 NaCl, 4 KCl, 2 CaCl2, 1 MgCl2, 5 HEPES, at pH 7.4, and the intracellular solution contained (in mM): 120 NaCl, 2 MgCl2, 5 EGTA, 10 HEPES, at pH 7.4. The initial pipette resistances were 1–2.5 megohms. Stray pipette capacitance was neutralized before establishing the whole cell configuration. All data acquisition and analysis were performed with the Windows-based patch clamp program, jClamp (SciSoft, Ridgefield, CT). Non-linear charge movement was calculated using a continuous high resolution (2.56 ms sampling) two-sine stimulus protocol (10 mV peaks at both 390.6 Hz and 781.2 Hz) superimposed onto voltage steps (150 ms duration) from either -200 mV to +80 mV or -160 mV to +120 mV (20). The voltage dependence of the non-linear capacitance was fit to the first derivative of a two-state Boltzmann function (21).

$$C(V) = \frac{\beta Q_{max} e^{-\beta(V-V_{1/2})}}{\left(1+e^{-\beta(V-V_{1/2})}\right)^2} + C_{lin} \tag{4.1}$$

where $\beta = ze_0\delta/k_BT$. In addition, Q_{max} is the maximum charge transferred across the membrane; $V_{1/2}$ is the potential at half-maximal charge transfer; z is the number of elementary charges, e_0, displaced across a fraction, δ, of the membrane dielectric; k_B is the Boltzmann constant, and T is the absolute temperature.

In co-transfected cells, the voltage dependence of the non-linear capacitance was fit with,

$$C(V) = p_{D154N}^2 \cdot C_{D154N} + (1 - p_{D154N})^2 \cdot C_{D342Q} + 2(1 - p_{D154N})\, p_{D154N} \cdot C_{Heterodimer} \tag{4.2}$$

where p_{D154N} is the percentage of subunits carrying the D154N mutation. C_{D154N}, C_{D342Q}, and $C_{Heterodimer}$ are voltage-dependent capacitances of homogenous populations of homodimeric mutant prestin or of heterodimeric prestin. Q_{max} was assumed to be identical for each non-linear capacitance term.

To measure Cl^-/SO_4^{2-} exchange by zebrafish prestin, external solutions containing (in mM) 135 NaCl, 5 Na_2SO_4, 4 KCl, 2 CaCl2, 1 MgCl2, 5 HEPES, pH 7.4, and internal solutions (in mM) containing: 30 Na_2SO_4, 90 NaCl, 2 MgCl2, 5 EGTA, 10 HEPES, pH 7.4, were used.

Purification of [^{35}S]Methionine-labeled Protein from *Xenopus* Oocytes cRNA-injected and non-injected control oocytes were incubated for the indicated time with Revidue L-[^{35}S]methionine (>37 TBq/mmol, GE Healthcare Biosciences) at ~25 Mbq/ml (~0.1 MBq/oocyte) in frog Ringer's solution at 19 °C for metabolic labeling. Either immediately after the pulse or after an additional chase period, the radiolabeled oocytes were extracted with digitonin (1.0%) in 0.1 M sodium phosphate buffer, pH 8.0. His-tagged proteins were isolated by metal affinity chromatography using Ni^{2+}-NTA-agarose (Qiagen), as detailed previously (18), with the modification that iodoacetamide was routinely included at 10 mM and 1 mM in the lysis and washing buffers, respectively (22). In some experiments, 1% perfluoro-octanoic acid, ammonium salt (PFO, Sigma-Aldrich) was used as detergent for membrane protein extraction and purification in 0.1 M sodium phosphate buffer, pH 8.0, with and without 10 mM iodoacetamide as indicated. Proteins were eluted from Ni^{2+}-NTA-agarose with PFO elution buffer consisting of 250 mM imidazole/HCl and 1% PFO at pH 7.4 and stored at 0 °C until analysis later on the same day.

Chemical Cross-linking His-tagged SLC26 protein bound to Ni^{2+}-NTA beads was washed in triplicate with imidazole-free sodium phosphate buffer (pH 8.0) supplemented with 0.2% digitonin. The Ni^{2+}-NTA beads (packed volume, ~15 µl) were resuspended in 50 µl of 0.2 M triethanolamine/HCl (pH 8.5), 0.5% digitonin. The cross-linking reaction was initiated by adding glutardialdehyde (Roth Chemicals) or dimethyl adipimidate (Pierce) from freshly prepared solutions in distilled water or 0.2 M triethanolamine/HCl (pH 8.5), respectively. After 30 min at room temperature, the cross-linking reaction was terminated by washing the Ni^{2+}-NTA-agarose beads twice with imidazole-free sodium phosphate buffer, 0.2% digitonin. Proteins were eluted from Ni^{2+}-NTA-agarose with non-denaturing elution buffer, consisting of 250 mM imidazole/HCl and 0.5% digitonin at pH 7.4, and then stored at 0 °C until analysis later on the same day.

Purification of YFP Fusion Proteins from Mammalian Cells tsA201 or HEK293 cell dishes were washed with cold phosphate-buffered saline and lysed with 800 µl of 0.1 M sodium phosphate buffer containing 1% digitonin, protease inhibitors, and 50 mM iodoacetamide. For lysis, the whole dish was incubated 15 min on ice, followed by complete transfer of the cell lysate into a microtube and subsequent quadruplicate vortexing during incubation on ice for another 15 min. SLC26 proteins were isolated by metal affinity chromatography using Ni^{2+}-NTA-agarose (Qiagen). In some experiments, 1% PFO in PFO extraction buffer was used for cell lysis.

SDS-PAGE, BN-PAGE, and PFO-PAGE-[^{35}S]Methionine- labeled proteins were denatured for 10 min at 56 °C with SDS sample buffer containing 20 mM dithiothreitol (DTT) and electrophoresed in parallel with ^{14}C-labeled molecular mass markers (Rainbow, GE Healthcare Biosciences, Freiberg, Germany) on linear SDS-polyacrylamide gels. BN-PAGE was performed as described (18) immediately after protein purification. We loaded the protein purified from the equivalent of 0.5 oocytes in each lane. Molecular masses were determined by comparison with the defined membrane protein complexes generated by partial denaturing of the homopentameric α1 GlyR (23). PFO-PAGE was performed as described using freshly poured Tris-glycine (Laemmli) gels without SDS and Tris-glycine running buffer supplemented with 0.5% (w/v) PFO instead of SDS (24, 25). The homopentameric α1 GlyR was used as a mass marker as above.

YFP-tagged proteins were visualized by scanning the wet PAGE gels with a fluorescence scanner (Typhoon, GE Healthcare Biosciences). PAGE gels with radioactive proteins were fixed and dried, exposed onto a phosphorscreen, and scanned with a Storm 820 PhosphorImager (GE Healthcare Biosciences). Individual bands were quantified with the Image-QuaNT software. To investigate the glycosylation state of the proteins, samples were treated for 2 h with either endoglycosidase H (EndoH) or PNGase F (New England Biolabs, Beverly,MA) in the presence of reducing SDS sample buffer and 1% (w/v) Nonidet P-40 to counteract SDS inactivation of PNGase F.

Data Analysis Protein intensities were quantified with the ImageQuaNT software (GE Healthcare Biosciences). Each experiment was performed at least in triplicate. Data are given as mean ± S.E.

Results

His and YFP Tags Leave Function of SLC26A3 and Prestin Unaltered We added carboxyl-terminal hexahistidine tags to various SLC26 isoforms to purify the proteins from *Xenopus* oocytes by a single Ni^{2+}-metal affinity chromatography step. Moreover, SLC26 isoforms were expressed as YFP fusion proteins in mammalian cells, to visualize protein bands using a fluorescence scanner. To test whether these sequence alterations affect functional properties, we compared chloride transport by WT and His-tagged SLC26A3, non-linear charge movement by WT and His- or YFP-tagged rat prestin, and Cl^-/SO_4^{2-} antiport by WT and His- or YFP-tagged

zebrafish prestin.

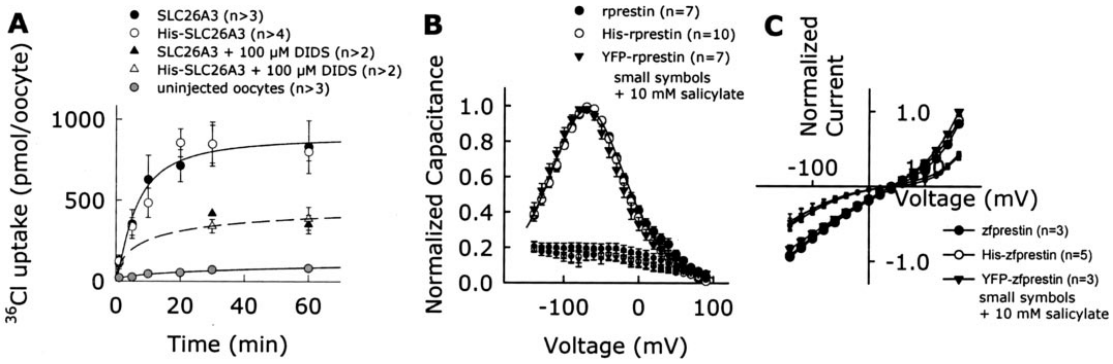

Abbildung 4.1: **Figure 1. His and YFP tags leave function of SLC26A3 and prestin unaltered.** *A*, time dependence of ^{36}Cl uptake into oocytes expressing human SLC26A3 and His-SLC26A3. To test the DIDS sensitivity of the hSLC26A3 transporters, 100 µM DIDS was added to the uptake solution. *B*, normalized non-linear charge movement associated with rat prestin, His-rprestin, and YFP-rprestin heterologously expressed in tsA201 cells. *C*, normalized current-voltage relationships from tsA201 cells expressing zebrafish prestin, His-zfprestin, and YFP-zfprestin. Salicylate was applied by moving cells into the stream of a perfusion solution containing 10 mM salicylate.

SLC26A3 was initially identified as a potential tumor suppressor that was down-regulated in adenoma and abundant in normal colonic mucosa (14). It was demonstrated to be a DIDS-sensitive anion exchanger (27, 28). We expressed tagged and untagged SLC26A3 in *Xenopus* oocytes and measured radioactive chloride uptake with and without added DIDS (27). Oocytes expressing WT or His-tagged SLC26A3 accumulated chloride with similar time courses and magnitudes (Fig. 1A). In both cases, ^{36}Cl uptake was significantly higher in oocytes expressing SLC26A3 than in control oocytes, and incubation with 100 µM DIDS caused a reduction of the chloride uptake to ~50%.

Rat prestin performs voltage-induced conformational changes that can be monitored as voltage-dependent capacitance changes (10, 29). We expressed WT and His- or YFP-tagged rat prestin in tsA201 cells and measured voltage-dependent capacitance using a software-based lock-in technique (phase tracking) in the whole cell patch clamp technique. Neither the absolute amplitude of the non-linear capacitance (data not shown) nor the voltage dependence of rat prestin (Fig. 1B) was affected by any of the added tags. Rat prestin charge movement is not affected by 100 µM DIDS (data not shown). However, non-linear capacitances by WT and tagged prestin were eliminated by salicylate (29) (Fig. 1B).

Zebrafish prestin is functionally different from rat prestin. In addition to mediating voltage-dependent charge movements (30), it functions as Cl^-/SO_4^{2-} exchanger with 1:1 stoichiometry (31). We measured currents in cells expressing WT or YFP or His fusion proteins of zebrafish prestin. The three tested proteins displayed anion currents with identical reversal potential and

therefore unchanged transport stoichiometry (Fig. 1C). Mean current amplitudes were comparable (data not shown), and 10 mM salicylate (31) reduced current amplitudes to ~50% in all cases (Fig. 1C). The addition of the His tag or YFP tag did not affect the function of the tested SLC26 isoforms. We conclude that none of the tags prevents oligomerization processes of SLC26 that are of functional importance.

His-tagged SLC26A3 and rat prestin were expressed and metabolically labeled in *Xenopus* oocytes. After extraction with 1% (w/v) digitonin, proteins were purified by metal affinity chromatography. Both proteins express well in *Xenopus* oocytes and are metabolically stable during a sustained chase. When resolved by reducing SDS-PAGE with a low percentage of acrylamide, as in Fig. 2A, the SLC26A3 and prestin polypeptides migrated at 15–20% lower masses than calculated from the amino acid sequences (85 kDa for His-SLC26A3 and 82 kDa for His-prestin). Both polypeptides shifted to higher apparent molecular masses at higher acrylamide concentrations (results not shown). This indicates that the mass deviations are due to anomalous migration in SDS-PAGE gels and not to post-translational processing of the polypeptide chains. Anomalous fast electrophoretic mobility has frequently been observed with highly hydrophobic membrane proteins (32).

Human SLC26A3 harbors four sequons for N-glycosylation, ^{153}NAT, ^{161}NNS, ^{164}NNS, and $^{165\text{NSS}}$, in the predicted second ectodomain loop, which is flanked by the transmembrane segments TM3 and TM4. Deglycosylation with either EndoH or PNGase F reduced the molecular mass by ~8 kDa (Fig. 2B, lanes 1–3), suggesting the presence of three N-linked high mannose-type oligosaccharides of 2–3 kDa each. Substitution of Asn^{153} by glutamine resulted in a di-glycosylated polypeptide (lanes 4–6), and additional glutamine substitution of Asn161, Asn^{164}, and Asn^{165} resulted in a non-glycosylated polypeptide (lanes 10–12). Thus, the three sequons that are in close proximity to one another acquire only two oligosaccharides, indicating that either Asn^{164} or Asn^{165} is sterically inaccessible for the oligosaccharyltransferase (32, 33).

Rat prestin carries five potential glycosylation sites, with two adjacent sequons – ^{163}NAT and ^{166}NGT – located in the second ectodomain. Deglycosylation produced a ~5-kDa mass shift (Fig. 2C, lanes 2–3), suggesting that two sites carry N-glycans. Glutamine substitution of Asn^{163} led to a monoglycosylated polypeptide (lanes 4 – 6), and no mass shift by PNGase F was observed when both sites, Asn^{163} and Asn^{166}, were replaced by glutamines (lanes 7–9). The three remaining N-glycosylation sequons, ^{589}NATV, ^{603}NATK, and ^{736}NATP, were not used.

SLC26A3 and Rat Prestin Migrate as Discrete Dimers in BN-PAGE Gels To examine whether SLC26 transporters assemble into stable higher order structures, we natively purified human SLC26A3 or rat prestin from *Xenopus* oocytes and resolved it on BN-PAGE gels. The non-denatured hSLC26A3 exchanger migrated as a distinct band of ~200 kDa (Fig. 3A, lane 1). The size of the native SLC26A3 oligomer was assessed by comparing it to a molecular weight standard produced by partial dissociation of the homopentameric α1 GlyR receptor (Fig. 3A, lane 8). This procedure results in the occurrence of oligomers consisting of one to five GlyR α1 subunits (molecular mass ~52 kDa), representing a reliable size standard for membrane proteins of up

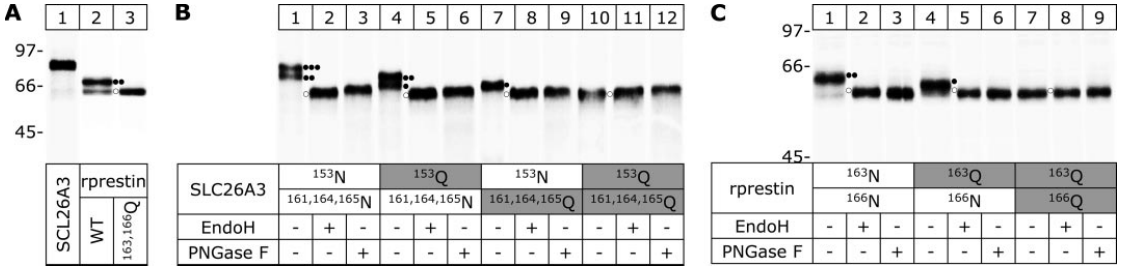

Abbildung 4.2: **Figure 2. Biochemical characterization of human SLC26A3 and rat prestin.** *A–C*, human SLC26A3 and rat prestin purified by Ni^{2+}-affinity chromatography after an overnight [^{35}S]methionine pulse and a 24-h chase from *X. laevis* oocytes were resolved on a reducing SDS-PAGE urea gel (6% acrylamide/8 M urea) in parallel with ^{14}C-labeled molecular mass markers (positions indicated in kDa at the left margins). Mutation of single or multiple asparagine glycosyl acceptors to glutamine combined with deglycosylation analysis as indicated reveals that SLC26A3 and prestin carry three (*B*) or two (*C*) high mannose type N-glycans, respectively. Glycosylated and non-glycosylated forms are indicated by black and white dots, respectively. Black dots indicate the number of glycans of the respective polypeptide.

to 260 kDa (32). To display the number of subunits incorporated in the SLC26A3 transporter complex, we weakened non-covalent subunit interactions by treating the natively purified protein with increasing concentrations of SDS. Incubation of the SLC26A3 exchanger with 0.01% SDS resulted in the complete disappearance of the 200-kDa band in favor of one faster migrating band of ~100 kDa (Fig. 3A, lane 4). The similarity with the calculated mass (91 kDa including the 6-kDa mass contributed by two N-linked glycans) and the absence of a faster migrating band in the presence of a 10-fold higher SDS concentration (Fig. 3A, lane 6) indicate that the 100-kDa band represents the monomeric state of SLC26A3, and the 200-kDa band represents the dimeric state. In the absence of the denaturant SDS, the 200-kDa band was resistant to 1-h incubation at 37 °C with Coomassie dye (Fig. 3A, lane 2) or Coomassie dye plus the strong reductant DTT (Fig. 3A, lane 3). Non-glycosylated SLC26A3 transporters also existed exclusively as dimers (results not shown). Other multimerization states were virtually absent (Fig. 3). Natively purified rat prestin migrated at three positions equal to ~97, ~190 kDa, and ~250 kDa in BN-PAGE gels (Fig. 3B, lane 3). Denaturing by SDS resulted in a complete dissociation of the oligomeric prestin into the ~90-kDa form (Fig. 3B, lanes 5 and 6), closely similar to the calculated mass of the rat prestin monomer of 87 kDa (protein core of 82 kDa including His tag plus 5 kDa of N-linked carbohydrate). No faster migrating protein species was observed, indicating that the 90-kDa band represents the monomer and the ~180-kDa band the dimer of rat prestin.

The ~250-kDa band (indicated by a star) was consistently observed when non-denatured prestin was resolved in BN-PAGE gels. Its intensity was about 10%–30% of that of the ~190-kDa band, as determined by quantitative PhosphorImager scanning. The non-glycosylated ^{163}Q^{166}Q-prestin mutant migrated only at two positions inthe BN-PAGE gel corresponding to ~90 kDa and ~190 kDa (Figs. 3B, lane 7). This suggests that the ~250-kDa band is related to the pre-

sence of N-linked glycans, and that both the ~190-kDa band and the ~250-kDa band represent dimeric states. Quantification of the relative intensity of the different bands revealed that dimers represented 52% of the total prestin in this experiment.

To rule out the possibility that the lowest molecular band corresponds to an unusually stable dimer and the higher molecular mass band to a tetrameric conformation, we engineered a concatenated rat prestin construct by linking two coding regions in a single open reading frame. After expression in *Xenopus* oocytes, two major bands were observed in BN-PAGE (Fig. 3B, compare lanes 9 and 3), corresponding to (prestin-prestin) and (prestin-prestin)$_2$. Both conformations are stable and occur with comparable probability, further corroborating the dimeric subunit stoichiometry of prestin. Under denaturing conditions, the ~190-kDa band of the covalently linked dimer became more prominent (Fig. 3B, lane 10), obviously due to the dissolution of the dimerized tandem dimer and higher mass aggregates. In addition, a faint band appeared that migrated at the same position as the prestin monomer (Fig. 3B, indicated by a cross in lane 10). This monomeric form arises most likely from a proteolytic cleavage in the linker region of the concatenated prestin dimer, as has been observed previously with all other concatamers studies in our laboratories (17, 32). Reducing SDS-PAGE resolved the full-length prestin concatamer as a 140-kDa polypeptide corresponding approxi mately to twice the apparent 63 kDa of the prestin monomer (Fig. 3C). In addition, proteolysis-derived monomers are visible as weak bands (indicated by a cross).

Our conclusions are in conflict with a recent report that postulated that gerbil prestin exists as a tetramer formed by association of two disulfide-linked dimers (34). To identify possible reasons for these differences in experimental results, we performed three experiments. We tested the effect of reducing agents on the oligomeric state for all studied SLC26 isoforms (Figs. 3D, 5C, and 5G). Next, we demonstrated that BN-PAGE correctly displays the dimeric structure of ClC channels, a protein family firmly established to form dimers (Fig. 3E). Lastly, we repeated some experiments on rat prestin using PFO as detergent (34) (see Fig. 7).

Prestin Multimers Are Not Covalently Linked by Disulfide Bonds Recombinant rat prestin migrated entirely as monomers in BN-PAGE gels after denaturing with low concentrations of SDS in the absence of added reductant (Fig. 3B, lanes4 – 6). Comparative resolution of non-reduced and DTT-reduced prestin on SDS-PAGE gels did not provide evidence for disulfide-linked multimers (Fig. 3D, lanes 3 and 4). Similar results were obtained with SLC26A3 (Fig. 3D, lanes 1 and 2) and zebrafish prestin (see Fig. 5C). We conclude that SLC26 dimers are held together by non-covalent forces rather than by covalent disulfide bonds.

BN-PAGE Displays the Dimeric Structure of the Human Muscle Chloride Channel hClC-1 The BN-PAGE technique has been shown to correctly display the quaternary state of various ion channels and transporters, including the pentameric structure of Cys-loop receptors (23, 35, 36) and the trimeric structure of glutamate transporters (32, 37, 38) and P2X receptors (18). To validate this experimental approach for a dimeric membrane protein, we expressed a member of

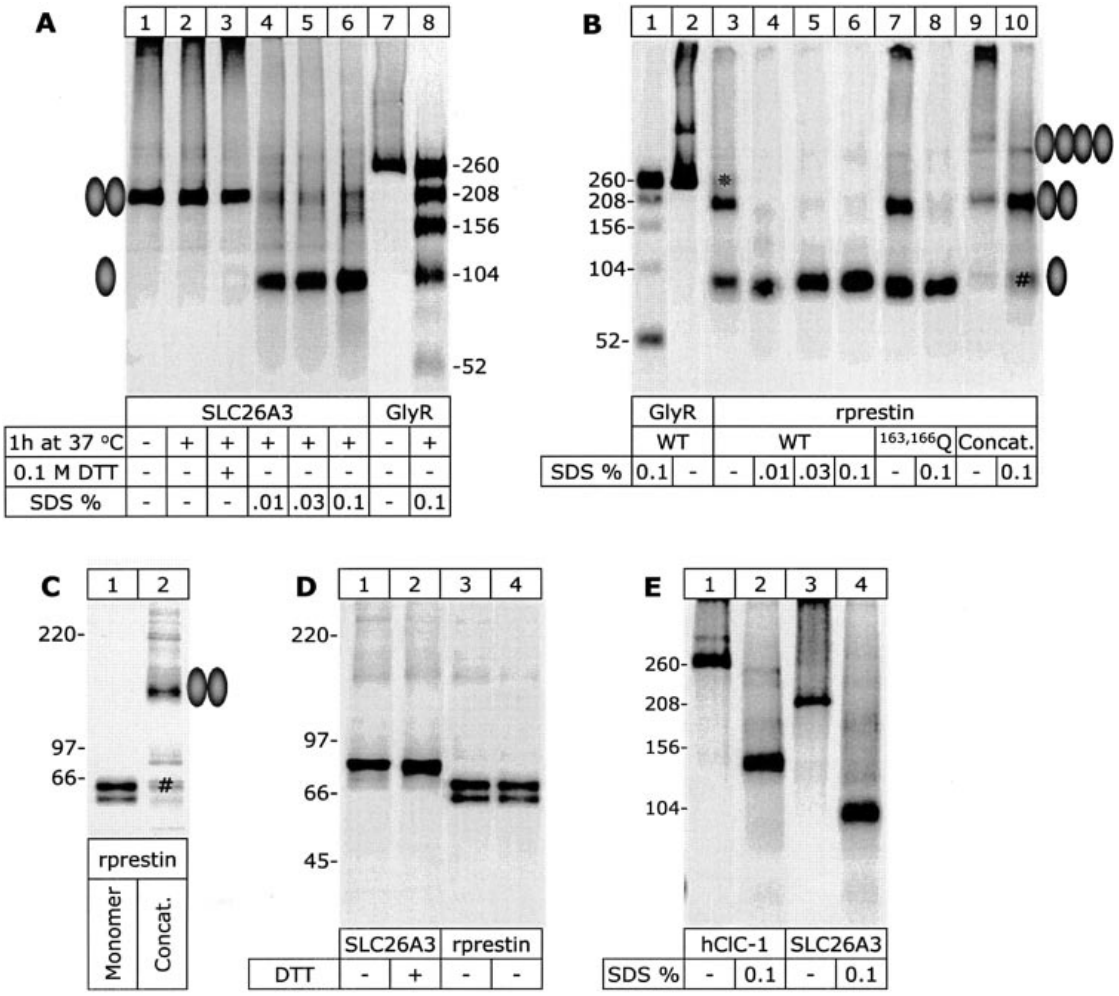

Abbildung 4.3: **Figure 3. Oligomeric state of human SLC26A3 and rat prestin in *Xenopus* oocytes as determined by BN-PAGE.** *A* and *B*, autoradiography of BN-PAGE gels of [^{35}S]methionine-labeled, recombinant SLC26A3 (*A*) and prestin (*B*) proteins purified from *X. laevis* oocytes. An additional band that most likely represents the complex-glycosylated prestin dimer is given as *, and monomeric by-products of the prestin concatamer as #. The treatment of the samples before loading is given in the tables below each figure. Recombinant α1 GlyR was purified from *X. laevis* oocytes to serve as a molecular mass standard. The ellipses schematically illustrate dimeric and monomeric states. *C*, SDS-PAGE analysis of monomeric and concatenated prestin-prestin as resolved in a reducing SDS-PAGE urea gel (10% acrylamide). *D*, SDS-PAGE analysis of SLC26A3 and prestin under non-reducing and reducing conditions. Doublet bands in *C* and *D* represent di- and mono-glycosylated forms of rprestin. *E*, comparative BN-PAGE analysis of the oligomeric state of hClC-1 and SLC26A3. Where indicated, the samples were denatured with SDS for 1 h at 37 °C before loading onto the gel.

the ClC family of voltage-gated chloride channels, the human muscle chloride channel (hClC-1), in *Xenopus laevis* oocytes (39, 40). Non-denatured recombinant hClC-1 channels purified by metal affinity chromatography from [^{35}S]methionine-labeled oocytes migrated as a single sharp band in the BN-PAGE gel (Fig. 3E, lane 1) at the same position as the non-denatured 260 kDa α1 GlyR. SDS led to a concentration-dependent appearance of a faster-migrating protein band of ~130 kDa (Fig. 3E, lane 2), closely similar to the calculated mass of the hClC-1 monomer (including a single 3-kDa oligosaccharide side chain at Asn^{430} (41)). BN-PAGE is therefore able to display correctly the quaternary structure of a dimeric membrane protein. The identity of the oligomeric states of both classes of proteins can be illustrated by directly comparing hClC-1 and SLC26A3 on the same BN-PAGE gel (Fig. 3E).

Cross-linking Generates Covalently Linked SLC26 Dimers Next we used chemical cross-linking as an alternative approach to determine the oligomeric state of SLC26 proteins. Glutardialdehyde efficiently cross-linked natively purified rat prestin to dimers (Fig. 4A). Quantification of the protein bands showed that 66%–71% of prestin migrated as covalently linked dimers in the reducing SDS-PAGE gel when incubated at $\geq$1 mM glutardialdehyde. The non-glycosylated prestin mutant was cross-linked to dimers with the same effectiveness as WT prestin (results not shown).

Cross-linking by glutardialdehyde increased the fraction of dimeric proteins from 60% (no cross-linker, Fig. 4B, lane 1) to up to 80% in BN-PAGE gel (10 mM glutardialdehyde, Fig. 4B, lane 8). Thus, a certain fraction of non-covalently linked prestin dimers dissociates into monomers during overnight BN-PAGE electrophoreses. The imidoester dimethyl adipimidate, which has a longer spacer arm than glutardialdehyde (8.6 Å versus ~5 Å), was much less efficient in generating covalently linked dimers, as visualized by reducing SDS-PAGE (Fig. 4A, lanes 6 – 8) and BN-PAGE (Fig. 4B, lanes 10 –13). SLC26A3 (Fig. 4C, lanes 1 and 2) could also be cross-linked to dimers. Glutardialdehyde cross-linking did not affect the migration of the SLC26 dimers in the BN-PAGE gel (Fig. 4D). However, cross-linking completely prevented the SDS-induced dissociation of the dimers into monomers (compare lanes 2 and 4). The co-analyzed concatenated rat prestin dimer migrated at exactly the same position as the glutardialdehyde-cross-linked prestin on the BN-PAGE gel (lanes 9 and 10). No adducts larger than dimers were observed for any tested SLC26 isoform.

Non-mammalian Eukaryotic and Prokaryotic SLC26 Paralogs Are Also Assembled as Dimers The SLC26 family contains paralogs in mammals, non-mammals, plants, fungi, and bacteria (2). To assess whether the oligomeric state is evolutionarily conserved in non-mammalian eukaryotes and prokaryotes, we studied the subunit stoichiometry of zebrafish (zf) prestin (15) and a bacterial isoform from *P. aeruginosa* (PASulP).

SLC26 paralogs were expressed as His fusion proteins in *Xenopus* oocytes and metabolically labeled. The zebrafish paralog acquired EndoH-resistant complex-type carbohydrates during a sustained pulse (Fig. 5A). Complex-glycosylation resulted in an ~25 kDa increase in the appa-

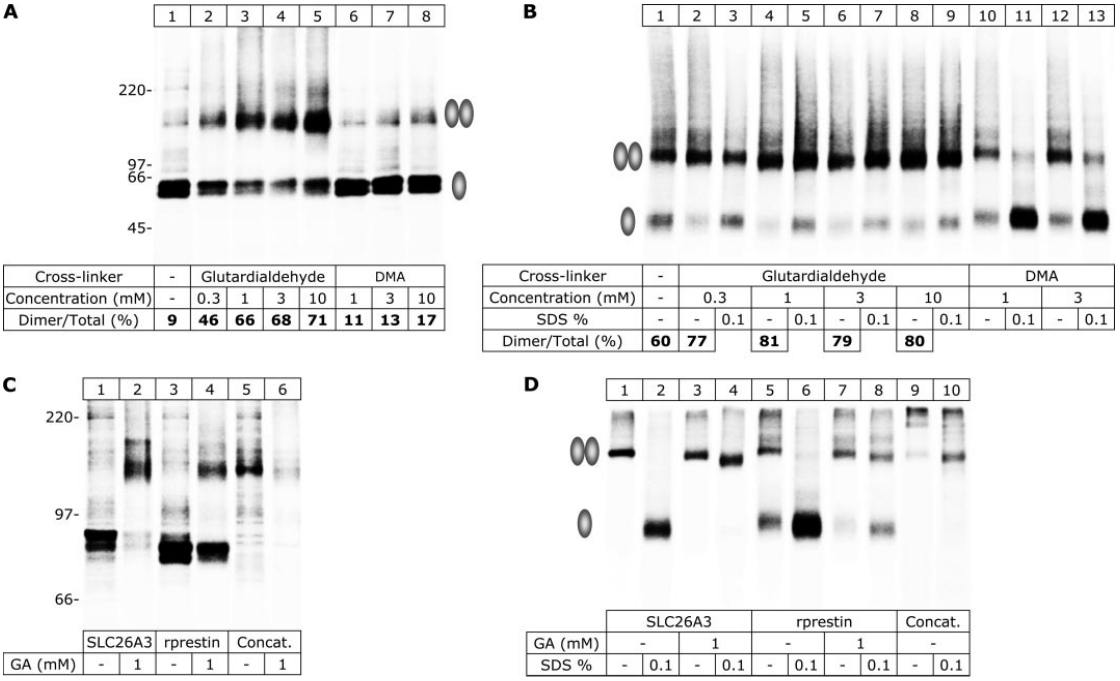

Abbildung 4.4: **Figure 4. Oligomeric state of human SLC26A3 and rat prestin in *Xenopus* oocytes as determined by chemical cross-linking.** *A*, autoradiography of SDS-PAGE urea gels of rat prestin after purification and incubation with cross-linkers as indicated. *B*, BN-PAGE analysis of the same samples as in *A* in the non-denatured and SDS-denatured state. Numbers in *A* and *B* indicate the percent of dimers relative to total prestin protein. *C*, SDS-PAGE analysis of SLC26A3, rat prestin, and the concatenated prestin-prestin tandem dimer. After elution with non-denaturing buffer, samples were supplemented with reducing SDS sample buffer and resolved in SDS-PAGE urea gels (4–10% acrylamide gradient). *D*, BN-PAGE analysis of the same samples as in *C* were resolved in the non-denatured and SDS-denatured state as indicated. The ellipses schematically illustrate dimeric and monomeric states.

rent molecular mass (indicated by a star). Elimination of two putative N-glycosylation sequons, ^{161}NGT and ^{164}NSS, by glutamine substitution of Asn^{161} and Asn^{164} prevented N-glycosylation and thus complex glycosylation (Fig. 5B). Comparative analysis under non-reducing and reducing conditions provided no evidence for the existence of disulfide-bonded zebrafish prestin oligomers (Fig. 5C).

In BN-PAGE, the non-denatured zebrafish prestin migrated predominantly as a dimer (~240 kDa) (Fig. 5D, lane 1) that dissociated into the monomeric ~120 kDa form when treated with SDS (Fig. 5D, lanes 2 and 3). The existence of dimeric prestin was further verified by cross-linking with glutardialdehyde (Fig. 5E). In contrast to the small amount of monomeric prestin visible in the BN-PAGE gel (Fig. 5F, lane 1), no such monomer could be detected in the cross-linked

sample (Fig.5F, lane 2). We conclude that zebrafish prestin exists as a homogenous population of dimers when expressed in *Xenopus* oocytes.

A prokaryotic SLC26 is also assembled as dimer (Fig. 5G). After expression in *Xenopus* oocytes, PASulP migrated as one distinct band of ~160 kDa in its non-denatured form (Fig. 5G, lane 1). Incubation for 1 h at 37°C in the presence of Coomassie dye led to the additional appearance of a ~82-kDa band (Fig. 5G, lane 2). Denaturing with SDS resulted in one distinct band of ~62 kDa, close to the calculated molecular mass of 64 kDa of the PASulP monomer. We conclude that the 160-kDa and 82-kDa bands represent the PASulP dimer and monomer, respectively, and that SDS increases the mobility of the PASulP monomer in the BN-PAGE gel.

Subunit Stoichiometry of SLC26 Is Not Affected by the Expression System To test whether oligomerization of eukaryotic SLC26s might be affected by the cellular environment, we resolved rat prestin, zebrafish prestin, and SLC26A3 by BN-PAGE after heterologous expression as YFP fusion protein in mammalian cells. The expressed proteins were extracted with 1% (w/v) digitonin and subjected to BN-PAGE either by application of the full lysate (rat and zebrafish prestin) or after purification by metal affinity chromatography (His-SLC26A3) (Fig. 6). In all cases, YFP-tagged SLC26 transporters migrated predominantly as bands of ~260 kDa (Fig. 6, lanes 3, 6, and 9) in BN-PAGE gels. The carboxyl-terminally GFP-tagged rP2X1 receptor served as a mass marker (Fig. 6, lanes 1 and 2). Incubation in SDS (Fig. 6, lanes 4 and 5, 7 and 8, and 10 and 11) led to a disappearance of the ~260-kDa SLC26 proteins and the appearance of one band with about half of the molecular mass, in agreement with a dimeric structure also in mammalian cells.

PFO-PAGE Does Not Display a Multimeric Structure of Rat Prestin Previous experiments on the subunit stoichiometry of prestin used a different detergent and PAGE systems. Whereas we employed digitonin as detergent and BN-PAGE, Zheng *et al.* used PFO and PFO-PAGE (34). To assess the consequences of this difference, we purified WT and glycosylation-deficient mutant rat prestin from oocytes using digitonin and PFO as detergents. When resolved by PFO-PAGE, WT, and glycosylation-deficient rat prestin migrated entirely as monomers, irrespective of the detergent used for purification (Fig. 7A, lanes 2 and 3, and 8 and 9). On PFO-PAGE gels, prestin dimers were only observed when digitonin-purified prestin was cross-linked with glutardialdehyde before application to the gel (Fig. 7A, lanes 6 and 7). Hence, the dimeric state of prestin is preserved during purification with digitonin, but lost during PFO-PAGE unless stabilized by cross-linking. PFO not only dissociates prestin oligomers, but also GlyR pentamers (Fig. 7A, lane 1). The appearance of GlyR monomers in the non-denatured GlyR sample that was co-analyzed as a mass marker also indicates a significantly stronger denaturing effect of PFO than of digitonin. On BN-PAGE gels, GlyR behaves as a very stably assembled homopentamer; monomers are only observed after denaturation with SDS (22).

We next extracted a YFP fusion protein of rat prestin from stably transfected mammalian cells using digitonin or PFO. Digitonin-extracted YFP-rprestin migrated in the PFO-PAGE gel exclu-

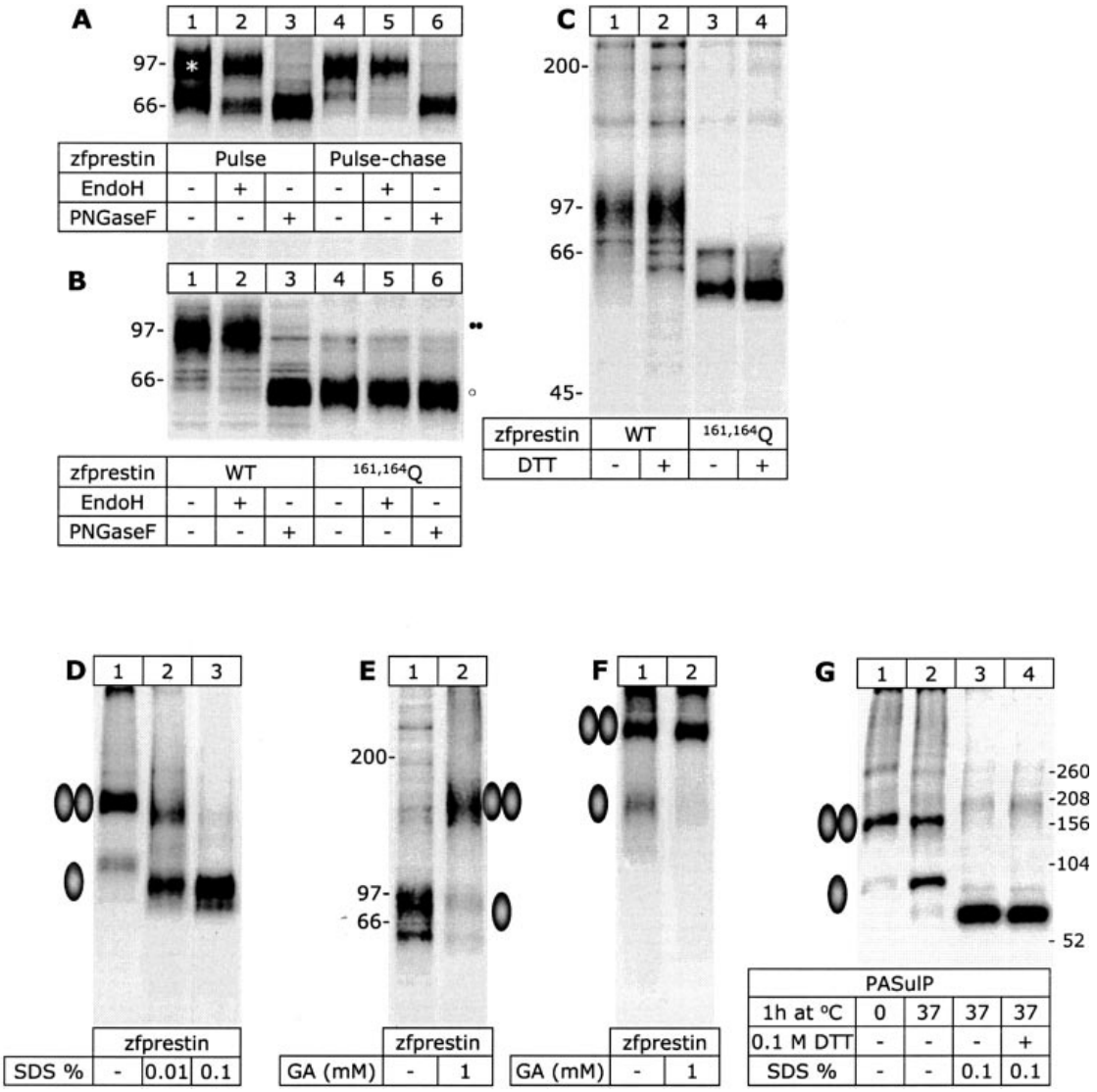

Abbildung 4.5: **Figure 5. Glycosylation and oligomeric states of zebrafish prestin and a SLC26 paralog from *P. aeruginosa*.** *A*, autoradiography of zebrafish prestin (zfprestin) purified directly after an overnight [^{35}S]methionine pulse and after an additional 24-h chase interval. Samples were deglycosylated with EndoH or PNGase F as indicated. *B*, SDS-PAGE analysis of WT and glycosylation-deficient mutant zfprestin, purified after an overnight pulse and 24-h chase, treated with EndoH or PNGase F, and resolved by reducing SDS-PAGE. *C*, SDS-PAGE of the same samples as in B, resolved under non-reducing and reducing conditions. *D*, BN-PAGE analysis of zfprestin. Samples were treated as indicated to induce dissociation into lower order intermediates, including monomers. *E*, oligomeric state of zfprestin as determined by glutardialdehyde (GA) cross-linking followed by reducing SDS-PAGE. *F*, BN-PAGE analysis of the same samples as in *E* were resolved in non-denatured states. The ellipses schematically illustrate dimeric and monomeric states. *G*, autoradiography of a BN-PAGE gel containing [^{35}S]methionine-labeled PASulP purified from *X. laevis* oocytes. Samples were treated as indicated before loading onto the gel.

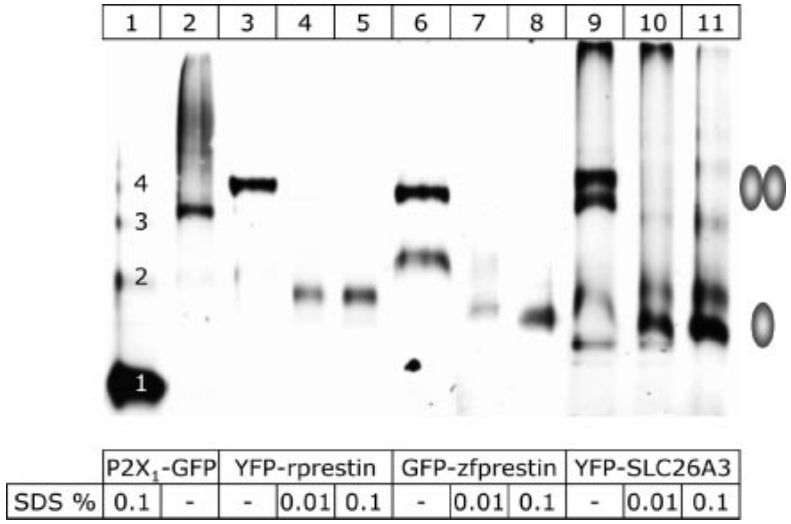

Abbildung 4.6: **Figure 6. Oligomeric state of human SLC26A3 and rat and zebrafish prestin in mammalian cells as determined by BN-PAGE.** BN-PAGE analysis of fluorophore-tagged proteins heterologously expressed in tsA201 cells or FRT/TO HEK293 cells. If indicated, samples were treated with SDS for 1 h at 37°C to induce dissociation into lower order intermediates before gel loading. YFP-tagged proteins were visualized by fluorescence scanning the wet BN-PAGE gel. Numbers specify the oligomeric state of P2X1 protein.

sively in the monomeric state (Fig. 7B, lane 2). Two proteins bands were resolved by PFO-PAGE and could be identified by deglycosylation analysis as the predominant complex-glycosylated (Endo H-resistant) form of prestin and a less abundant (Endo H-sensitive) core-glycosylated form (Fig. 7D). The dimeric state that is predominant on BN-PAGE gels (Fig. 6) is not present under these conditions. PFO-extracted YFP-prestin migrated neither in BN-PAGE gels (data not shown) nor in PFO-PAGE gels (Fig. 7B, lane 1) as oligomer. Neither the addition of DTT nor of iodoacetamide resulted in the appearance of protein bands with lower molecular weight, verifying the absence of disulfide-bonded YFP-rprestin oligomers (Fig. 7C). We conclude that PFO does not conserve the oligomeric state of rat prestin.

Functional Interaction between Prestin Subunits In a dimeric assembly, each subunit can be functionally independent, or alternatively, the two neighboring subunits can cooperate in performing a certain protein function. To study whether the two subunits of the motor protein prestin interact functionally, we co-expressed two mutant proteins – D154N and D342Q (29). In agreement with an earlier report (29), D154N shifts the voltage dependence of the non-linear capacitance to more negative voltages and D342Q shifts the voltage dependence to more positive ones (Fig. 8A). The voltage dependence of the non-linear capacitance of prestin can be fit with a derivative of a Boltzmann equation, providing values for the potential at which the half-maximal charge transfer has occurred ($V_{1/2}$) and the number of elementary charges displaced across a fraction of the membrane during the voltage-dependent conformational change (Table 1).

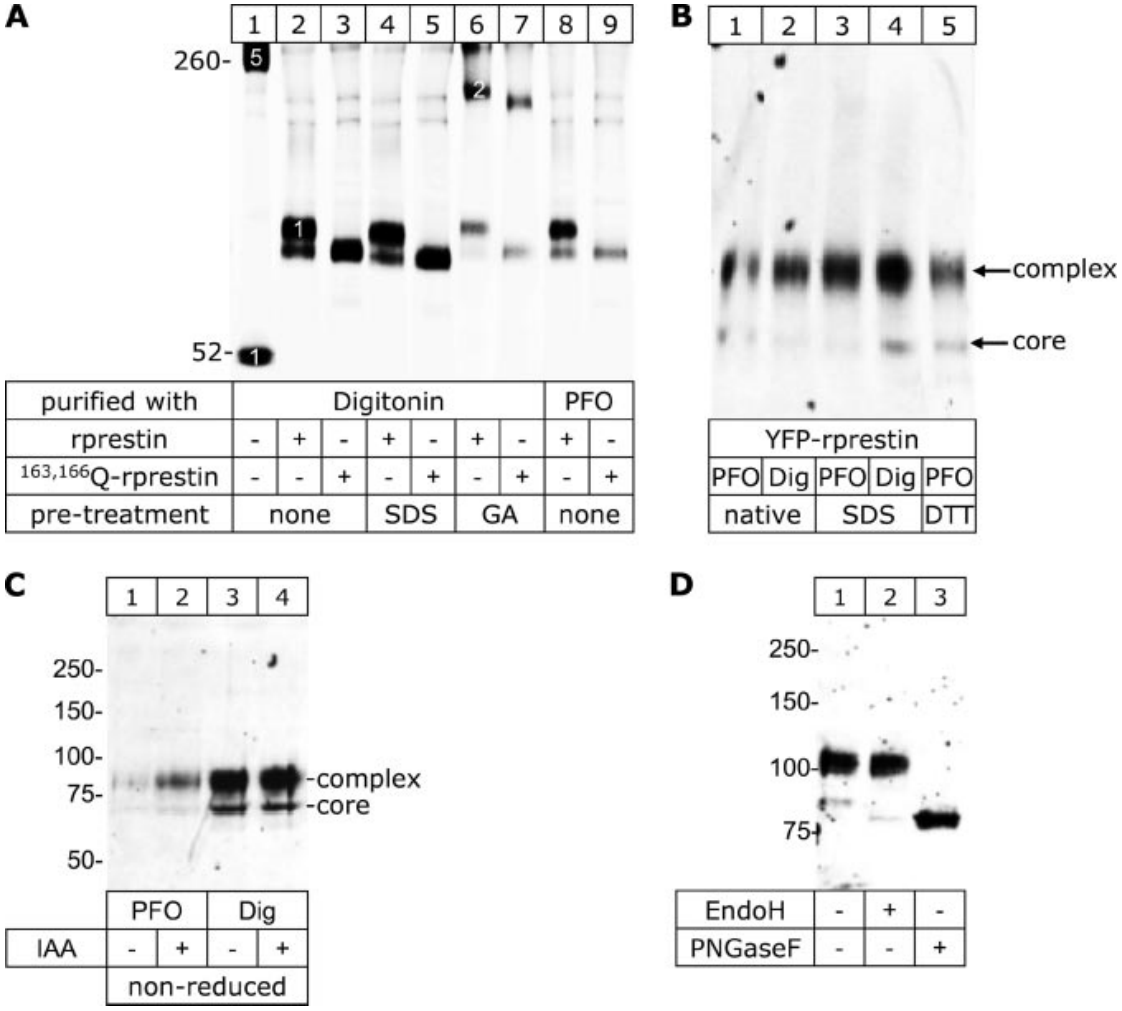

Abbildung 4.7: **Figure 7. PFO and PFO-PAGE exert protein-denaturing functions.** *A*, autoradiography of a PFO-PAGE gel (8% acrylamide) of rat prestins isolated from 1% digitonin extracts of *X. laevis* oocytes after a 24-h chase following overnight [^{35}S]methionine labeling. Digitonin (0.5%) and PFO (1%) indicate the detergent used for elution from the Ni^{2+}-NTA-agarose. Where indicated, samples were partially denatured with 0.1% SDS (1 h at 37 °C). GA indicates that digitonin-solubilized prestin was cross-linked by 10 mM glutardialdehyde before elution from the beads. *B*, PFO-PAGE gel (6% acrylamide) of YFP-rprestin extracted with 1% digitonin or 1% PFO from Flp-In-T-Rex cells stably expressing YFP-rprestin cells induced by 1 µg/ml of tetracycline for 24 h. Where indicated, samples were incubated with 0.1% SDS or 0.1 M DTT for 1 h at 37 °C before being loaded onto the gel. *C*, YFP-rprestin samples from the same experiment as shown in *B* were resolved by non-reducing SDS-PAGE. *IAA* indicates whether or not 10 mM iodoacetamide was present in the extraction buffer. *D*, the same YFP-prestin sample as in lane 4 of *C* was deglycosylated with EndoH or PNGase F as indicated and resolved by reducing SDS-PAGE. Masses of the All Blue Precision Plus Protein standard (Bio-Rad) are given on the left.

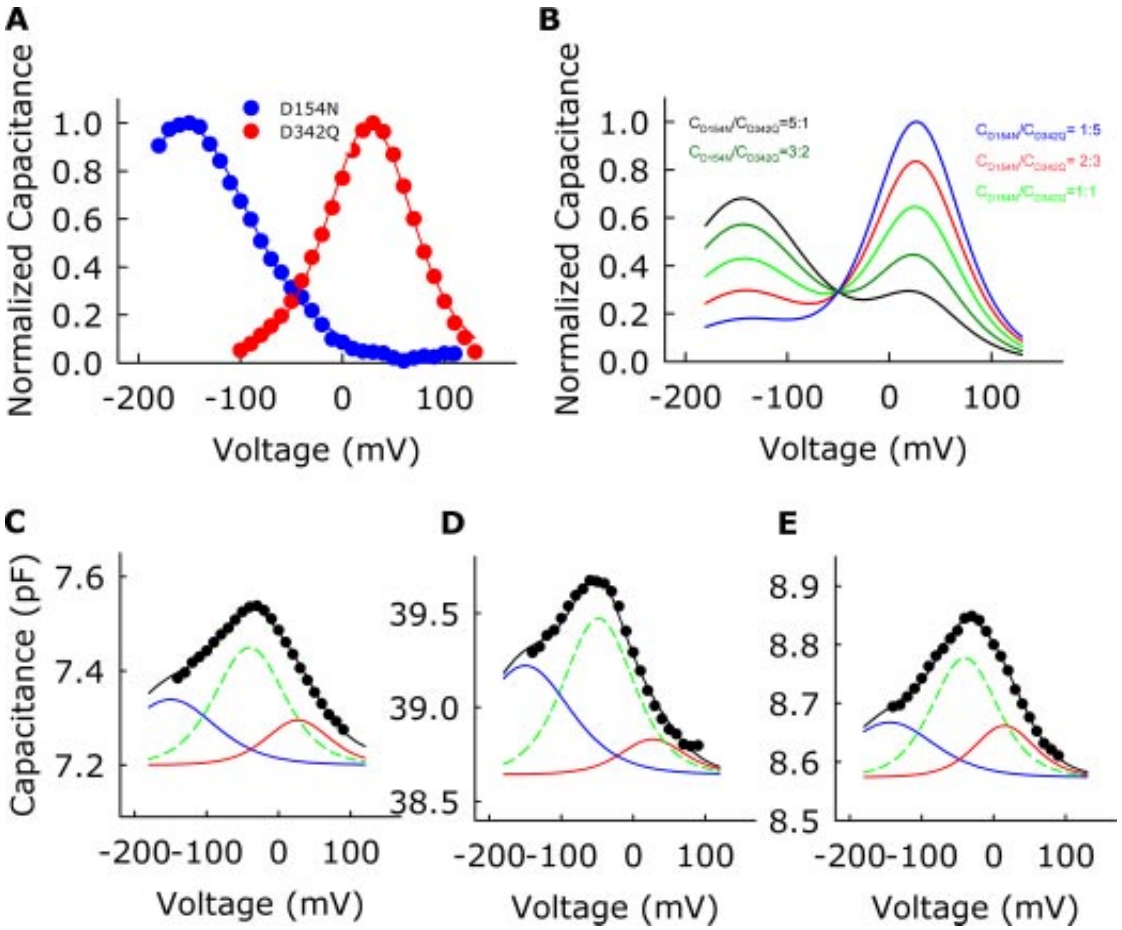

Abbildung 4.8: **Figure 8. Non-linear capacitance in tsA201 cells co-expressing mutant rat prestin.** *A*, voltage dependence of the non-linear capacitance of tsA201 cells expressing either D154N or D342Q prestin. *B*, simulated voltage dependence of the non-linear capacitance of cells co-expressing D154N and D342Q prestin without functional interaction between the subunits. *C–E*, voltage dependence of the non-linear capacitance measured on three different cells co-transfected with D154N and D342Q prestin. The solid black line represents a fit of a sum of three first derivatives of a Boltzmann term to the measured values. Colored lines show the voltage dependence of the three components: red and blue correspond to the capacitance conferred by the homodimeric motor proteins, green corresponds to the hetero-oligomers.

Table 1. Fit parameters of the voltage dependences of non-linear charge movement of homodimeric mutant and heterodimeric rat prestin.

	$V_{1/2}$ (mV)	β (mV^{-1})
D154N (n = 6)	-144 ± 13	0.024 ± 0.004
D342Q (n = 4)	15 ± 12	0.036 ± 0.001
Heterodimer (n = 3)	-43 ± 4	0.034 ± 0.003

In case of a parallel action of the two subunits without functional interactions, the voltage dependence of the non-linear capacitance of heterodimeric prestin will be the addition of the respective voltage dependences of each homo-dimeric transporter. In contrast, any cooperative interaction during the voltage-dependent conformational change will cause a deviation of the voltage dependence of the heterodimeric motor protein from this superposition. Fig. 8B shows the simulated voltage dependences of the non-linear capacitance ($C_{nonlin} - V$) curves, assuming no interaction between D154N and D342Q prestin in a heterodimeric motor protein. All the simulated $C_{nonlin} - V$ curves showed two clearly separated maxima with amplitudes that correspond to the relative amplitude of the individual components.

Non-linear capacitances from co-transfected cells are different from the simple sum of the capacitances generated by the two mutant motor proteins (Fig. 8, C–E). The $C_{nonlin} - V$ curves exhibit a single peak that is significantly broader than the ones observed in cells expressing only a single type of prestin. Heterodimeric motor proteins thus undergo conformational changes whose voltage dependence is jointly determined by both subunits. Such a behavior can only be found in case of a functional interaction of the two subunits. Conformational changes of one prestin molecule are modified by the contralateral subunit in the dimeric motor protein.

This functional assay did not only provide evidence for a functional interaction between subunits but also further support for a dimeric structure of prestin. For a dimeric protein, cells co-transfected with two plasmids are expected to express three populations, homodimeric D154N, homodimeric D342Q, and heterodimeric motor proteins consisting of one D154N and one D342Q subunit. We thus fitted the experimentally observed voltage dependences of non-linear capacitances with the sum of three first derivatives of a two-state Boltzmann function. For the two of the three that corresponded to the homodimeric populations, $V_{1/2}$ and $z\delta$ were fixed to the values obtained from cells only transfected with one mutant, and only the relative amplitude Q_{max} was adjusted as a fit parameter. For the third term, $V_{1/2}$, $z\delta$, and Q_{max} were optimized as fit parameters. For all tested cells, the values for $V_{1/2}$ and $z\delta$ of the third fitted component were very similar (Table 1). Such behavior is in full agreement with a dimeric assembly. It is inconsistent with a tetramer, for which the third capacitance component would represent three hetero-multimeric components, whose relative contribution would depend on the relative number of the two mutant subunits in the oligomer.

Discussion

SLC26 is a gene family encoding anion transporters, anion channels, and membrane-bound motor proteins. The first evidence for SLC26 multimerization came from fluorescence resonance energy transfer experiments that demonstrated a close proximity between fluorescently tagged carboxyl termini of two prestin subunits (42–44). The number of subunits necessary to form a functional motor protein was first addressed by Zheng *et al.* (34). In that study, native and recombinant prestin were shown to form stable oligomers that resisted dissociation into monomers by SDS. Chemical cross-linking and PFO-PAGE combined with immunoblotting and affinity purification suggested a tetrameric subunit stoichiometry of prestin. SDS dissociated the tetramer into dimers that could be converted to monomers by hydrophobic reducing agents but not by the hydrophilic ones. The authors concluded that prestin monomers are covalently linked to dimers by disulfide bonds located in the hydrophobic membrane core and that these covalently linked dimers associate to form a tetramer.

Our results are in contrast to those published findings. BN-PAGE and chemical cross-linking demonstrated that neither prestin nor any other tested SLC26 isoform was linked by disulfide bonds, and all SLC26s formed dimers as predominant oligomeric state. Oligomers dissociated entirely into monomers under non-reducing conditions in the presence of low concentrations of SDS. The use of a tandem concatamer as a mass marker corroborated the correct assignment of BN-PAGE bands to certain oligomeric states of rat prestin. Not only all tested eukaryotic, but also a prokaryotic SLC26 exhibits a dimeric subunit stoichiometry. After expression in *Xenopus* oocytes, a paralog from *P. aeruginosa* migrates exclusively as dimer in BN-PAGE. Because our experiments were performed with rat and zebrafish prestin and those of the other study with gerbil SLC26A5/prestin (34), these differences might be due to isoform-specific locations of cysteine residues. This is not the case: all cysteines are fully conserved in human, rat, mouse, and gerbil prestin, but not in the zebrafish isoform (supplemental Fig. S2). It appears furthermore possible that SLC26s exhibit both oligomerization states, dimers as well as tetramers, as reported for a member of another anion transporter family (SLC4) (45). However, the complete absence of tetramers in all our assays argues against this possibility. We can thus only speculate about the reasons for the different results of our group and those by Zheng *et al.* (34). We solubilized prestin with digitonin, whereas Zheng et al. used PFO (34). Digitonin has a strong record as an efficient and gentle detergent for the extraction of membrane protein complexes prone to dissociation by treatment with other detergents (46, 47). The combination of digitonin solubilization and BN-PAGE has been demonstrated to faithfully display the subunit stoichiometry of various membrane proteins, such as the mitochondrial protein import machinery, oxidative phosphorylation supercomplexes (47), various ligand-gated ion channels (18, 32, 35), transporters (32, 48), and membrane-bound enzymes (49). In contrast, PFO-PAGE dissociates membrane-bound enzymes (50), ion channels (ionotropic γ-aminobutyric acid (24) and glycine receptors (Fig. 7)), as well as transporters (a bacterial glutamate transporter6). PFO also dissociates prestin (Fig. 7, A and B). To explain the occurrence of oligomers resistant to both SDS and DTT (see Zheng *et al.* Fig. 6, A and B), we suggest that prestin may have aggregated during or after protein solubiliza-

tion to form random oligomers. Alternatively, intersubunit disulfide bond formation could have occurred during purification in those experiments in which iodoacetamide was not added. Even small amounts of such non-physiological higher order oligomers can be detected by the highly sensitive Western blot technique (34). In contrast, we used metabolic labeling or labeling with fluorescent proteins, both permitting a quantification of the relative amounts of several protein fractions.

The difference in detection might also explain the dissimilar outcome of the chemical cross-linking. In the previous study, dimers were the predominant state, although trimers and tetramers were observed (34). Cross-linking combined with Western blotting provides semi-quantitative data about the abundance of the distinct oligomeric states. Moreover, at high membrane densities, which are likely to occur in the mammalian cochlea, unspecific cross-linking can occur between neighboring protein complexes. A limitation of BN-PAGE analysis in determining the native oligomeric state of proteins is that solubilization of the protein might dissociate weak protein-protein interactions. It thus appears possible that SLC26s form stable dimers that associate to higher order oligomers in the native membrane, i.e. tetramers that are dissociated during solubilization or gel electrophoresis. The results of our cross-linking experiments (Figs. 4, 5E, and 7A) and the functional analysis of cells co-transfected with two mutant prestin proteins with different voltage dependences of the non-linear capacitance (Fig. 8) argue against this possibility. Co-transfection resulted in the formation of heterooligomers with distinct voltage dependences. The voltage dependence of the non-linear capacitance of co-transfected cells could be well fit assuming only a single population of hetero-oligomers without evidence for a cooperative interaction of more than two subunits. These data demonstrate that a dimeric assembly is the functional unit of prestin.

Heterodimeric D154N-D342Q prestin exhibits voltage-dependent capacitances that are different from D154N and D342Q homodimeric proteins. The two mutations thus do not exert an additive effect, as expected in case of two independently functioning subunits. The two subunits rather jointly determine the voltage dependence of conformational changes of the dimeric protein. This inter-subunit interaction explains the recent finding of a missense mutation in the *pres* gene found in a heterozygous hearing-impaired patient (51). The mutation results in a shift of the voltage dependence of non-linear capacitance. It can result in a dominant inheritance mode, because heterodimeric prestin consisting of WT and mutant prestin exhibits an intermediate phenotype. At present, it is unknown if inter-subunit interactions occur in SLC26 transporters and channels. For all inherited diseases linked to these SLC26 genes, the inheritance mode is recessive (3). The interaction between prestin subunits is weak. BN-PAGE of rat prestin reveals a significant percentage of monomeric proteins (Fig. 3), and cross-linking increases the percentage of dimers to only ~80% (Fig. 4). Hence, a certain fraction of monomers exists in intracellular compartments or in the surface membrane.

Many known transporter families have been shown to form oligomeric proteins. Members of the SLC1 family are assembled as trimers (32, 38), whereas SLC4, SLC6, and ClC transporters form dimers (40, 52, 53). In oligomeric transporters two different forms of intersubunit inter-

actions are possible. The subunits could jointly contribute to a central carrier or motor protein domain, or each subunit might be capable of functioning by itself. SLC1 (38), SLC4 (52), and ClC (40) transporters exhibit multibarreled structures with two or three carrier domains each formed by a single subunit. The ClC family contains channels and transporters, and for ClC channels cooperative gating steps have been reported (54). In SLC1 transporters, each subunit appears to function independently of each other (55). Because prestin dimers are not very stable (Fig. 3) and because the inheritance mode of SLC26-linked diseases is in general recessive, the formation of a common carrier or motor protein domain appears unlikely. A likely explanation for all our results is that two SLC26 subunits work in parallel but interact allosterically.

Two different transmembrane topology models of prestin are currently considered. Both place the amino and the carboxyl termini at the intracellular membrane side, but differ in the number of transmembrane helices. Although Zheng and colleagues postulated 12 transmembrane helices (56), a revised topology model contains only 10 transmembrane domains (42). We here confirm that rat prestin is a glycoprotein with two N-glycans at Asn^{163} and Asn^{166} (26) and demonstrate that zebrafish prestin and human SLC26A3 carry two N-glycans at corresponding localizations. SLC26A3 harbors one additional N-glycan in position Asn^{153}, which is also located in the predicted second extracellular loop. Three N-glycosylation sequons in the rat prestin sequence remain unused: ^{589}NATV, ^{603}NATK, and ^{736}NATP. The non-usage of ^{736}NATP does not provide topological information, because a proline in the +4 position is known to prevent N-glycosylation. In contrast, the lack of glycosylation of ^{589}NATV and ^{603}NATK supports the cytosolic localization of these residues. The glycosylation states of various SLC26s strongly support the topology model with 12 transmembrane domains.

We conclude that a dimeric subunit stoichiometry is general to prokaryotic and eukaryotic SLC26 isoforms. Three different approaches demonstrated a dimeric subunit stoichiometry for one mammalian anion exchanger, one mammalian motor pro- tein, one zebrafish prestin homologue, and one prokaryotic paralog. Isoform-specific functional differences therefore do not originate from differences in the quaternary structure.

Acknowledgments *— We thank Drs. B. Fakler and D. B. Mount for providing expression constructs for rat prestin, zebrafish prestin, and human SLC26A3.*

References

1. Bissig, M., Hagenbuch, B., Stieger, B., Koller, T., and Meier, P. J. (1994) *J. Biol. Chem.* **269**, 3017–3021

2. Mount, D. B., and Romero, M. F. (2004) *Pflugers Arch.* **447**, 710–721

3. Everett, L. A., and Green, E. D. (1999) *Hum. Mol. Genet.* **8**, 1883–1891

4. Liu, X. Z., Ouyang, X. M., Xia, X. J., Zheng, J., Pandya, A., Li, F., Du, L. L., Welch, K.

O., Petit, C., Smith, R. J., Webb, B. T., Yan, D., Arnos, K. S., Corey, D., Dallos, P., Nance, W. E., and Chen, Z. Y. (2003) *Hum. Mol. Genet*. **12**, 1155–1162

5. Jiang, Z., Grichtchenko, I. I., Boron, W. F., and Aronson, P. S. (2002) *J. Biol. Chem*. **277**, 33963–33967

6. Moseley, R. H., Hoglund, P., Wu, G. D., Silberg, D. G., Haila, S., de la Chapelle, A., Holmberg, C., and Kere, J. (1999) *Am. J. Physiol*. **276**, G185–G192

7. Scott, D. A., and Karniski, L. P. (2000) *Am. J. Physiol*. **278**, C207–C211

8. Soleimani, M., Greeley, T., Petrovic, S., Wang, Z., Amlal, H., Kopp, P., and Burnham, C. E. (2001) *Am. J. Physiol*. **280**, F356–F364

9. Xie, Q., Welch, R., Mercado, A., Romero, M. F., and Mount, D. B. (2002) *Am. J. Physiol*. **283**, F826–F838

10. Zheng, J., Shen, W., He, D. Z., Long, K. B., Madison, L. D., and Dallos, P. (2000) *Nature* **405**, 149–155

11. Dallos, P., and Fakler, B. (2002) *Nat. Rev. Mol. Cell. Biol*. 3, 104–111

12. Kim, K. H., Shcheynikov, N., Wang, Y., and Muallem, S. (2005) *J. Biol. Chem*. **280**, 6463–6470

13. Dorwart, M. R., Shcheynikov, N., Wang, Y., Stippec, S., and Muallem, S. (2007) *J. Physiol*. **584**, 333–345

14. Schweinfest, C. W., Henderson, K. W., Suster, S., Kondoh, N., and Papas, T. S. (1993) *Proc. Natl. Acad. Sci. U.S.A*. **90**, 4166–4170

15. Weber, T., Gopfert, M. C., Winter, H., Zimmermann, U., Kohler, H., Meier, A., Hendrich, O., Rohbock, K., Robert, D., and Knipper, M. (2003) *Proc. Natl. Acad. Sci. U.S.A*. **100**, 7690–7695

16. Liman, E. R., Tytgat, J., and Hess, P. (1992) *Neuron* **9**, 861–871

17. Nicke, A., Rettinger, J., and Schmalzing, G. (2003) *Mol. Pharmacol*. **63**, 243–252

18. Nicke, A., Baumert, H. G., Rettinger, J., Eichele, A., Lambrecht, G., Mutschler, E., and Schmalzing, G. (1998) *EMBO J*. **17**, 3016–3028

19. Hebeisen, S., Biela, A., Giese, B., Muller-Newen, G., Hidalgo, P., and Fahlke, Ch. (2004) *J. Biol. Chem*. **279**, 13140–13147

20. Santos-Sacchi, J., Kakehata, S., and Takahashi, S. (1998) *J. Physiol*. **510**, 225–235

21. Santos-Sacchi, J. (1991) *J. Neurosci*. **11**, 3096–3110

22. Sadtler, S., Laube, B., Lashub, A., Nicke, A., Betz, H., and Schmalzing, G. (2003) *J. Biol. Chem*. **278**, 16782–16790

23. Griffon, N., Buttner, C., Nicke, A., Kuhse, J., Schmalzing, G., and Betz, H. (1999) *EMBO J*. **18**, 4711–4721

24. Ramjeesingh, M., Huan, L. J., Garami, E., and Bear, C. E. (1999) *Biochem. J*. **342**, 119–123

25. Xu, J., Liu, Y., Yang, Y., Bates, S., and Zhang, J. T. (2004) *J. Biol. Chem*. **279**, 19781–19789

26. Matsuda, K., Zheng, J., Du, G. G., Klocker, N., Madison, L. D., and Dallos, P. (2004) *J. Neurochem*. **89**, 928–938

27. Moseley, R. H., Hoglund, P., Wu, G. D., Silberg, D. G., Haila, S., de la, C. A., Holmberg, C., and Kere, J. (1999) *Am. J. Physiol*. **276**, G185–G192

28. Melvin, J. E., Park, K., Richardson, L., Schultheis, P. J., and Shull, G. E. (1999) *J. Biol. Chem*. **274**, 22855–22861

29. Oliver, D., He, D. Z., Klocker, N., Ludwig, J., Schulte, U., Waldegger, S., Ruppersberg, J. P., Dallos, P., and Fakler, B. (2001) *Science* **292**, 2340–2343

30. Albert, J. T., Winter, H., Schaechinger, T. J., Weber, T., Wang, X., He, D. Z., Hendrich, O., Geisler, H. S., Zimmermann, U., Oelmann, K., Knipper, M., Gopfert, M. C., and Oliver, D. (2007) *J. Physiol*. **580**, 451–461

31. Schaechinger, T. J., and Oliver, D. (2007) *Proc. Natl. Acad. Sci. U.S.A*. **104**, 7693–7698

32. Gendreau, S., Voswinkel, S., Torres-Salazar, D., Lang, N., Heidtmann, H., Detro-Dassen, S., Schmalzing, G., Hidalgo, P., and Fahlke, Ch. (2004) *J. Biol. Chem*. **279**, 39505–39512

33. Gavel, Y., and von Heijne, G. (1990) *Protein Eng*. **3**, 433–442

34. Zheng, J., Du, G. G., Anderson, C. T., Keller, J. P., Orem, A., Dallos, P., and Cheatham, M. (2006) *J. Biol. Chem*. **281**, 19916–19924

35. Nicke, A., Rettinger, J., Mutschler, E., and Schmalzing, G. (1999) *J. Receptor & Signal Transd. Res*. **19**, 493–507

36. Buttner, C., Sadtler, S., Leyendecker, A., Laube, B., Griffon, N., Betz, H., and Schmalzing, G. (2001) *J. Biol. Chem*. **276**, 42978–42985

37. Koch, H. P., and Larsson, H. P. (2005) *J. Neurosci*. **25**, 1730–1736

38. Yernool, D., Boudker, O., Jin, Y., and Gouaux, E. (2004) Nature **431**, 811–818

39. Fahlke, Ch., Knittle, T. J., Gurnett, C. A., Campbell, K. P., and George, A. L., Jr. (1997) *J. Gen. Physiol*. **109**, 93–104

40. Dutzler, R., Campbell, E. D., Cadene, M., Chait, M. B., and MacKinnon, R. (2002) *Nature* **415**, 287–294

41. Schmidt-Rose, T., and Jentsch, T. J. (1997) *Proc. Natl. Acad. Sci. U.S.A*. **94**, 7633–7638

42. Navaratnam, D., Bai, J. P., Samaranayake, H., and Santos-Sacchi, J. (2005) *Biophys. J*. **89**, 3345–3352

43. Wu, X., Currall, B., Yamashita, T., Parker, L. L., Hallworth, R., and Zuo, J. (2007) *Dev. Neurobiol*. **67**, 483–497

44. Greeson, J. N., Organ, L. E., Pereira, F. A., and Raphael, R. M. (2006) *Brain Res*. **1091**, 140–150

45. Casey, J. R., and Reithmeier, R. A. (1991) *J. Biol. Chem*. 266, 15726–15737

46. Schmalzing, G., Kroner, S., Schachner, M., and Gloor, S. (1992) *J. Biol. Chem*. **267**, 20212–20216

47. Krause, F. (2006) *Electrophoresis* **27**, 2759–2781

48. Fernandez, E., Jimenez-Vidal, M., Calvo, M., Zorzano, A., Tebar, F., Pala- cin, M., and Chillaron, J. (2006) *J. Biol. Chem*. **281**, 26552–26561

49. Failer, B. U., Aschrafi, A., Schmalzing, G., and Zimmermann, H. (2003) *Eur. J. Biochem*. **270**, 1802–1809

50. Lieberman, R. L., Shrestha, D. B., Doan, P. E., Hoffman, B. M., Stemmler, T. L., and Rosenzweig, A. C. (2003) *Proc. Natl. Acad. Sci. U.S.A*. **100**, 3820–3825

51. Toth, T., Deak, L., Fazakas, F., Zheng, J., Muszbek, L., and Sziklai, I. (2007) *Int. J. Mol. Med*. **20**, 545–550

52. Wang, D. N., Sarabia, V. E., Reithmeier, R. A., and Kuhlbrandt, W. (1994) *EMBO J*. **13**, 3230–3235

53. Yamashita, A., Singh, S. K., Kawate, T., Jin, Y., and Gouaux, E. (2005) *Nature* **437**, 215–223

54. Miller, C. (1982) Philos. Trans. R. *Soc. Lond. B. Biol. Sci*. **299**, 401–411

55. Grewer, C., Balani, P., Weidenfeller, C., Bartusel, T., Tao, Z., and Rauen, T. (2005) *Biochemistry* **44**, 11913–11923

56. Zheng, J., Long, K. B., Shen, W., Madison, L. D., and Dallos, P. (2001) *Neuroreport* **12**, 1929–1935

Anion transport by the cochlear motor protein prestin

Michael Schänzler[1] and Christoph Fahlke[1,2]

[1]Institut für Neurophysiologie, Medizinische Hochschule, Hannover, Germany

[2]Zentrum für Systemische Neurowissenschaften, Hannover (ZSN), Germany

Prestin is a member of the SLC26 solute carrier family and functions as a motor protein in cochlear outer hair cells. While other SLC26 homologues were demonstrated to transport a wide variety of anions, no electrogenic transport activity has been assigned so far to mammalian prestin. We here use heterologous expression in mammalian cells, patch clamp recordings and measurements of expression levels of individual cells to study anion transport by rat prestin. We demonstrated that cells expressing rat prestin exhibit SCN^- currents that are proportional to the number of prestin molecules. Variation of the SCN^- concentration resulted in changes of the current reversal potential that obey the Nernst equation indicating that SCN^- transport is not stoichiometrically coupled to other anions. Application of external SCN^- causes large increases of anion currents, but only minor changes in non-linear charge movements suggesting that only a very small percentage of prestin molecules function as SCN^- transporters under these conditions. Unitary current amplitudes are below the resolution limit of noise analysis and thus much smaller than expected for pore-mediated anion transport. A comparison with a non-mammalian prestin from D. rerio – recently shown to function as Cl^-/SO_4^{2-} antiporter – and an SLC26 anion channel, human SLC26A7, revealed that SCN^- transport is conserved in these distinct members of the SLC26 family. We conclude that mammalian prestin is capable of mediating electrogenic anion transport and suggest that SLC26 proteins converting membrane voltage oscillations into conformational changes and those functioning as channels or transporters share certain transport capabilities.

The solute carrier 26 (SLC26) gene family encodes multifunctional membrane proteins in numerous tissues and organs (Mount & Romero, 2004). Eleven human members have been identified including one non-coding pseudogene. The physiological importance of these proteins is highlighted by several inherited human diseases caused by mutations in SLC26 genes (Everett & Green, 1999; Liu *et al*. 2003), such as diastrophic dysplasia, congenital chloride diarrhoea, and inner ear deafness. The symptomatic diversity of these diseases illustrates the variety of cellular functions relating to this class of transport proteins. Most mammalian SLC26 proteins operate as anion exchangers with distinct substrate specificities (Bissig *et al*. 1994; Moseley *et*

al. 1999; Scott & Karniski, 2000; Soleimani *et al*. 2001; Jiang *et al*. 2002; Xie *et al*. 2002). However, there are also family members that exhibit additional transport properties. SLC26A7 and SLC26A9 have been reported to function as anion carriers (Petrovic *et al*. 2004; Xu *et al*. 2005), but there is also experimental evidence for anion channel activity (Kim *et al*. 2005; Dorwart *et al*. 2007; Chang *et al*. 2009). SLC26A5/prestin represents a motor protein that allows outer hair cells in the mammalian cochlea to change length in response to acoustic signals (Zheng *et al*. 2000; Dallos & Fakler, 2002). This function results in mechanical sound amplification and enhances the hearing sensitivity by more than 40 dB. The basis for these length changes are voltage-dependent conformational changes that result in voltage-dependent capacitances of cells expressing prestin (Santos-Sacchi, 1991; Zheng *et al*. 2000). Non-mammalian prestin orthologues from chicken and zebrafish (Weber *et al*. 2003; Albert *et al*. 2007; Tan *et al*. 2011) function as electrogenic chloride/sulfate antiporters, suggesting that the mechanism by which prestin generates electromotility is evolutionarily derived from a transport cycle (Schaechinger & Oliver, 2007). At present, it is unclear whether mammalian prestin can mediate anion transport. Whereas Bai *et al*. (2009) recently demonstrated that mammalian cells expressing gerbil prestin were capable of accumulating radioactive formate and oxalate, a subsequent study by Tan *et al*. (2010) did not observe a statistically significant difference between mammalian prestin and negative controls.

Using electrophysiological techniques, we studied here the transport of another anion, the pseudohalide thiocyanate (SCN^-), by a mammalian prestin and compared it to SCN^-transport by zebrafish prestin and human SLC26A7. The aim of our study was to define the similarities and differences in anion transport between the three functional branches of the SLC26 family, anion channels, transporters and motor proteins, through the functional evaluation of SCN^- currents by human SLC26A7, Slc26a5 (DANRE)/prestin from *Danio rerio* (zebrafish) and SLC26A5 (RAT)/prestin from *Rattus norvegicus*.

Methods

Construction of expression plasmids and heterologous expression

pcDNA3.1(+)Zeo-(RAT) Slc26a5-His and pcDNA5/FRT/ TO-(RAT) Slc26a5-YFP encoding rat prestin (GenBank accession number NM_030840), pcDNA5FRT/TO-(DANRE) slc26a5-YFP encoding prestin from *Danio rerio* (zebrafish) (GenBank accession number BX571796) (Weber *et al*. 2003), and pcDNA5/FRT/TO-(HUMAN) SLC26A7-YFP encoding human SLC26A7 (GenBank accession number BC094730.1) (Kim *et al*. 2005) were created by PCR-based techniques, as described (Detro-Dassen *et al*. 2008). All fluorescent tags were added to the carboxy-terminus of the coding region. We expressed SLC26A5 (RAT)/prestin transiently in HEK293T cells, as described (Melzer *et al*. 2005). Moreover, we generated four inducible stable cell lines by selecting Flp-In T-REx cells (Invitrogen, Carlsbad, CA, USA) transfected with pcDNA5/FRT/TO-(RAT) Slc26a5-YFP, pcDNA5/FRT/TO-(DANRE) slc26a5-YFP, pcDNA5/FRT/TO-(HUMAN) SLC26A7-YFP or pcDNA5 /FRT/TO-YFP. Cells expressing rat or zebrafish prestin were used

after 24–48 h incubation with 1 µg ml^{-1} tetracycline, whereas inducible cells expressing human SLC26A7 or yellow fluorescent protein (YFP) alone were incubated only for 8 h prior to electrophysiological characterization (Trapani & Korn, 2003). Mammalian cells were usually cultivated in media containing fetal serum. To minimize background expression of SLC26s, we used tetracycline-free sera (fetal bovine serum (FBS) certified, Invitrogen). For all inducible cell lines expressing SLC26 fusion proteins, current amplitudes were markedly increased by induction with tetracycline. However, there was also a faint fluorescent membrane staining in the absence of tetracycline (data not shown), suggesting that expression of SLC26s also occurs in the absence of tetracycline. For control experiments, we created pcDNA3.1(+)YFP for transient expression in HEK293T cells and pcDNA5/FRT/TO-YFP for generating an inducible stable cell line expressing YFP alone.

Functional properties of YFP fusion proteins were unaltered for SLC26A5 (RAT)/prestin (Detro-Dassen *et al*. 2008), Slc26a5 (DANRE)/prestin (Detro-Dassen *et al*. 2008) and human SLC26A7 (Supplementary Fig. 1). Comparison of SCN^- currents in cells expressing YFP-tagged (Figs 3 and 4) and untagged (Figs 1 and 2) proteins demonstrate that these tags do not modify SLC26A5/prestin anion currents.

Functional characterization of SLC26A5 and SLC26A7

Transfected HEK293 or HEK293T cells were studied through whole-cell patch clamping using an Axopatch 200B amplifier (Torres-Salazar & Fahlke, 2007). Two different standard solutions with different anion current reversal potentials were used. Solution A contained (mM): 100 NaSCN, 20 CsCl, 20 TEA-Cl, 2 KCl, 2 $CaCl_2$, 2 $MgCl_2$, 2 $CoCl_2$, 5 Hepes (extracellular); and 120 CsCl, 2 $MgCl_2$, 5 EGTA, 10 Hepes (intracellular). Solution B contained (mM): 5 NaSCN, 100 NaCl, 15 CsCl, 20 TEA-Cl, 2 KCl, 2 $CaCl_2$, 2 $MgCl_2$, 2 $CoCl_2$, 5 Hepes (extracellular); and 30 NaSCN, 90 CsCl, 2 $MgCl_2$, 5 EGTA, 10 Hepes (intracellular). To compare non-linear capacitances in the presence of external Cl^- or SCN^- (Fig. 1B), external solution A was modified by replacement of external NaSCN with NaCl and sodium gluconate so that concentrations of SCN^- and Cl^- were comparable. For the experiments shown in Fig. 5, solutions were modified equimolarly by replacing NaCl or NaSCN with sodium gluconate. For experiments studying block by Cl^-/SO_4^{2-}, a bath solution containing (mM) 75 Na_2SO_4, 30 NaSCN, 2 potassium gluconate, 2 $Ca(gluconate)_2$, 2 $Mg(gluconate)_2$, 5 Hepes, and pipette solution A were used. Na_2SO_4 was replaced with sodium gluconate at a ratio of 2:3 to determine the concentration dependence of block, and NaSCN was equimolarly replaced by sodium gluconate to study isolated Cl^-/SO_4^{2-} antiport. Calculated osmolarities were 274 mosmol l^{-1} for all pipette solutions and between 310 and 312 mosmol l^{-1} for external solutions. The pH was adjusted to 7.4 for all solutions. For all experiments, absence of cell swelling was visually tested during the different phases of each experiment. The initial pipette resistances were 1–2.5 MΩ. Stray pipette capacitance was neutralized before establishing the whole-cell configuration. Agar salt bridges were used and the recorded data for Fig. 4 was additionally corrected for liquid junction potentials. In experiments determining transmembrane currents, pCLAMP9 (Molecular Devices,

Sunnyvale, CA, USA) was used for data acquisition and analysis (Detro-Dassen *et al*. 2008). To measure voltage-dependent capacitance, data acquisition and analysis were performed with the Windows-based patch-clamp program, jClamp (SciSoft, Ridgefield, CT, USA). Non-linear charge movement was calculated using a continuous high-resolution (2.56 ms sampling) two-sine stimulus protocol (10 mV peak at both 390.6 and 781.2 Hz) superimposed onto voltage steps (150 ms duration) from -160 mV to +100 mV (Santos-Sacchi *et al*. 1998). The voltage dependence of the non-linear capacitance was fit to the first derivative of a two-state Boltzmann function (Santos-Sacchi, 1991).

$$C(V) = \frac{\beta Q_{max} \, e^{-\beta(V-V_{1/2})}}{\left(1+e^{-\beta(V-V_{1/2})}\right)^2} + C_{lin} \tag{4.3}$$

with

$$\beta = z\frac{e_0\delta}{k_B T} \tag{4.4}$$

Q_{max} is the maximum charge transferred across the membrane; $V_{1/2}$ is the potential at half-maximal charge transfer; z is the number of elementary charges, e_0, displaced across a fraction, δ, of the membrane dielectric; k_B is Boltzmann's constant, and T is the absolute temperature. For experiments correlating currents and the number of SLC26-YFP fusion proteins, cells were cultivated on collagen coated glass coverslips and mounted in a perfusion chamber on an inverted IX71 micro- scope with UPlanSApo 60x/1.35 oil immersion objective (Olympus, Hamburg, Germany). YFP was excited at 500 nm using a Polychrome V fast switching monochromator and emitted fluorescence light was detected at 530 nm using a photomultiplier tube equipped ViewFinder III (Till Photonics, Gräfelfelfing, Germany) (Alekov & Fahlke, 2009). Fluorescence excitation and detection were software-controlled by the Photometry extension of PATCHMASTER. Fluorescence was measured in the linear range of the photomultiplier and detected in V. Unless otherwise stated all values are given as means ± SEM.

Confocal imaging

Live cell confocal imaging was carried out with Flp-In T-REx cells cultured in µ-Dishes (ibidi GmbH, Munich, Germany) (Riazuddin *et al*. 2009) on an Olympus IX81 inverted microscope. Image acquisition was done using the Fluoview FV1000 system (Olympus, Tokyo, Japan) with 515 nm excitation wavelength and fluorescence detection at 535–565 nm. Confocal images were superimposed on differential interference contrast (DIC) images taken simultaneously.

Results

Mammalian prestin can mediate SCN^- currents

SCN^- was recently shown to uncouple SLC26A3 and SLC26A6 anion exchangers (Shcheynikov *et al*. 2006; Ohana *et al*. 2011). To test whether SCN^- exerts similar actions on the motor

protein prestin, we studied ionic currents in HEK293T cells transiently expressing SLC26A5 (RAT)/prestin (Detro-Dassen *et al*. 2008) using whole-cell patch clamp recordings under conditions that have been shown to minimize endogenous current amplitudes in HEK293 cells (Santos-Sacchi, 2002; Farrell *et al*. 2006). With Cl^- as predominant internal and external anions, only negligible whole-cell currents could be observed (Fig. 1A, Zheng *et al*. 2000). Currents were very small in external NO_3^- (data not shown). After substitution of external Cl^- by SCN^- outwardly rectifying currents could be observed (Fig. 1A and B). Whole cell currents reversed at negative potentials as expected of anion selective currents with higher permeability for SCN^- than for Cl^-. In control cells transfected with a vector encoding YFP alone, anion current amplitudes in SCN^- are significantly smaller than those of prestin-expressing cells and negligible in external Cl^- (Fig. 1A and B).

The electrophysiological signature of prestin is voltage-dependent charge movements that report on voltage-dependent conformational changes of these proteins (Zheng *et al*. 2000). Figure 1B shows mean values for charge–voltage relationships from HEK293T cells transiently expressing SLC26A5 (RAT)/prestin in Cl^- or SCN^--based solutions. Exchange of external Cl^- to SCN^- slightly modifies prestin-associated charge movement. It shifts the operating range to more negative voltages and decreases the slope of the C–V curve. Non-linear capacitance of prestin can be described with eqn (1), the first derivative of a two-state Boltzmann probability distribution, from which the parameters Q_{max} , $V_{1/2}$ and β can be obtained by least square fitting. Q_{max} is the total amount of charge moved if all active prestin molecules transition into its alternate state (Rybalchenko & Santos-Sacchi, 2008). $V_{1/2}$ is the membrane potential resulting in a uniform distribution of prestin molecules between the two states and, as a direct consequence, the voltage at peak capacitance. The slope factor β specifies the apparent charge of the translocatable entity. Replacement of Cl^- by SCN^- decreases β and shifts the midpoint $V_{1/2}$ to more negative voltages, but does not reduce Q_{max} (Table 1).

Tabelle 4.1: **Table 1.** Fit parameters of the voltage dependences of non-linear charge movement of rat prestin in external Cl^- or SCN^-.

	$\beta\,(mV^{-1})$	$V_{1/2}\,(mV)$	$Q_{max}\,(fC)$
Cl^- (n = 10)	0.0308 ± 0.00052	-69 ± 1.4	266 ± 46
SCN^- (n = 8)	0.0231 ± 0.00089	-102 ± 3.2	290 ± 72

Heterologous expression of prestin might cause upregulation of endogenous anion channels, and the observed currents might be conducted by such channels rather than by prestin itself. SCN^- currents in transfected cells are small, and background currents are not insignificant under these conditions, making additional tests necessary to demonstrate that SLC26A5 (RAT)/prestin itself conducts SCN^-. Figure 1C plots the current amplitude at +160 mV versus Q_{max} for 30 cells. Q_{max} is proportional to the total number of functional prestin molecules in the membrane. Anion current amplitudes change linearly with the non-linear capacitance over a more than 20-

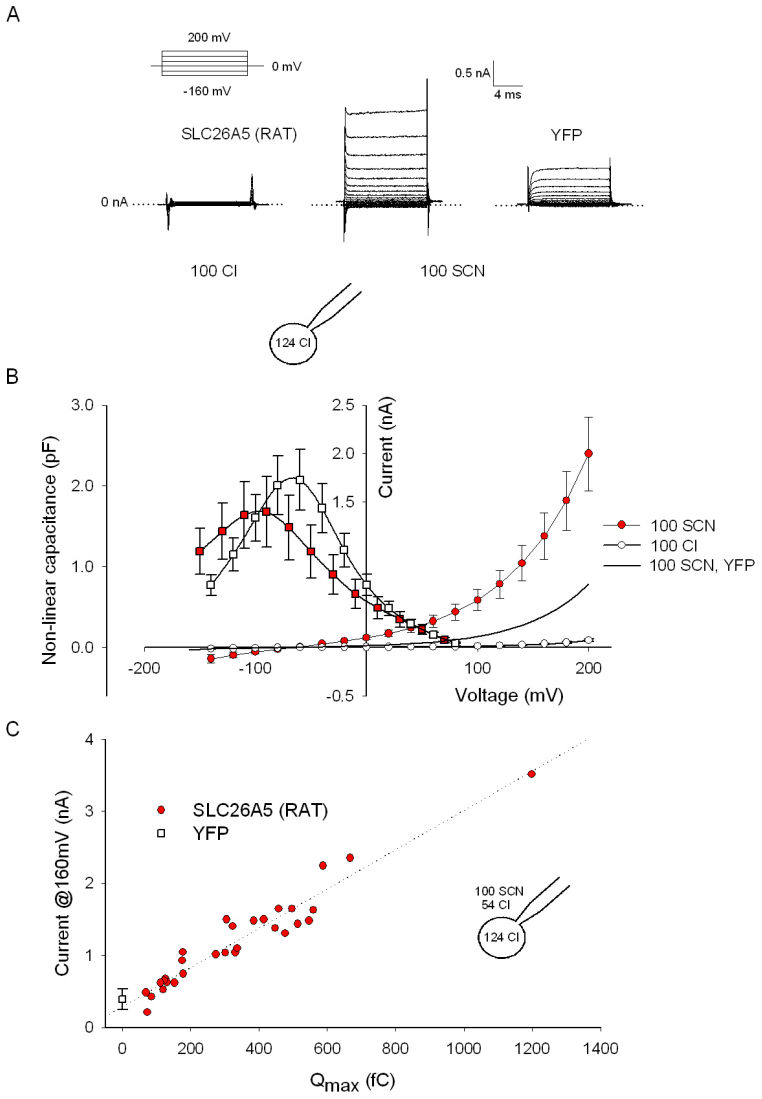

Abbildung 4.9: **Figure 1. SCN^- currents are conducted by mammalian prestin**
A, representative whole-cell currents in HEK293T cells transiently expressing SLC26A5 (RAT)/prestin with Cl^- or SCN^- as main extracellular anion. Membrane voltage was driven by a simple step protocol from –160 mV to +200 mV (upper left). The cartoon depicting the whole cell configuration illustrates the relevant ionic constituents. HEK293T cells expressing YFP were used as negative controls. *B*, voltage dependence of whole-cell capacitance (□) and current–voltage relationships (○) for SCN^-- or Cl^--based external solutions. Means ± SEM, n = (8, 10). *C*, plot of current amplitudes at +160 mV versus Q_{max} for 30 different cells. Q_{max} is proportional to the total number of active prestin molecules and was obtained by fitting the measured voltage-dependent capacitance with eqn (1). Cells expressing YFP do not exhibit non-linear capacitance and control current amplitudes are therefore given as means ± standard deviation at Q_{max} = 0 fC. The slope of the linear regression line is 2.6 pA fC^{-1}.

fold variation in the number of SLC26A5 (RAT)/prestin, demonstrating that SCN^- is transported by mammalian prestin and not by endogenous channels/transporters up-regulated by overexpression of prestin.

Noise analysis of macroscopic currents often provides information about underlying unitary current events (DeFelice, 1981). In ion channels, high unitary transport rates result in macroscopic currents whose variance is dominated by the opening and closing of individual channels. Such Lorentzian type noise is characterized by $1/f^2$ frequency dependence of the spectral density (Anderson & Stevens, 1973; DeFelice, 1981). We determined the power spectra of SLC26A5 (RAT)/prestin-mediated SCN^- currents and found them not to resemble Lorentzian noise, but rather $1/f$ frequency dependence (Fig. 2A). Since $1/f$ noise can be also observed in untransfected cells (Alekov & Fahlke, 2009), separation of prestin-associated noise from background is not possible. Moreover, no correlation between the number of prestin proteins and the whole cell current variance could be observed. Figure 2B plots the current variance at +160 mV versus the maximum voltage-dependent capacitances for 30 different cells expressing largely different amounts of SLC26A5 (RAT)/prestin. Expression of SLC26A5 (RAT)/prestin therefore does not add significant current noise above background levels, and unitary current amplitudes of SLC26A5 (RAT)/prestin cannot be determined by noise analysis. Ion channels that never close do not generate Lorentzian noise (Alvarez *et al*. 2002). The observed lack of prestin-specific noise might therefore be either due to very low unitary current amplitudes or to very high absolute open probabilities. To estimate the probability that SLC26A5 (RAT)/prestin assumes the anion conducting mode, we compared non-linear capacitances from individual cells that were consecutively perfused with external Cl^-- and SCN^--based solution (Fig. 2C). SCN^- resulted in a dramatic increase of macroscopic anion currents, but did not reduce non-linear capacitances. We rather observed in all cells a slight increase by 16 ± 7% after perfusion with SCN (n = 6), indicating that SCN^- converts only a very small number of prestin molecules into an SCN^- conducting state. Transported anions cannot stably bind to ion channels or trans- porters, and SCN^- is thus likely to induce frequent transitions between non-transporting and transporting states of SLC26A5 (RAT)/prestin. In this case, the percentage of conducting proteins equals the probability of this state, and we can thus conclude that the probability of SLC26A5 (RAT)/prestin being in a transporting/conducting mode is very low in the presence of SCN^-. The observed low current variances are therefore not due to very high open probabilities, but rather to unitary current amplitudes of SLC26A5 (RAT)/prestin that are too small to be resolved by macroscopic current noise measurements.

SCN^- currents in SLC26A5 and SLC26A7

To compare the observed prestin-mediated currents with SCN^- currents by other SLC26 proteins, we engineered inducible cell lines for fusion proteins of YFP with SLC26A5 (RAT)/prestin, Slc26a5 (DANRE)/prestin or human SLC26A7, and compared SCN^- currents by these SLC26 proteins (Fig. 3). SLC26A7 was the first SLC26 for which anion channel activity was demonstrated (Kim *et al*. 2005), and Slc26a5 (DANRE)/prestin is firmly established to function as coupled

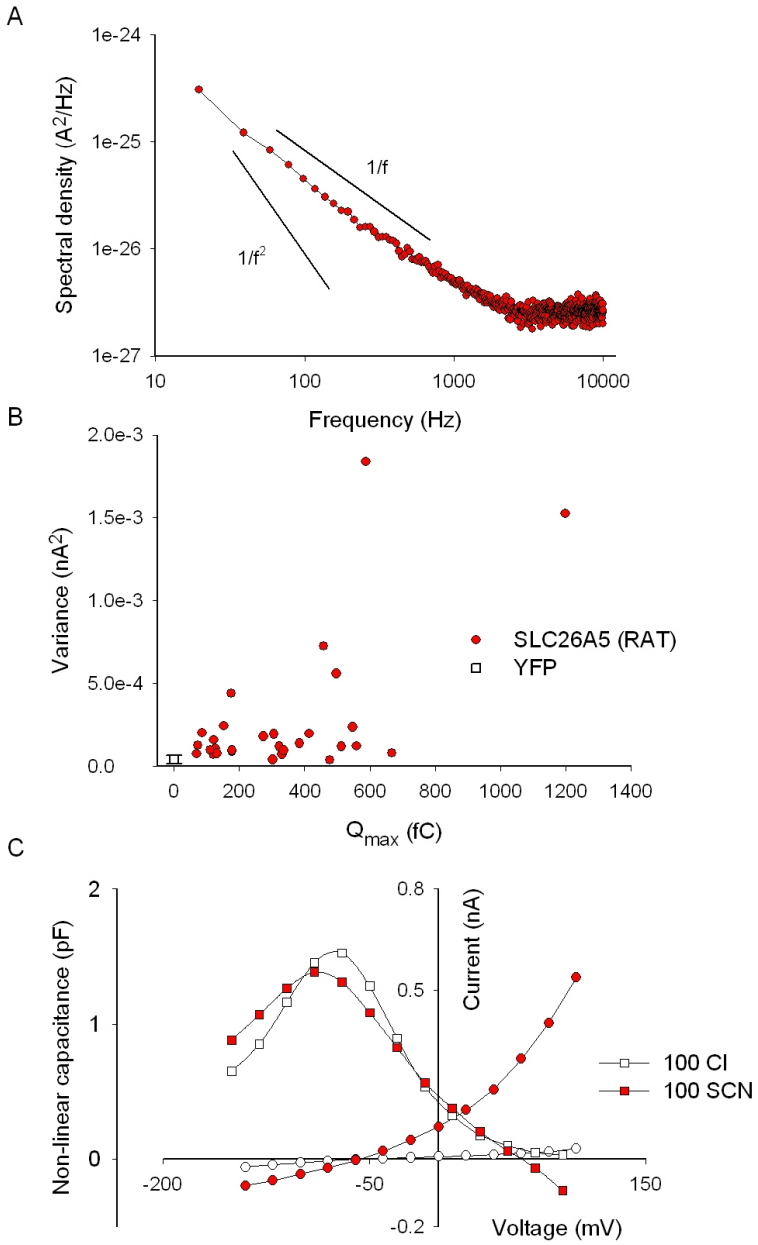

Abbildung 4.10: **Figure 2. Noise analysis of SCN^- currents mediated by SLC26A5 (RAT)/prestin** *A*, averaged power spectrum of SCN^- currents from cells expressing rat prestin. More than 30 individual current responses to +200 mV were averaged and corrected for background noise. Arbitrary continuous lines represent the expected slopes for $1/f$ noise or Lorentzian $1/f^2$ noise for comparison. *B*, variance from 10 ms long current traces at +160 mV membrane potential versus Q_{max}. Data were generated from the same experiments used for Fig. 1C. *C*, representative voltage dependence of the whole-cell capacitance (□) and SCN^- currents (•) before and following perfusion with external solutions containing 100 mM Cl^- or 100 mM SCN^-. All experiments used HEK293T cells transiently transfected with SLC26A5 (RAT)/prestin or YFP.

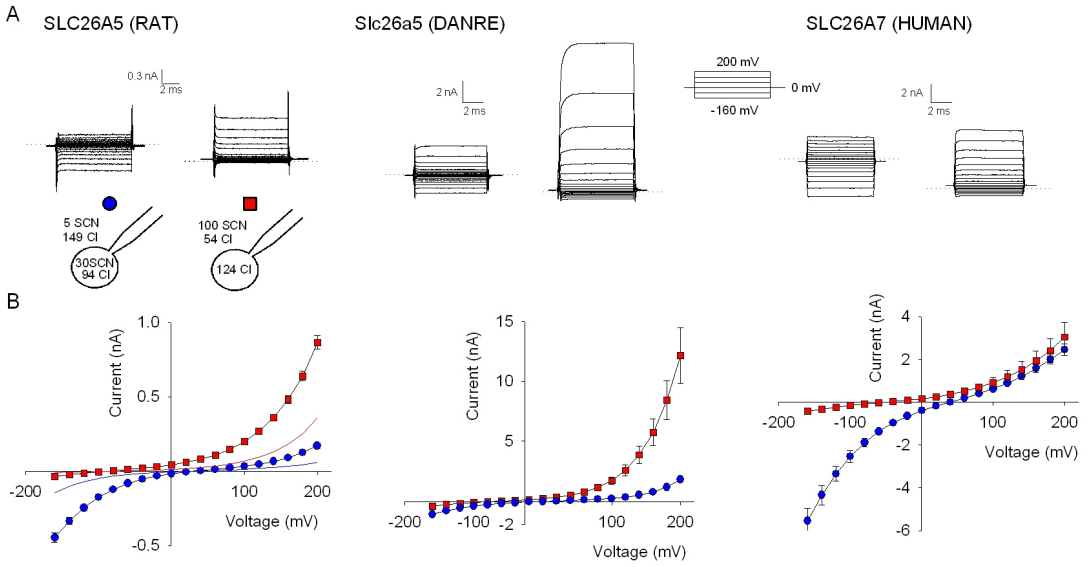

Abbildung 4.11: **Figure 3. SCN^- currents in cells stably expressing mammalian prestin, teleost prestin and human SLC26A7**
A, representative whole-cell SCN^- currents in Flp-In T-REx cells stably expressing YFP-tagged SLC26A5 (RAT)/prestin, Slc26a5 (DANRE)/prestin or human SLC26A7 for two different anion distributions shown in the cartoon. The dotted lines indicate the zero current reference level. *B*, current–voltage relationships for YFP-tagged SLC26A5 (RAT)/prestin, Slc26a5 (DANRE)/prestin or human SLC26A7 determined by current recordings as shown in A. Means ± SEM from more than 7 cells. Protein expression was induced with tetracycline 24 h before electrophysiological characterization for the two prestins and 8 h before characterization of SLC26A7.

anion exchanger (Schaechinger & Oliver, 2007). Figure 3A shows representative whole-cell currents from cells stably and inducibly expressing SLC26A5 (RAT)/prestin, Slc26a5 (DANRE)/prestin and human SLC26A7 for two different anion compositions. All tested SLC26s displayed whole-cell currents with reversal potentials that depend on the SCN^- distribution across the membrane (Fig. 3B, Table 2). SCN^- currents by Slc26a5 (DANRE)/prestin or by human SLC26A7 were larger than those of rat prestin. With external solutions containing high concentrations of thiocyanate ($[SCN^-]_o$ = 100 mM) and SCN^--free internal solutions), SLC26A5 (RAT)/prestin currents were usually below 1 nA at +200 mV after 24 h induction with tetracycline, but exceeded 10 nA in cells expressing zebrafish prestin. For human SLC26A7, currents were too large under these induction conditions, and we therefore used cells after induction for only 8 h. Plotting non-linear charge movements versus SCN^- current amplitudes allowed a comparison of protein amounts and SCN^- currents with SLC26A5 (RAT)/prestin (Fig. 1C). Since non-linear charge movement is a unique property of SLC26A5 (RAT)/prestin (Zheng *et al*. 2000; Albert *et al*. 2007), we used another approach to include all three proteins in such

comparison. SLC26 proteins were expressed as YFP fusion proteins, and YFP fluorescence thus provides a measure for the number of SLC26 proteins. Figure 4A plots whole-cell current versus whole-cell fluorescence for the three SLC26 proteins. For rat and zebrafish prestin, a linear correlation was observed, in agreement with the notion that SCN^- currents are mediated by the SLC26-YFP fusion protein. Current/fluorescence ratios are larger for Slc26a5 (DANRE)/prestin than for SLC26A5 (RAT)/prestin. Currents associated with human SLC26A7 were very large even at small fluorescence amplitudes, precluding measurements of current amplitudes over a wide variety of expression levels. However, at a given fluorescence, these currents were much larger than for the two prestins (Fig. 4A, inset).

Since the fluorescence value used does not distinguish between fusion proteins inserted into internal compartments or the surface membrane, the different slopes might be due to separate subcellular distributions of the distinct proteins. Confocal imaging of cells stably expressing SLC26A5 (RAT)/prestin or human SLC26A7 demonstrated that rat and zebrafish prestin show predominant surface staining (Fig. 4B). Although current/fluorescence ratios were much larger for human SLC26A7 than for prestin, intracellular fluorescence staining was more prominent in cells expressing human SLC26A7. SLC26A7 whole-cell currents were therefore larger than prestin currents, although a smaller percentage of protein was inserted into the surface membrane. The distinct SCN^- currents by fluorescence ratios of the three SLC26 proteins thus must be caused either by separate unitary current amplitudes or separate percentages of protein functioning as SCN^- transporters.

Concentration dependence of reversal potentials

The SLC26 family encompasses coupled anion transporters as well as anion channels (Mount & Romero, 2004, Kim et al. 2005; Dorwart et al. 2007). To distinguish between SLC26A5 functioning as coupled Cl^-/SCN^- exchanger – with a transport stoichiometry yet to be defined – or SCN^- uniporter or channel, we measured reversal potentials for a variety of SCN^- distributions across the membrane. In these experiments, the external [SCN^-] was always 5 mM. Internal and external [Cl^-] were adjusted to 94 mM and 149 mM, and internal [SCN^-] was varied between 2 and 30 mM. Figure 5A gives the concentration dependence of the reversal potential from measurements in cells expressing SLC26A5 (RAT)/prestin (filled symbol) or Slc26a5 (DANRE)/prestin (open symbol). Measured current reversal potentials were compared with predicted SCN^--diffusion potentials calculated by the Nernst equation:

$$V_{rev(SCN)} = \frac{RT}{zF} \ln \frac{[SCN^-]_i}{[SCN^-]_o} \tag{4.5}$$

or with predictions of the equilibrium potential of coupled transporters

$$V_{rev} = \frac{1}{1-r} \left(V_{rev(Cl} - rV_{rev(SCN)} \right) \tag{4.6}$$

In this formula, the coupling ratio r is defined as the ratio of the stoichiometric numbers of SCN^-($n(SCN)$) and Cl^-ions ($m(Cl)$) transported in one transport cycle ($r = n(SCN)/m(Cl)$).

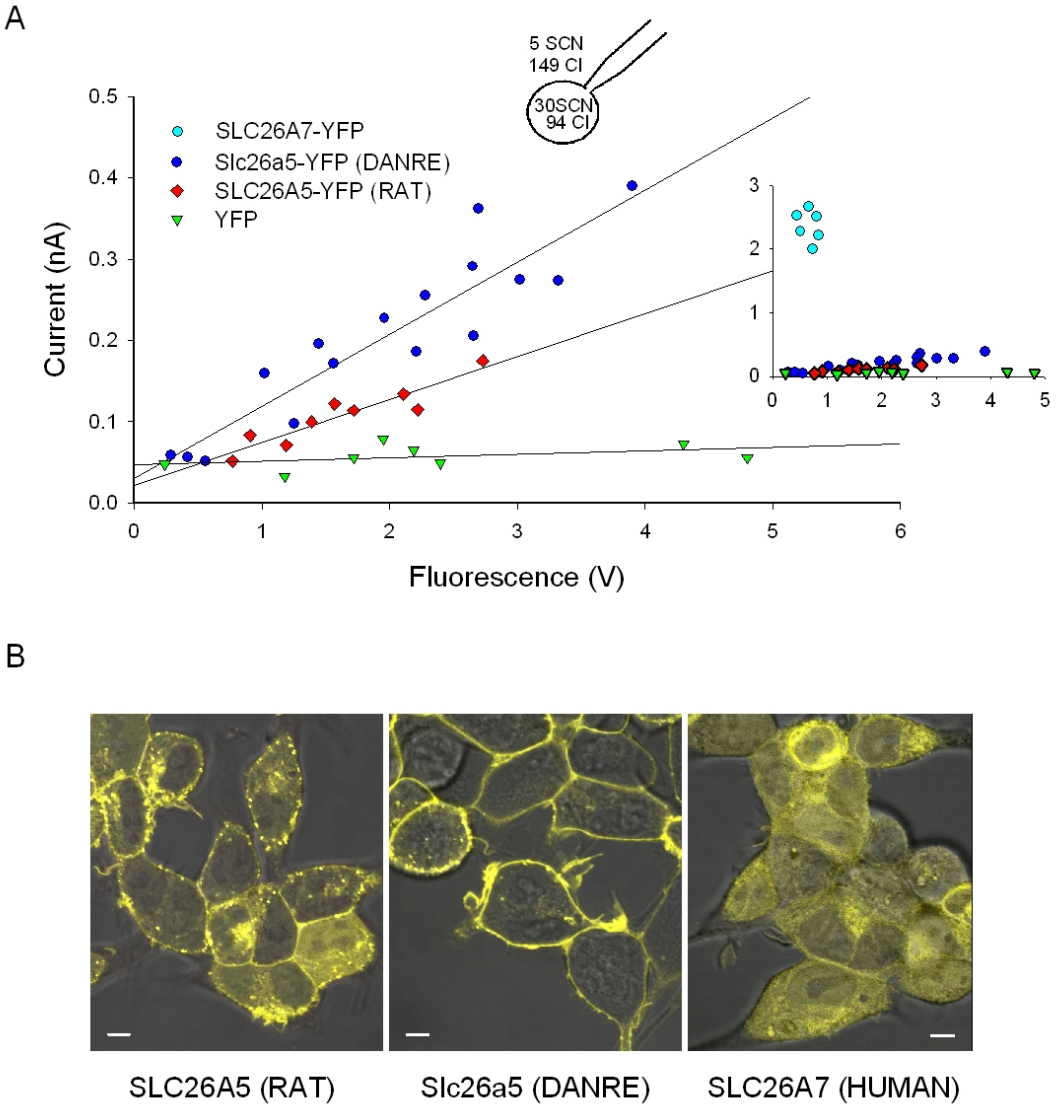

Abbildung 4.12: **Figure 4. Comparison of SCN^- transport by different SLC26s**
A, plot of whole-cell current amplitudes at –110 mV versus whole-cell fluorescence for Flip-In T-REx cells expressing YFP-tagged SLC26A5 (RAT)/prestin, Slc26a5 (DANRE)/prestin or human SLC26A7 (inset). An inducible stable cell line expressing only YFP was used as negative control. *B*, confocal images of Flp-In T-REx cells expressing the indicated YFP-tagged proteins superimposed on differential interference contrast images. Cells were incubated with tetracycline for either 24–48 h (SLC26A5 (RAT), Slc26a5 (DANRE)) or 8 h (YFP, human SLC26A7). Bar = 5 µm.

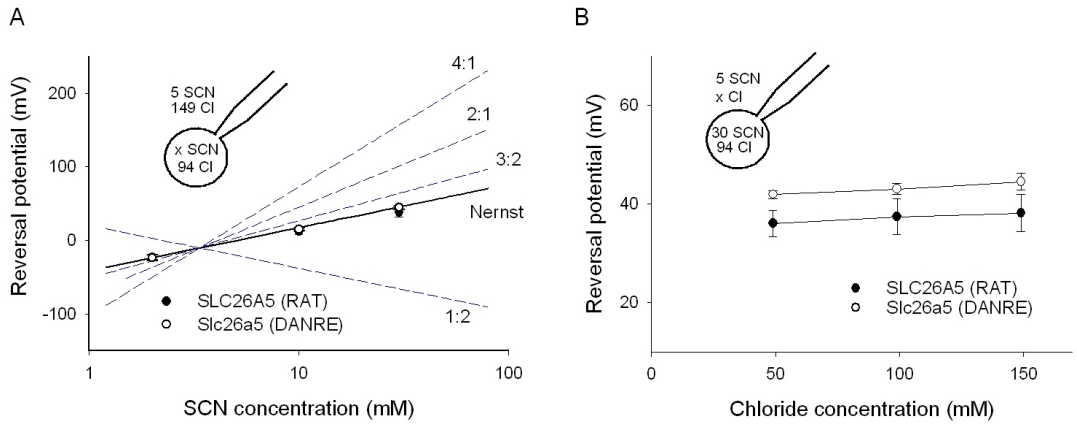

Abbildung 4.13: **Figure 5. Current reversal potentials are independent of [Cl^-] and obey the Nernst equation for [SCN^-]**

A, reversal potentials from cells expressing SLC26A5 (RAT)/prestin or Slc26a5 (DANRE)/prestin at different internal SCN^- concentrations. Symbols are means ± SEM from 5 or more experiments, whereas continuous and dashed lines provide predictions for different Cl^-/SCN^- exchange stoichiometries or SCN^- diffusion potentials calculated using eqns (3) and (4), respectively. The external solution contained 5 mM SCN^- and 149 mM Cl^-. *B*, reversal potentials from cells expressing SLC26A5 (RAT)/prestin or Slc26a5 (DANRE)/prestin at varying external [Cl^-] and $[SCN^-]_o$ /$[SCN^-]_i$ = 30/5 versus external [Cl^-]. Means ± SEM from 5 or more cells. The Nernst potential for SCN^- is +45 mV.

The experimentally observed reversal potentials for SLC26A5 (RAT)/prestin and Slc26a5 (DANRE)/prestin are different from predictions for coupled transport with various coupling stoichiometries, but closely similar to predictions of the Nernst equation for SCN^-. This finding supports the notion that SCN^- transport is not coupled to transmembrane Cl^- movement. As a further test, we studied whether reversal potentials are affected by the concentration of Cl^- (Fig. 5B). In these experiments, [SCN^-] was kept constant on both sides of the membrane, and external [Cl^-] was modified between 49 mM and 149 mM. Again, Cl^- did not exert any effect on the current reversal potential, providing further support for SCN^- currents that are not coupled to Cl^-. We conclude that prestin-mediated currents reverse at potentials closely similar to equilibrium potentials for SCN^-, indicating that rat and zebrafish prestin do not mediate a coupled SCN^-/Cl^- transport. Prestin-mediated SCN^- transport might thus either occur in a channel-mediated fashion as diffusion along an aqueous pore or by a uniporter that moves SCN^- across the membrane via conformational changes.

Tabelle 4.2: **Table 2.** Current reversal potentials for rat prestin, zebrafish prestin and human SLC26A7 at two different anion compositions.

$[SCN^-]_o$ /$[SCN^-]_i$	5/30	100/0
SLC26A5 (RAT)	35 mV ± 1.5 mV (n = 7)	-83 mV ± 2 mV (n = 9)
Slc26a5 (DANRE)	37 mV ± 3 mV (n = 8)	-50 mV ± 5 mV (n = 8)
SLC26A7 (HUMAN)	39 mV ± 1 mV (n = 7)	-48 mV ± 8 mV (n = 8)

SCN^- currents are reduced by external SO_4^{2-}

A large number of SLC26 proteins transport SO_4^{2-} (Bissig et al. 1994; Schaechinger & Oliver, 2007; Ohana et al. 2009). Assuming an alternating access transport mechanism coupled transport requires the existence of SO_4^{2-} sites in the inward and as well as in the outward facing conformation. Moreover, a recent theoretical treatment of the function of mammalian prestin proposed an external high affinity SO_4^{2-}-binding site (Muallem & Ashmore, 2006). We decided to study the effects of SO_4^{2-} on rat and zebrafish prestin-mediated SCN^- currents (Fig. 6). Ionic current measurements under uncoupling conditions has allowed characterization of substrate association for various transporters (Otis & Jahr, 1998; Watzke et al. 2001; Kovermann et al. 2010). We used a similar approach and determined currents first in the presence of SCN^- and SO_4^{2-} and thereafter at the same cell after switching to an external solution in which SO_4^{2-} was replaced by $gluconate^-$.

SO_4^{2-} blocked SCN^- currents through SLC26A5 (RAT)/prestin and through Slc26a5 (DANRE)/prestin in a reversible manner (Fig. 6A and D). SO_4^{2-} caused a small, but significant reduction of SLC26A5 (RAT)/prestin currents (170 pA ± 50 pA at +200 mV, n = 11, $P < 0.005$). We observed also a SO_4^{2-}-induced reduction of currents in control cells expressing only YFP (37 pA ± 14 pA at +200 mV, n = 8, $P < 0.01$). However, the current reduction was significantly smaller in control cells than in cells expressing rat prestin ($P < 0.01$, one-tailed Mann–Whitney U test). We used Wilcoxon's signed-rank test to test statistical significance since current differences were not normal-distributed.

To further separate effects of SO_4^{2-} on endogenous currents and on heterologously expressed SLC26A5 (RAT)/prestin we compared SO_4^{2-}- induced current block and non-linear capacitance in transiently transfected HEK293T cells with differing expression levels (Fig. 6C). For a given cell, the non-linear capacitance is proportional to the number of prestin proteins in the surface membrane. If SO_4^{2-} blocks SLC26A5 (RAT)/prestin, the relative block by SO_4^{2-} has to be linearly related to the number of prestin molecules. We indeed observed a linear relationship between these two parameters supporting the notion that SO_4^{2-} blocks SLC26A5 (RAT)/prestin. The small relative reduction of rat prestin-mediated SCN^- currents is thus either due to a very low binding affinity for SO_4^{2-} or to a very small percentage of SLC26A5 (RAT)/prestin being SO_4^{2-} sensitive. At present, we cannot distinguish between these two possibilities. The relatively

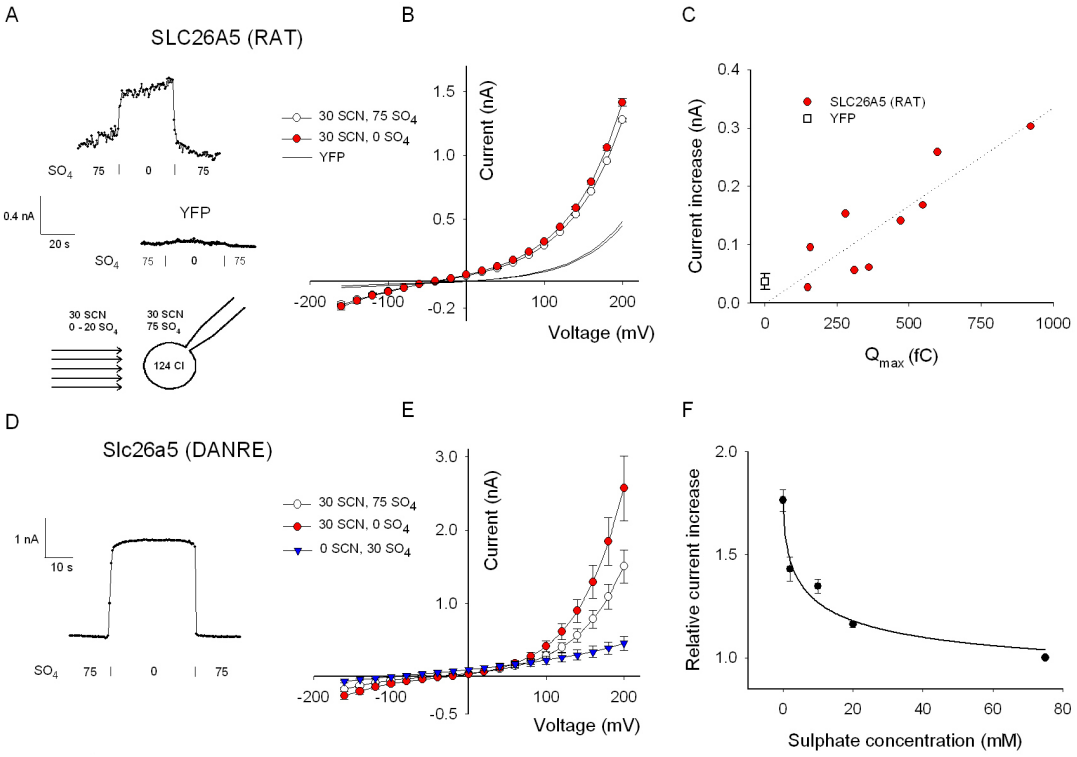

Abbildung 4.14: **Figure 6. SCN^- currents are blocked by external SO_4^{2-}** *A* and *D*, time course of current increases for rat prestin (A) and zebrafish prestin (D) upon removal of external SO_4^{2-}. Current amplitudes were measured at repetitive voltage steps to +200 mV, and $[SO_4^{2-}]$ is given below the time dependence of the current amplitude. *B*, current–voltage relationships from cells transiently expressing SLC26A5 (RAT)/prestin in solutions with SCN^- and varying $[SO_4^{2-}]$. Means ± relative standard error (RSE) from 9 cells. continuous lines show data from cells expressing only YFP as negative control (n = 5). *C*, plot of SO_4^{2-}-induced current amplitude reduction at +200 mV versus non-linear capacitance measured under the same ionic conditions for 9 different cells. In these experiments, transiently transfected HEK293T cells were used. Cells expressing YFP were accumulated into a single bin at Qmax = 0 fC and the current amplitude is shown as the mean ± standard deviation. *E*, current–voltage relationships from cells stably expressing Slc26a5 (DANRE)/prestin in solutions with varying $[SO_4^{2-}]$ and $[SCN^-]$. Means ± SEM from 7 cells. *F*, dose–response relationship for sulphate block of SCN^- currents mediated by Slc26a5 (DANRE)/prestin. Means ± SEM (n = 7). Currents were recorded at +200 mV membrane potential and then normalized to the current amplitude at $[SO_4^{2-}]$ = 75 mM.

small reduction of SLC26A5 (RAT)/prestin currents prevented determination of its concentration dependence.

Figure 6E gives the voltage dependence of zebrafish prestin SCN^- currents in the presence as well as in the absence of SO_4^{2-}. With external SCN^-, currents reversed at –39 mV ± 12 mV (n = 7) in the absence of SO_4^{2-} and at –61 mV ± 15 mV (n = 7) in the presence of SO_4^{2-} (Fig. 6E). The SO_4^{2-}-induced current reduction was associated with a shift of the current reversal potential. After replacement of SCN^- by gluconate the external solution contained SO_4^{2-} as the sole transportable anion permitting observation of coupled Cl^-/SO_4^{2-} antiport. Under these conditions the reversal potential was more negative than in the presence of SCN^- (–106 mV± 12 mV, n = 4; Fig. 6E). This shift in the reversal potential suggests that in external SO_4^{2-} and SCN^- a certain percentage of zebrafish prestin proteins function as Cl^-/SO_4^{2-} antiporters, and that SO_4^{2-} reduces the number of Slc26a5 (DANRE)/prestin functioning as SCN^- uniporters/channels. In the presence of external SO_4^{2-}, SCN^- uncouples Slc26a5 (DANRE)/prestin to a lower extent than in its absence. SO_4^{2-} at 75 mM blocked Slc26a5 (DANRE)/prestin currents by about 50%, and the pronounced block allowed determination of the SO_4^{2-}-concentration dependence of Slc26a5 (DANRE)/prestin currents (Fig. 6F). The data were well fit with a Michaelis–Menten relationship providing an apparent dissociation constant, K_d, of 7.7 mM.

Discussion

Mammalian SLC26A5/prestin is unique among the SLC26 family in its ability to convert changes of voltage into conformational changes that result in alteration of cell lengths (Zheng et al. 2000). Recently, non-mammalian prestin homologues were identified in zebrafish (Albert et al. 2007), as well as in chicken (Schaechinger & Oliver, 2007). These non-mammalian prestins exhibit non-linear capacitance; however, they also mediate stoichiometrically coupled transport of monovalent and divalent anions (Tan et al. 2011). Under the same conditions that resulted in coupled transport by non-mammalian homologues, no electrogenic transport activity could be determined for mammalian prestin (Schaechinger & Oliver, 2007). We here demonstrate that SLC26A5 (RAT)/prestin mediates electrogenic SCN^- transport. In transfected cells, SCN^- current amplitudes were well above background currents determined with transfected cells heterologously expressing a cytoplasmic protein (Fig. 1A). Moreover, we could demonstrate that SCN^- current amplitudes change linearly with expression levels of SLC26A5 (RAT)/prestin, either measured by non-linear capacitance (Fig. 1C) or whole-cell fluorescence (Fig. 4A). We observed such linear relationship over pronounced differences in the number of SLC26A5 (RAT)/prestin molecules as shown by a more than 20-fold variation in non-linear capacitance (Fig. 1C). This correlation provides strong evidence that SCN^- transport is mediated by SLC26A5 (RAT)/prestin itself. Such behaviour would not be expected if expression of mammalian prestin only upregulated endogenous anion channels, since upregulation of endogenous channels does not follow a linear relationship to the expressed protein. Moreover, background anion channels have been extensively studied in cultured mammalian cells, and no endogenous

channels with similar characteristics have been observed so far. Lastly, the functional similarity between rat and zebrafish prestin despite the clear difference in current amplitude further supports the notion of SLC26A5 (RAT)/prestin-mediated anion conduction (Figs 3 and 6). We did not test for electrogenic transport of formate and oxalate, but it appears likely that mammalian prestin is not perfectly selective and might also transport other anions (Bai et al. 2009). We observed measurable anion currents by prestin only for the non-physiological anion SCN^-. Moreover, even for this anion, macroscopic current conductances were very small making high and non-physiological voltages necessary to obtain significant current amplitudes. Most likely, anion currents by mammalian prestin thus do not exert a physiological function.

Two SLC26 anion exchangers, SLC26A3 and SLC26A6, were recently shown to function as conductive anion pathways in the presence of uncoupling anions such as NO_3^- and SCN^- (Shcheynikov et al. 2006; Ohana et al. 2011). Charge inverting mutations in a conserved glutamate residue, E367 in SLC26A3 and E357 in SLC26A6, inhibit coupled as well as uncoupled transport, indicating that NO_3^- and SCN^- transport occur through the same conduction path as anion exchange (Ohana et al. 2011). In the case that SCN^- transport by the related SLC26A5 occurs by a similar mechanism, SLC26A5 is expected to assume two conformational states and switch between these two states. In one state, the anion conduction pathway is open and can conduct SCN^-. In the other state, no transport occurs, and voltage steps cause conformational changes that result in charge movements resembling an incomplete transport cycle in transporters (Loo et al. 1993; Mager et al. 1993). We interpret all our finding in the framework of this model and assume that SLC26A5 (RAT)/prestin exclusively functions as a motor protein in the absence of SCN^- and that SCN^- can switch the motor protein into an anion-conducting mode. In the presence of external SCN^- the maximum capacitance is almost unaltered as compared to external Cl^- (Fig. 1B), indicating that the majority of rat prestin proteins assume the functional state characterized by voltage-dependent conformational changes. SCN^- thus seems to uncouple only a very small fraction of SLC26A5 (RAT)/prestin into anion channels. Since association and dissociation of SCN^- is expected to be fast (Alekov & Fahlke, 2009), the fraction of uncoupled proteins exactly translates into the absolute probability of being in the conducting mode. For ion channels/transporters with very small open probability, the unitary current amplitude can be calculated as the ratio of the current variance by the macroscopic current (Alvarez et al. 2002). Noise analysis revealed SCN^- current variances that were not different from background indicating that the unitary SCN^- transport rate of SLC26A5 (RAT)/prestin is very small. Our data indicate that – in external SCN^- – a very small fraction of SLC26A5 (RAT)/prestin assumes an anion conducting mode with very small transport rate.

Reversal potentials in mixtures of SCN^- and Cl^- are independent of the Cl^- concentration (Fig. 5), indicating that SCN^- transport is not thermodynamically coupled to Cl^- movement across the membrane. This finding suggests that prestin operates as an anion channel in the presence of external SCN^-. Alternatively, these currents might be mediated in a transporter mode that involves conformational changes mediating SCN^- transport. Unitary transport rates are too low to unambiguously distinguish between these two transport processes. However, since

SLC26 proteins encompass motor proteins, anion exchangers and anion channels, but no anion uniporter, and since channel-like transport has been shown for SLC26A3 and SLC26A6 (Ohana *et al*. 2011), we suggest that prestin assumes a channel mode of conduction in the presence of SCN^-.

We compared SCN^- transport by mammalian SLC26A5 (RAT)/prestin with Slc26a5 (DANRE)/prestin and human SLC26A7. All tested SLC26 proteins transported SCN^-, in agreement with the notion that this transport function is conserved within different functional branches of the SLC26 family. However, at comparable whole-cell fluorescences and thus protein expression levels human SLC26A7-mediated SCN^- current amplitudes were much bigger than for both prestins (Fig. 4). The different current amplitudes demonstrate that SCN^- transport rates by a given number of proteins are different for SLC26A5 (RAT)/prestin, Slc26a5 (DANRE)/prestin and human SLC26A7. This might suggest different unitary transport rates or different percentages of proteins functioning as SCN^- transporters, with very few SLC26A5 (RAT)/prestin, but a much larger percentage of Slc26a5 (DANRE)/prestin and human SLC26A7 functioning as SCN^- channels. At present, accurate determination of unitary current amplitudes are available neither for SLC26A5 nor for SLC26A7, precluding discrimination between distinct unitary transport rates or transport probabilities for these SLC26 proteins. The notion that only a certain percentage of SLC26 proteins function as SCN^- channels/uniporters is supported by experiments on Slc26a5 (DANRE)/prestin in mixtures of SCN^- and SO_4^{2-} (Fig. 6). SO_4^{2-} shifted reversal potentials to more negative potentials, indicating that zebrafish prestin can still function as an anion antiporter in the presence of SCN^-. Our results together with earlier findings (Shcheynikov *et al*. 2006; Ohana *et al*. 2011) suggest that all SLC26 proteins might be able to conduct polyatomic anions as a distinctive common feature of this family of transport proteins.

Since prestin is closely related to SLC26 anion exchangers (Zheng *et al*. 2000; Mount & Romero, 2004), various complete and incomplete transport processes have been implicated to be the basis of its voltage-dependent conformational changes. Oliver and colleagues (2001) studied the effects of internal anions on the non-linear capacitance of prestin, and proposed that monovalent anions like Cl^- or HCO_3^- bind to an intracellular binding site as an initial step in voltage-dependent conformational changes by prestin. An electric gradient translocates the anions across a fraction of the membrane and thereby triggers a conformational modification of the protein, resembling an incomplete transport cycle. Charge movement through the membrane dielectric manifests itself in non-linear capacitance, the distinct electrophysiological signature of prestin. Although the voltage-dependent capacitance predicted by this model is in excellent agreement with many experimental data, the model fails to correctly explain the observed effects of internal anion concentration and anion valence on non-linear charge movement. Subsequently, theoretical work by Muallem & Ashmore (2006) demonstrated that a transport model with an anion antiporter associated with intrinsic charge movement correctly predicts the anion and voltage dependence of the linear charge movement of prestin. The authors (Muallem & Ashmore, 2006) suggested that prestin functions as a Cl^-/SO_4^{2-} antiporter. This prediction was experimentally supported for non-mammalian prestin homologues from chicken and zebrafish (Schaechinger

& Oliver, 2007). However, since zebrafish prestin differs from mammalian prestin in a charge movement with shifted voltage dependence and lower speed (Schaechinger & Oliver, 2007), these experiments were not sufficient to unequivocally support the Muallem–Ashmore model. Our results support many of the predictions of this model. There is one transport mode that is shared by SLC26A5 (RAT)/prestin, Slc26a5 (DANRE)/prestin and human SLC26A7. SCN^- transport by SLC26A5 (RAT)/prestin is blocked by external SO_4^{2-}, indicating that there is an external SO_4^{2-} binding site. Our findings, together with recent results that internal SO_4^{2-} supports the non-linear capacitance of prestin (Rybalchenko & Santos-Sacchi, 2003; Rybalchenko & Santos-Sacchi, 2008), indicate that mammalian prestin exhibits monovalent and also divalent anion binding sites on both membrane sides, as expected for a Cl^-/SO_4^{2-} antiporter.

In summary, we demonstrated a transport function of the motor protein prestin that is conserved in other members of the SLC26 family operating as channels or transporters. The observed transport process is unlikely to have any direct physiological function, but could be useful to further characterize mechanisms underlying the function of the motor protein prestin or related SLC26 proteins.

Acknowledgements

We would like to thank Dr B. Fakler for providing expression constructs for rat and zebrafish prestin and to the members of the Institut für Neurophysiologie, MHH, for helpful discussions.

References

1. Albert JT, Winter H, Schaechinger TJ, Weber T, Wang X, He DZ, Hendrich O, Geisler HS, Zimmermann U, Oelmann K, Knipper M, Gopfert MC & Oliver D (2007). Voltage-sensitive prestin orthologue expressed in zebrafish hair cells. *J Physiol* **580**, 451–461.

2. Alekov A & Fahlke Ch (2009). Channel-like slippage modes in the human anion/proton exchanger ClC-4. *J Gen Physiol* **133**, 485–496.

3. Alvarez O, Gonzalez C & Latorre R (2002). Counting channels: a tutorial guide on ion channel fluctuation analysis. *Adv Physiol Educ* **26**, 327–341.

4. Anderson CR & Stevens CF (1973). Voltage clamp analysis of acetylcholine produced end-plate current fluctuations at frog neuromuscular junction. *J Physiol* **235**, 655–691.

5. Bai JP, Surguchev A, Montoya S, Aronson PS, Santos-Sacchi J & Navaratnam D (2009). Prestin's anion transport and voltage-sensing capabilities are independent. *Biophys J* **96**, 3179–3186.

6. Bissig M, Hagenbuch B, Stieger B, Koller T & Meier PJ (1994). Functional expression cloning of the canalicular sulfate transport system of rat hepatocytes. *J Biol Chem* **269**, 3017–3021.

7. Chang MH, Plata C, Zandi-Nejad K, Sindic A, Sussman CR, Mercado A, Broumand V, Raghuram V, Mount DB & Romero MF (2009). Slc26a9-anion exchanger, channel and Na+ transporter. *J Membr Biol* **228**, 125–140.

8. Dallos P & Fakler B (2002). Prestin, a new type of motor protein. *Nat Rev Mol Cell Biol* **3**, 104–111.

9. DeFelice LJ (1981). Introduction to Membrane Noise. *Plenum Press*, New York.

10. Detro-Dassen S, Schanzler M, Lauks H, Martin I, zu Berstenhorst SM, Nothmann D, Torres-Salazar D, Hidalgo P, Schmalzing G & Fahlke Ch (2008). Conserved dimeric subunit stoichiometry of SLC26 multifunctional anion exchangers. *J Biol Chem* **283**, 4177–4188.

11. Dorwart MR, Shcheynikov N, Wang Y, Stippec S & Muallem S (2007). SLC26A9 is a Cl- channel regulated by the WNK kinases. *J Physiol* **584**, 333–345.

12. Everett LA & Green ED (1999). A family of mammalian anion transporters and their involvement in human genetic diseases. *Hum Mol Genet* **8**, 1883–1891.

13. Farrell B, Do Scope C & Brownell WE (2006). Voltage-dependent capacitance of human embryonic kidney cells. *Phys Rev E* **73**, 041930.

14. Jiang Z, Grichtchenko II, Boron WF & Aronson PS (2002). Specificity of anion exchange mediated by mouse Slc26a6. *J Biol Chem* **277**, 33963–33967.

15. Kim KH, Shcheynikov N, Wang Y & Muallem S (2005). SLC26A7 is a Cl- channel regulated by intracellular pH. *J Biol Chem* **280**, 6463–6470.

16. Kovermann P, Machtens JP, Ewers D & Fahlke Ch (2010). A conserved aspartate determines pore properties of anion channels associated with excitatory amino acid transporter 4 (EAAT4). *J Biol Chem* **285**, 23676–23686.

17. Liu XZ, Ouyang XM, Xia XJ, Zheng J, Pandya A, Li F, Du LL, Welch KO, Petit C, Smith RJ, Webb BT, Yan D, Arnos KS, Corey D, Dallos P, Nance WE & Chen ZY (2003). Prestin, a cochlear motor protein, is defective in non-syndromic hearing loss. *Hum Mol Genet* **12**, 1155–1162.

18. Loo DD, Hazama A, Supplisson S, Turk E & Wright EM (1993). Relaxation kinetics of the Na+/glucose cotransporter. *Proc Natl Acad Sci U S A* **90**, 5767–5771.

19. Mager S, Naeve J, Quick M, Labarca C, Davidson N & Lester HA (1993). Steady states, charge movements, and rates for a cloned GABA transporter expressed in Xenopus oocytes. *Neuron* **10**, 177–188.

20. Melzer N, Torres-Salazar D & Fahlke Ch (2005). A dynamic switch between inhibitory and excitatory currents in a neuronal glutamate transporter. *Proc Natl Acad Sci U S A* **102**, 19214–19218.

21. Moseley RH, Hoglund P, Wu GD, Silberg DG, Haila S, de la Chapelle A, Holmberg C & Kere J (1999). Downregulated in adenoma gene encodes a chloride transporter defective in congenital chloride diarrhea. *Am J Physiol* **276**, G185–G192.

22. Mount DB & Romero MF (2004). The SLC26 gene family of multifunctional anion exchangers. *Pflugers Arch* **447**, 710–721.

23. Muallem D & Ashmore J (2006). An anion antiporter model of prestin, the outer hair cell motor protein. *Biophys J* **90**, 4035–4045.

24. Ohana E, Shcheynikov N, Yang D, So I & Muallem S (2011). Determinants of coupled transport and uncoupled current by the electrogenic SLC26 transporters. *J Gen Physiol* **137**, 239–251.

25. Ohana E, Yang D, Shcheynikov N & Muallem S (2009). Diverse transport modes by the solute carrier 26 family of anion transporters. *J Physiol* **587**, 2179–2185.

26. Otis TS & Jahr CE (1998). Anion currents and predicted glutamate flux through a neuronal glutamate transporter. *J Neurosci* **18**, 7099–7110.

27. Petrovic S, Barone S, Xu J, Conforti L, Ma L, Kujala M, Kere J & Soleimani M (2004). SLC26A7: a basolateral Cl-/HCO3- exchanger specific to intercalated cells of the outer medullary collecting duct. *Am J Physiol Renal Physiol* **286**, F161–F169.

28. Riazuddin S, Anwar S, Fischer M, Ahmed ZM, Khan SY, Janssen AG, Zafar AU, Scholl U, Husnain T, Belyantseva IA, Friedman PL, Riazuddin S, Friedman TB & Fahlke Ch (2009). Molecular basis of DFNB73: mutations of BSND can cause nonsyndromic deafness or Bartter syndrome. *Am J Hum Genet* **85**, 273–280.

29. Rybalchenko V & Santos-Sacchi J (2008). Anion control of voltage sensing by the motor protein prestin in outer hair cells. *Biophys J* **95**, 4439–4447.

30. Rybalchenko V & Santos-Sacchi J (2003). Cl- flux through a non-selective, stretch-sensitive conductance influences the outer hair cell motor of the guinea-pig. *J Physiol* **547**, 873–891.

31. Santos-Sacchi J (1991). Reversible inhibition of voltage-dependent outer hair cell motility and capacitance. *J Neurosci* **11**, 3096–3110.

32. Santos-Sacchi J (2002). Functional motor microdomains of the outer hair cell lateral membrane. *Pflugers Arch* **445**, 331–336.

33. Santos-Sacchi J, Kakehata S & Takahashi S (1998). Effects of membrane potential on the voltage dependence of motility-related charge in outer hair cells of the guinea-pig. *J Physiol* **510**, 225–235.

34. Schaechinger TJ & Oliver D (2007). Nonmammalian orthologs of prestin (SLC26A5) are electrogenic divalent/chloride anion exchangers. *Proc Natl Acad Sci U S A* **104**, 7693–7698.

35. Scott DA & Karniski LP (2000). Human pendrin expressed in Xenopus laevis oocytes mediates chloride/formate exchange. *Am J Physiol Cell Physiol* **278**, C207–C211.

36. Shcheynikov N, Wang Y, Park M, Ko SB, Dorwart M, Naruse S, Thomas PJ & Muallem S (2006). Coupling modes and stoichiometry of Cl-/HCO3- exchange by slc26a3 and slc26a6. *J Gen Physiol* **127**, 511–524.

37. Soleimani M, Greeley T, Petrovic S, Wang Z, Amlal H, Kopp P & Burnham CE (2001). Pendrin: an apical Cl-/OH- exchanger. *Am J Physiol Renal Physiol* **280**, F356–F364.

38. Tan X, Pecka JL, Tang J, Okoruwa OE, Zhang Q, Beisel KW & He DZ (2011). From zebrafish to mammal: functional evolution of prestin, the motor protein of cochlear outer hair cells. *J Neurophysiol* **105**, 36–44.

39. Torres-Salazar D & Fahlke Ch (2007). Neuronal glutamate transporters vary in substrate transport rate but not in unitary anion channel conductance. *J Biol Chem* **282**, 34719–34726.

40. Watzke N, Bamberg E & Grewer C (2001). Early intermediates in the transport cycle of the neuronal excitatory amino acid carrier EAAC1. *J Gen Physiol* **117**, 547–562.

41. Weber T, Gopfert MC, Winter H, Zimmermann U, Kohler H, Meier A, Hendrich O, Rohbock K, Robert D & Knipper M (2003). Expression of prestin-homologous solute carrier (SLC26) in auditory organs of nonmammalian vertebrates and insects. *Proc Natl Acad Sci U S A* **100**, 7690–7695.

42. Xie Q, Welch R, Mercado A, Romero MF & Mount DB (2002). Molecular characterization of the murine Slc26a6 anion exchanger: functional comparison with Slc26a1. *Am J Physiol Renal Physiol* **283**, F826–F838.

43. Xu J, Henriksnas J, Barone S, Witte D, Shull GE, Forte JG, Holm L & Soleimani M (2005). SLC26A9 is expressed in gastric surface epithelial cells, mediates Cl-/HCO3- exchange, and is inhibited by NH4+. *Am J Physiol Cell Physiol* **289**, C493–C505.

44. Zheng J, Shen W, He DZ, Long KB, Madison LD & Dallos P (2000). Prestin is the motor protein of cochlear outer hair cells. *Nature* **405**, 149–155.

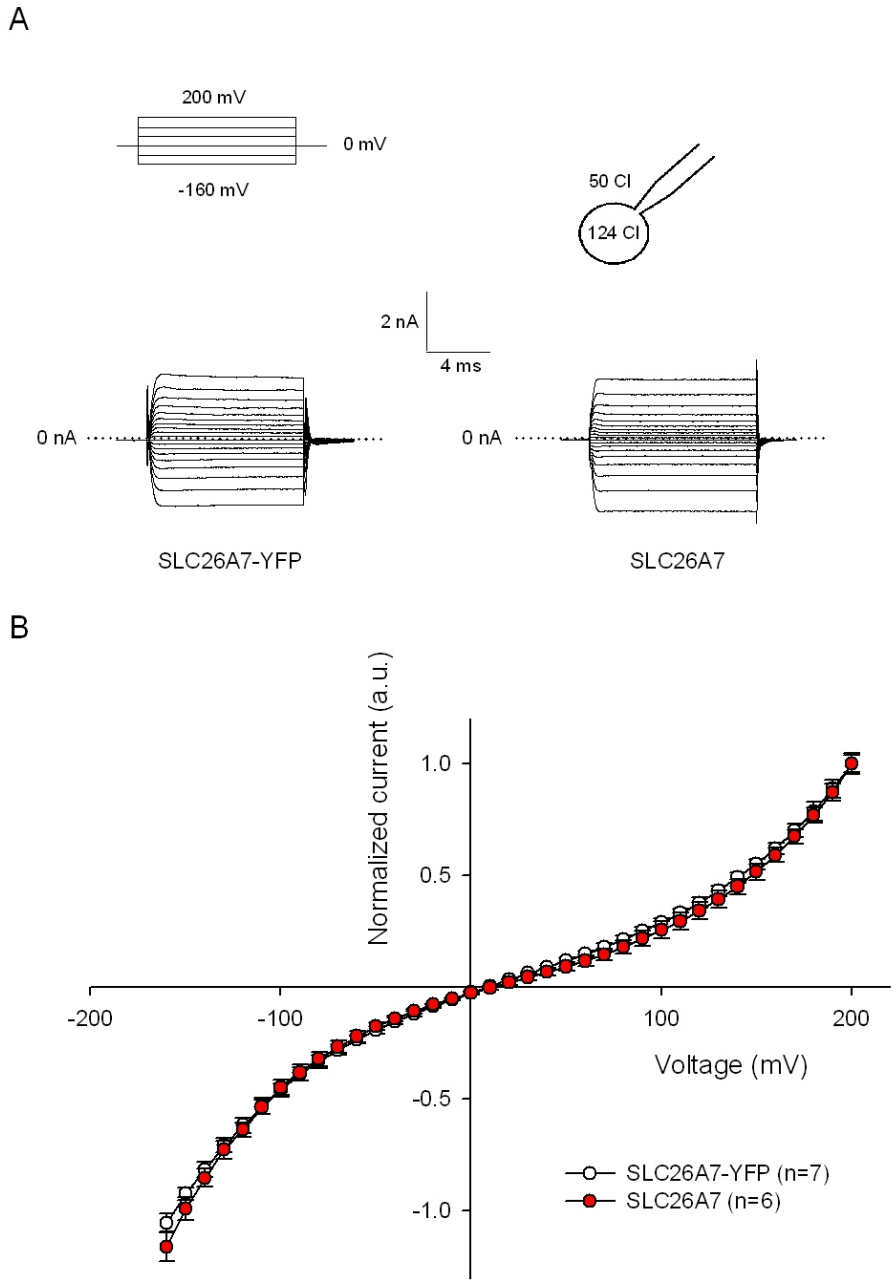

Supplemental Figure 1.

Danksagung

Die vorliegende Arbeit wurde am Institut für Neurophysiologie der Medizinischen Hochschule Hannover unter der Leitung von Prof. Dr. med. Christoph Fahlke angefertigt.

Christoph Fahlke danke ich für die Möglichkeit, diese Dissertation an seinem Institut anfertigen zu dürfen, gerade auch weil die Rahmenbedingungen etwas ungewöhnlich waren. Das Physik-Praktikum war mein 'zweiter Arbeitsplatz'; ich habe wohl mehr Zeit im Praktikum als im Labor verbracht. Die Tutoren und Mitarbeiter des Physik-Praktikums haben dazu beigetragen, dass ich das Praktikum immer gerne betreut habe. Ohne die gute Zusammenarbeit mit den Mitarbeitern des Instituts für Neurophysiologie, die immer hilfsbereit waren, wäre diese Arbeit schwer möglich gewesen. Die im Rahmen der Arbeit verwendeten Plasmide sowie die stabilen Zelllinien wurden von Sonja Meyer zu Berstenhorst hergestellt. Ein besonderer Dank gilt Peter Kovermann für das Korrekturlesen dieser Arbeit und kritische Kommentare zum Manuskript.

Selbständigkeitserklärung

gemäß §6(1) der Promotionsordnung der Naturwissenschaftlichen Fakultät der Gottfried Wilhelm Leibniz Universität Hannover für die Promotion zum Dr. rer. nat.

Hierdurch erkläre ich, dass ich meine Dissertation mit dem Titel

Anionentransport durch das Motorprotein Prestin

selbständig verfasst und die benutzten Hilfsmittel und Quellen sowie gegebenenfalls die zu Hilfeleistungen herangezogenen Institutionen vollständig angegeben habe. Die Dissertation wurde nicht schon als Masterarbeit, Diplomarbeit oder andere Prüfungsarbeit verwendet.

Lebenslauf

Michael Schänzler

03.03.1969	geboren in Karlsruhe
1975 bis 1979	Grundschule in Munster (Örtze)
1979 bis 1998	Gymnasium Soltau
Juni 1988	Abitur
1988 bis 1989	Grundwehrdienst
1989 bis 1997	Studium der Physik an der Universität Hannover
August 1997	Diplom
1998 bis 1999	Universität Hannover, Gravitationswellendetektor GEO 600
1999 bis 2001	Halcyonics GmbH, Göttingen
2002 bis 2004	Universität Hannover, Institut für Quantenoptik, Wissenschaftlicher Mitarbeiter
2005 bis heute	Medizinische Hochschule Hannover, Institut für Neurophysiologie, Wissenschaftlicher Mitarbeiter